Theoretical and Experimental Investigation of All-Optical Gain-Clamped Discrete Fiber Raman Amplifiers

A thesis submitted to McGill University in partial fulfillment of the requirements of the degree of Master of Engineering

Theodore Zambelis
Photonics Systems Group, Electrical and Computer Engineering
McGill University, Montreal, Quebec, Canada
October 15, 2003

Your file Votre référence
ISBN: 0-612-98577-6
Our file Notre référence
ISBN: 0-612-98577-6

Analyse théorique et expérimentale d'amplificateurs tout-fibre Raman discrets et clampés

Theodore Zambelis

Résumé

A partir de simulations numériques, nous concevons et analysons les performances des amplificateurs tout-fibre Raman, discrets et clampés. En particulier, nous nous intéressons à une configuration qui génére un signal dit de "feedback", grâce à l'utilisation de réseaux de Bragg. Nous examinons l'impact de la longueur d'onde de feedback sur les propriétés du "clamping".

A partir des résultats des simulations, nous concluons que, pour parvenir à un clamping du gain uniforme à travers la bande DWDM qui nous intéresse, les pompes optiques doivent être réduites également par le signal de feedback. L'effet de ce dernier signal sur l'amplificateur peut surtout être prédit à partir des coefficients de gain Raman correspondant à la séparation en fréquence entre le signal de feedback et les pompes. Nous avons développé un amplificateur Raman qui est uniformément clampé sur une bande de 58 nm et qui présente un gain d'au moins 20 dB ainsi qu'une puissance critique de -3 dBm.

Nous vérifions aussi, de manière expérimentale, le clamping du gain de cette configuration.

Theoretical and Experimental Investigation of All-Optical Gain-Clamped Discrete Fiber Raman Amplifiers

Theodore Zambelis

Abstract

Using numerical simulations, we design and analyze the performance of gain-clamped discrete fiber Raman amplifiers. In particular, we investigate a configuration which generates a feedback signal through the use of fiber Bragg gratings. We examine the impact of the feedback wavelength on the gain-clamping properties.

From the simulation results, we conclude that in order to achieve uniform gain-clamping across the DWDM band of interest, the optical pumps must be depleted evenly by the feedback signal. The effect of the feedback signal on the amplifier may be mostly predicted based on the Raman gain coefficients corresponding to the frequency separation between the feedback signal and the pumps. A 58 nm wide uniformly gain-clamped Raman amplifier having over 20 dB gain and a critical power of -3 dBm is developed.

We also verify gain-clamping for this configuration experimentally.

Acknowledgements

Firstly, I thank Dr. Lawrence Chen, for giving me the opportunity to be a member of his team during these past two years, and also for his support, good advice and for the many things he taught me. I would like to thank fellow students, Nikolaos Gryspolakis, Johann Gest and Bing Xia for their wisdom, patience and teamwork. I would like to give a special word of thanks to Chris Rolston, who tirelessly made sure that our working conditions were second-to-none. I thank MPB Communications for generously loaning us a high-powered fiber Raman laser, which made a huge difference in the experiments. Jacek Kierzenka of Mathworks Inc., author of the 'bvp4c' Matlab function, was also very helpful.

This experience would not have been the same had it not been for the good people in the Photonics group, particularly my colleagues and friends in room 848. Finally, I thank my family and friends, Kostas, Elaine, Yaya, Stacy and family, Greg, Pauline, Victoria, Sam, Nancy, Jimmy, Rami, Ali and of course my other friends for their love and encouragement.

Table of Contents

List of Figures

List of Tables

1 Introduction and Motivation

1.1 Fiber Raman Amplifiers in Optical Communications

Fiber Raman Amplifiers (FRAs) are being deployed in almost every new long-haul and ultralong-haul fiber-optic transmission system, making them one of the first widely commercialized nonlinear optical devices in telecommunications [5]. FRAs, found either in **distributed** or **discrete** configurations, offer an increase in the capacity of fiber-optic transmission systems. Distributed FRAs have primarily been used to upgrade existing long-haul systems since they provide an improvement in the noise figure (NF) and reduce the nonlinear penalty of fiber systems. Discrete FRAs, which are the subject of this thesis, have until now been used mostly in long-haul applications to open up new wavelength windows in Dense Wavelength Division Multiplexing (DWDM) systems, particularly in the short wavelength S-band (1470 to 1520 nm) [6], [13] or in the ultra-long wavelength U-band (1600 to 1670 nm) [39]. As enabling technologies become increasingly available, particularly in the areas of high-powered laser diode pump sources and highly nonlinear fibers having large Raman gain, discrete FRAs are becoming a practical technology option for a growing number of applications.

The main advantage of FRAs, both discrete and distributed, is that they offer an adjustable gain spectrum in terms of bandwidth, gain window and gain spectrum shape. This allows them to have an ultra-wide and flat gain band, and this without the use of any gain flattening filters. The bandwidth of Raman amplification is very broad; when a single optical pump is used, the gain bandwidth is roughly 60 nm in terms of Full Width at Half Maximum (FWHM). When multiple pump sources are employed, the gain spectrum becomes a superposition of the gain spectra that would have been provided by each pump individually (if we ignore pump-to-pump interactions), and therefore, the total bandwidth may be greatly extended, see Fig. 1-1. Meanwhile, the actual gain band is determined by the pump wavelengths since the interaction is not resonant. On the other hand, in Erbium Doped Fiber Amplifiers (EDFAs), the gain bandwidth is limited by the fluorescence of the erbium ion in silica, and therefore only part of the potential transmission bandwidth is covered [19], namely the C-band (1530 – 1565 nm) and L-band (1570 – 1605 nm). With Raman amplifiers, any wavelength window may be amplified, as long as the appropriate optical pumps are available. In particular, the S- and U-bands are of interest for transmission systems since fiber attenuation is still relatively low in these regions. Finally, the shape of the gain spectrum may be tailored by the selection of pump wavelengths and launch powers (shown schematically in Fig. 1-1).

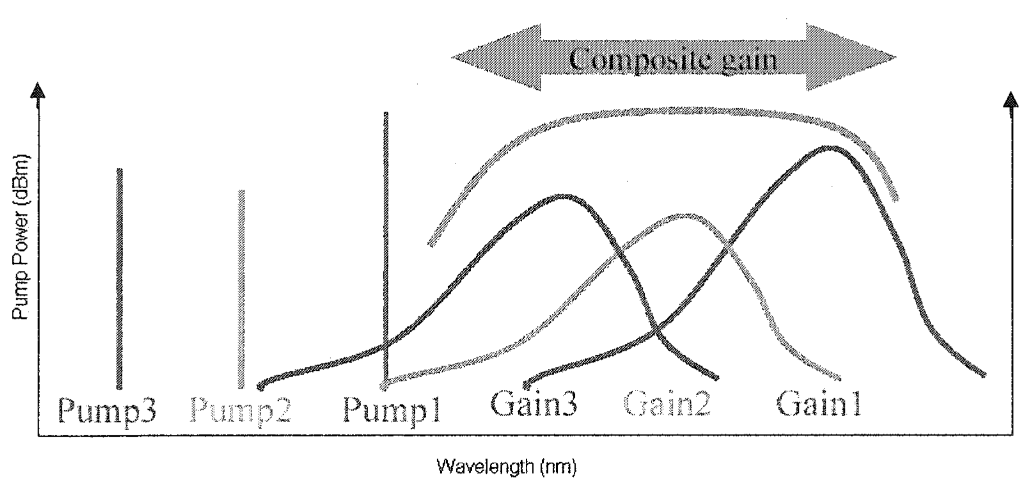

Fig. 1-1 Total Raman gain is the result of a superposition of the gain of the individual pumps. [4]

1.1.1 Distributed FRAs

An amplifier is said to be distributed when the amplification occurs directly in the transmission medium, rather than at a discrete point as in discrete or **lumped** amplifiers. Distributed FRAs offer improved noise figure and also reduce the non-linear penalty, which allows for longer amplifier spans, higher bit rates, closer channel spacing, and operation near the zero-dispersion wavelength [5].

EDFAs are inherently discrete amplifiers. As shown in Fig. 1-2, in long-haul systems that use only EDFAs (labeled "lumped amplification"), the signals are boosted at regular intervals; the optical reach of this system is limited by the ASE noise produced by the amplifiers themselves and also by the nonlinearities of the transmission fiber [8]. This is explained as follows: as the signal is amplified, ASE noise is also added to the signal, which degrades the OSNR. In order to counter this effect, more signal power may be launched into the fiber, but higher signal power results in the appearance of undesirable nonlinear effects, which also degrade the signal. This is remedied by a system which employs both discrete and distributed amplification, as shown in Fig. 2-1 (labeled "with distributed amplification"). Since amplification occurs as the signal is propagating in the transmission medium, the signal need not be launched at such high powers at the amplification point. This increases the overall OSNR of the link and increases the overall power budget. In [11], an increase in the power budget of 7.4 dB was obtained by using distributed FRAs, which allowed an enhancement of spectral efficiency: a four-fold increase in either the TDM or WDM channels was permitted when the distributed FRA was employed. Alternatively, the increase in the power budget may be used to extend the fiber-span distance between consecutive amplifiers [1].

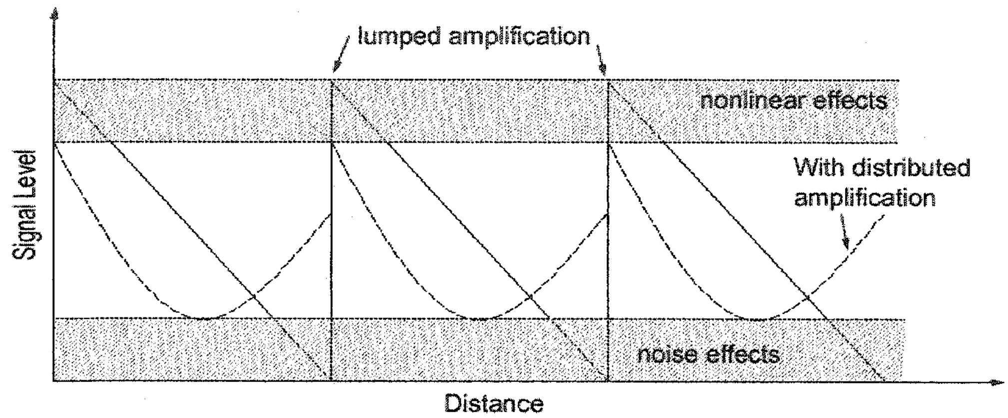

Fig. 1-2 Comparison of long-haul systems. One uses distributed and lumped amplification and the other uses lumped amplification only. [1]

Since distributed Raman amplification can be achieved in any conventional transmission fiber, it is attractive as an upgrade method for already installed systems. Nowadays, Raman amplification is considered to be essential for high-bit rate (> 40 Gbps) systems.

1.1.2 Discrete FRAs

A discrete FRA (DFRA) is like an EDFA in that it is an element placed into the transmission link to provide localized gain. In DFRAs, optical fiber with high Raman gain efficiency is used to give high gain with a short fiber length. In particular, Dispersion Compensating Fiber (DCF) and Highly Non-Linear Fiber (HNLF) are commonly employed in DFRAs. Several configurations are possible including copropagating pumps and signals, counter-propagating pumps and signals, and multiple-stage designs in which the gain medium is divided into two or more sections.

While not offering the advantages of distributed amplifiers mentioned in the previous section, namely an increase in the power budget due to the countering of noise and of nonlinear effects by amplification directly in the transmission medium, DFRAs still maintain the advantage of gain-spectrum design flexibility. Meanwhile, the discrete configuration allows for the use of all-optical gain-clamping, which is discussed in the following section.

1.2 Significance of the Gain-Clamped Discrete FRA

In DWDM networks of the future, channels will be added and dropped continuously in order to meet the dynamically varying capacity demands [22]. Also, fiber cuts or other unexpected events could contribute to the variation in the number and power of signals in a link. As in EDFAs, the performance of FRAs is dependent on input signal power, both in terms of the **steady-state noise and gain levels** and in terms of the **transient effects**.

In a typical optical amplifier without gain control, as the total input signal power is increased, the steady-state gain provided by the amplifier decreases. Due to this effect, certain signals in the system may not receive sufficient gain, in which case their power would be too low for detection at the receiver. On the other hand, as the total input signal power to an amplifier is decreased, the gain that the amplifier provides increases so that a certain signal may receive too much gain and be at too high a power level to be properly detected at the receiver, or its high-power may result in the appearance of undesirable nonlinear effects. **Saturation power** is the total input signal power (optical amplifiers saturate on a total input power basis [26]) at which point the amplifier's steady-state gain begins to decrease as the overall input power is increased. The saturation power in FRAs has been shown to be on the order of tens of milliwatts [22]; albeit higher than EDFAs, in DWDM systems where tens or even hundreds of channels may be simultaneously present, this saturation power is still low and the steady-state gain variation effect will be present.

Transient effects also occur as a result of a change in the input signal power to the amplifier: if the input power to the amplifier is decreased, there is momentary sharp increase in the gain which eventually settles down to a new steady-state value. If the input signal power is increased, there is a sharp decrease in the gain, which eventually settles up to a new steady-state value. In both cases, the signal power seen by the receiver may either be too high or too low for proper detection. Furthermore, when amplifiers are cascaded down a link, the transient effects can accumulate and severely degrade the system performance [26].

Fig. 1-3 summarizes the effect of input power fluctuations to the amplifier. In (a) the steady-state gain fluctuation is shown while in (b) the transient effects are shown.

In order to maintain a constant gain level for the surviving signals and to counter transient effects, a **gain control mechanism** is needed in the FRA. Two main approaches have been used thus far to achieve gain-control in FRAs, as well as in EDFAs: pump control and gain-clamping.

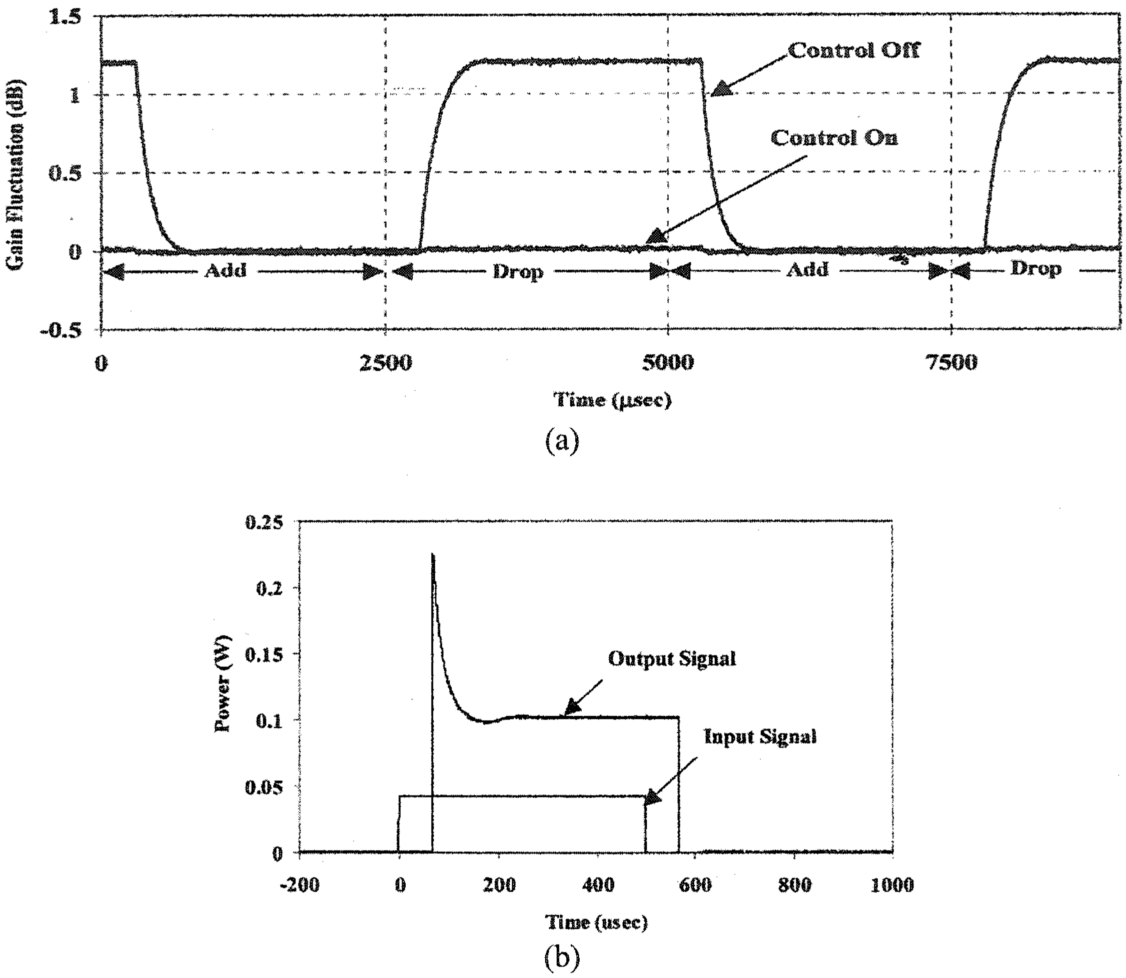

Fig. 1-3 Effects of channel add/drop on the output of the amplifier. (a) Fluctuation of steady-state gain, and (b) transient effects. [30]

1.2.1 Pump Control

Pump control, shown schematically in Fig. 1-4, is simple in concept: there is a monitoring of either the output of the amplifier (feedback), the input to the amplifier (feed-forward) or a combination of both (feedback and feed-forward), and an electrical control system adjusts the pump power in order to maintain a constant gain value and to counter transient effects. One of the main advantages of pump control over all-optical gain-clamping (described in the next section) is that it may be used in both distributed and discrete modes, as shown in [26] and [27], whereas gain-clamping is normally found only in discrete systems. In [26], a proportional-integral-derivative (PID) control circuit was used to control the transients in an 8-channel single-pump distributed system. One of eight channels and the total output power were used as controls to the feedback circuit. When four channels were dropped, the gain variation was maintained under 0.02 dB, compared to 0.35 dB with no pump control. Similar results were obtained for lumped amplifiers. In [27], it was found that using a combination of proportional and differential feedback (PD control) gives superior control performance than when using the PID feedback function alone (as was done in [26]). Also in [27], the results were extended to multi-pump, multi-channel wideband FRAs. It was found that in a 100 channel DWDM system spanning 1520 to 1629 nm, with an 8 pump (ranging from 1416 to 1502 nm) gain-flattened distributed amplifier, the use of a single control channel was insufficient. On the other hand, the use of two control channels resulted in a marked improvement in the transients compared to the uncontrolled case. A control channel at 1520 nm was used to control the powers of the four shorter wavelength pumps, and a second channel at 1540 nm was used to control the remaining four pumps. A response time of approximately 100 μs was required to return the system to the original gain level, which is in the acceptable range for telecommunications applications.

Although pump control shows promise, the complexity of the required additional electronic circuitry poses serious difficulties for practical implementation. The speed requirements are very stringent; pump control circuitry must be able to process fall/rise times of less than 30 μs [27]. When multi-wavelength pumps are used, calculating the appropriate pump powers needed to maintain a constant gain spectrum for these dynamic input conditions is much more complicated than simply applying a power ratio amongst the pumps as shown in [24]; pump-to-pump interactions play a very important role in determining the gain spectrum, and therefore they must also be considered in the control system's calculation.

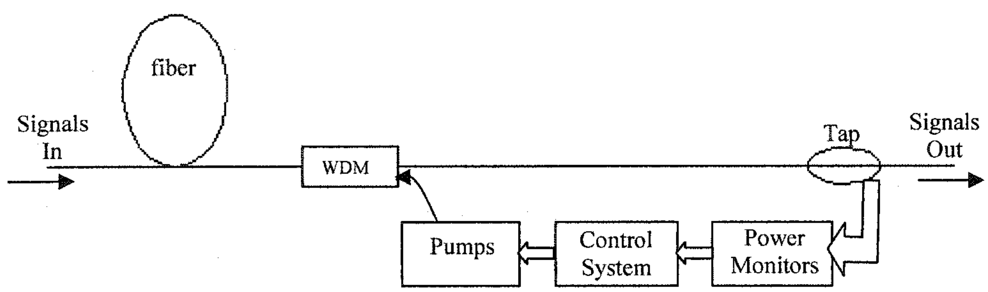

Fig. 1-4 Dynamic gain control by feedback pump-control.

1.2.2 All-Optical Gain-Clamping

All optical gain-clamping is the gain control mechanism that is studied in this thesis. It uses only passive optical components to achieve dynamic gain-clamping and it is inherently better suited for discrete systems. The principle of operation is as follows: a feedback lasing signal is generated at a wavelength outside the WDM band of interest. By having a higher power than the WDM signals, the lasing signal may force the amplifier to operate in saturation and dominate its gain and noise characteristics, i.e. the amplifier becomes clamped to the lasing signal. As WDM channels are added and dropped, the gain and noise performance of the surviving channels are maintained (more) constant. Gain-clamping will cease to take effect once the input signal powers exceed the **critical power**, at which point the lasing signal no longer has the dominant effect (the critical power is quantified as the input signal power for which the amplifier gain drops by 0.5 dB from its small-signal value).

Two potential configurations for this system are shown in Fig. 1-5. In Fig. 1-5 (a), the lasing signal is generated in a feedback ring. This type of system is investigated theoretically in [28] and [29] and experimentally in [17] and [18]. In [18], a gain variation of less than 0.3 dB is demonstrated for total input signal power ranging from –20 dBm to 2.7 dBm (a single pump and four DWDM signals are used). As will be seen throughout this work, the selection of the lasing wavelength is of central importance in the design of a gain-clamped DFRA (GC-DFRA). In [28], it is stated that "better gain-clamping is achieved when the clamping wavelength is in a relatively low-gain regime", which is also supported by our work. In the feedback ring GC-DFRA, the lasing wavelength is determined by the passband of the filter in the feedback loop. In [28], a multi-passband filter was used, which resulted in multiple lasing wavelengths which improved the clamping (higher critical power); however this also leads to a further decrease in the gain since the pumps are **depleted** to a greater extent, i.e. more power is drawn from the pumps. The degree of gain-clamping may also be increased by decreasing the attenuation in the loop: this increases the lasing signal power which also depletes the pumps more strongly, which reinforces the clamping effect but lowers the number of photons available for gain.

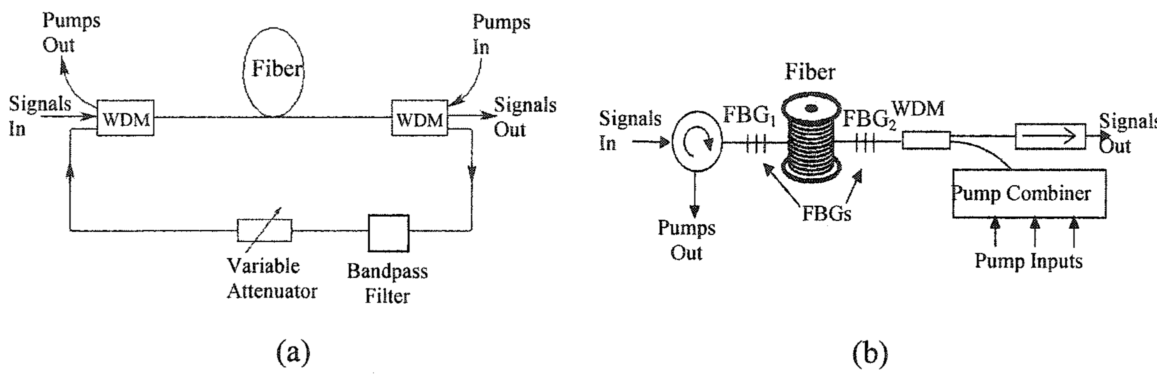

Fig. 1-5 Two configurations for all-optical gain-clamping. (a) uses a ring-laser configuration. (b) uses resonant cavity by FBGs.

1.3 Thesis Contributions

In this work, the steady-state gain-clamping properties of the DFRA configuration shown in Fig. 1-5 (b) are theoretically and experimentally analyzed. This configuration also controls the transient effects, but the detailed study of this is not treated herein. The fiber Bragg gratings (FBGs) create a resonant cavity in which a lasing feedback signal is generated at the gratings' reflective wavelengths, which leads to gain-clamping. FBG_1 and FBG_2 have reflectivities R_1 and R_2, respectively, which can be used to control the power of the lasing signal (analogous to the variable attenuator in the ring-laser design). By using multiple gratings on each side of the gain fiber (in series), several lasing signals may be obtained, analogous to the use of a multi-passband filter in the feedback ring loop design. In this work, clamping with a single lasing wavelength was analyzed. **In particular, a method of systematically locating an optimum feedback wavelength for uniform gain-clamping is developed.** As will be seen in detail in chapter 4, uniform gain-clamping refers to maintaining constant gain-clamping performance across the DWDM band of interest.

1.4 Thesis Outline

The remainder of this thesis is organized as follows. In chapter 2, a background of the physical processes involved in FRAs is given. This is followed by a review of the sources of noise and of the polarization dependence of Raman gain. In chapter 3, two models of the steady-state behavior of the FRA are presented: one simplified which is used for estimation purposes, and one full model which accurately accounts for the main physical interactions. This model was incorporated into a computer simulation program which was used to analyze a GC-DFRA, the results of which are presented in chapter 4. A method of designing a uniformly gain-clamped wideband DFRA is arrived at based on the Raman gain spectrum and on the pump wavelengths. The trends observed in the simulations were then replicated experimentally, and the procedures and results are found in chapter 5. In chapter 6, a summary is given and future work is outlined.

2 Raman Amplification

An optical fiber is capable of guiding light over long propagation distances while confining it to a small cross-sectional area, thus providing a long interaction region with large electric field intensity, which is especially favorable for nonlinear phenomena, such as Raman scattering, Brillouin scattering and four-wave mixing [7]. While each of these mentioned nonlinear processes may be harnessed to achieve stimulated amplification, Stimulated Raman Scattering (SRS) has the advantages of self phase-matching between the pump and the signal, and high speed response [8].

2.1 Physical Processes in the Raman Amplifier

2.1.1 The Spontaneous Raman Effect

A molecule may absorb photons either by converting their energy into its vibrational or rotational motion, or through the mechanism of electronic transition [9]. As shown in Fig. 2-1 (a), a molecule in a certain vibrational, rotational or electronic state, say *state 1*, may absorb a photon with energy $h\nu_i$ which raises the molecule to some intermediate or virtual state, whereupon it makes an immediate Stokes transition of energy $h\nu_s$, down to *state 2*. A Stokes transition is one in which the emitted photon has lower energy than the incident primary photon. In conserving energy, the difference $h\nu_i - h\nu_s = h\nu_{12}$ goes into exciting the molecule to the higher energy level of *state 2*. Similarly, if the molecule was initially in state 2 when it was excited by an incident photon, as in Fig. 2-1 (b), it may undergo an anti-Stokes transition to state 1, whereby the emitted photon has greater energy than the incident photon. Both of these phenomena are called **Raman Scattering**.

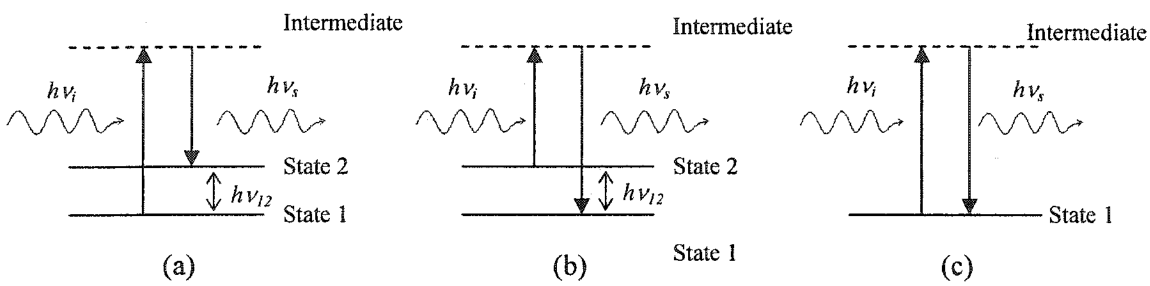

Fig. 2-1 (a) and (b) show Raman scattering, with stokes and anti-Stokes shifts, respectively. (c) depicts Rayleigh scattering [9].

The mechanism by which the incident radiation is absorbed depends on the wavelength of this radiation. For the visible spectrum and ultraviolet regions, energy is usually absorbed by electronic transition. For the far-infrared and microwave regions, the energy is converted to rotational kinetic energy. Infrared photons, which are of concern for telecommunications applications, contribute to the vibrational motion of the silica molecule via the **Kerr nonlinear effect** when they are absorbed, with a response time on the order of 10 femtoseconds. Even though this is an extremely fast response, it introduces a finite delay of nonlinear polarization with respect to the electric field of the incident light wave which allows the real vibrational modes (also called optical **phonons**) to exist [32].

The spontaneous Raman effect was predicted in 1923 by Adolf Smekal and first observed experimentally in 1928 by Sir Chandrasekhara Vankata Raman, then professor of physics at the University of Calcutta. The effect was difficult to put to use at the time due to the unavailability of strong optical sources, which of course changed with the advent of the laser. Raman Spectroscopy, which uses the resulting energy differences between the incident and emitted fields, is a unique and powerful analytical tool that yields insight into a molecule's structure [9].

2.1.2 The Stimulated Raman Effect

Stimulated Raman Scattering (SRS) was first noticed by chance in 1962 by Eric J. Woodbury and Won K. Ng. While working with a high powered laser at 694.3 nm whose beam traveled through a nitrobenzene shutter, they noticed that 10% of the incident energy appeared as a coherent beam at 766.0 nm, a shift characteristic of one of the vibrational modes of nitrobenzene [9]. The effect is shown schematically in Fig. 2-2. In the presence of a photon from the scattered beam at frequency ν_s, the Raman scattering process is stimulated such that the incident beam loses a photon, while the scattered beam coherently gains a photon.

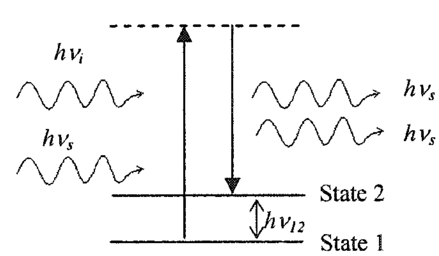

Fig. 2-2 Stimulated Raman Scattering [9]

This is the basis of the FRA: when a silica fiber is optically pumped, signals at a lower energy can experience stimulated Raman amplification.

2.1.3 Rayleigh scattering

Rayleigh scattering occurs in an optical amplifier when an incident photon interacts with microscopic glass composition non-uniformities in the optical fiber [5]. The incident photon is absorbed by the molecule and a scattering event occurs; unlike Raman scattering, the molecule returns to its original state after re-emitting the photon, and therefore the emitted photon has the same frequency as the incident one, see Fig. 2-1(c). The majority of scattering events that occur when a solid, liquid or gas is permeated with light is from Rayleigh scattering. In optical fibers where there are only two directions of propagation, forward Rayleigh scattering is when the scattered photons retain their original direction of propagation, whereas Rayleigh backscattering is when the scattered photons propagate in the reverse direction.

2.2 Sources of Noise in FRAs

There are four primary sources of noise in FRAs [5]. First, ASE noise is a result of spontaneous Raman scattering (SRS) that is amplified as it travels down the gain medium (analogous to ASE in EDFAs). The **noise figure** (NF) relates the amount of ASE noise that is added to the signal relative to amount of gain and can be written as in Equation 2-1.

$$NF = \frac{1}{G}\left(\frac{2 \cdot S_{ASE}(v)}{hv} + 1\right) \qquad \textbf{(Equation 2-1)}$$

$$S_{ASE}(v) = (G-1) \cdot hv \cdot \left[\frac{N_2}{N_2 - N_1}\right] \qquad \textbf{(Equation 2-2)}$$

S_{ASE} is the ASE power spectral density which can be written as in Equation 2-2, h is Plank's constant, v is the signal frequency, G is the observed gain, and N_2 and N_1

respectively represent the upper and lower state carrier populations. Fortunately, the FRA always acts as a fully inverted system, i.e. the upper state population N_2 is much greater than the lower state population N_1, which reduces the $(N_2 / N_2 - N_1)$ factor in Equation 2-2 to unity. If fiber attenuation is ignored, FRAs would achieve the theoretical quantum limit NF of 3 dB. However, due to long propagation distances in FRAs (on the order of kilometers), the attenuation in the fiber contributes in reducing gain and hence the NF increases. ASE noise may be countered by using a multiple-stage design; by dividing the amplification in more than one stage, the pump launch powers are reduced and the backward propagating ASE, which contributes to the forward propagating ASE through Rayleigh backscattering, may be removed through the use of isolators. In [15], the NF was reduced by 1.5 dB using a dual-stage design.

The second source is thermal noise. As shown in [12], the closer the signal and pump are spaced closer together, the higher the thermal noise generation. Due to this effect, for multi-pump gain flattened systems, the NF is higher for the shorter wavelength signals since they are closest to the pumps. Consequently, there is a tradeoff between low ASE noise and the amplifier's bandwidth of operation. The effect is due to **phonon-stimulated optical noise**: at room or elevated temperatures, there is a population of thermally induced phonons in the glass fiber that can spontaneously experience gain from the pumps, thereby creating additional noise for signals close to the pump wavelengths [5]. A configuration that uses both co- and counter-propagating pumps for the pumps which amplify these lower wavelength (higher noise) signals can be used to achieve **noise-flattening** in discrete amplifiers, as shown in Fig. 2-3 [23].

Since optical amplification prior to transmission loss can suppress ASE, co-propagation leads to lower ASE noise than counter-propagation. But counter-propagation is preferred in terms of avoiding polarization-dependent gain (see Section 2.3) and for eliminating the coupling of pump-fluctuations to the signal (see fourth noise source in this section). By using both co- and counter-propagation for the shorter wavelength pumps and counter-propagation only for the remaining pumps, the NF of the shorter wavelength signals can be lowered such that a flat NF is obtained [4], [23].

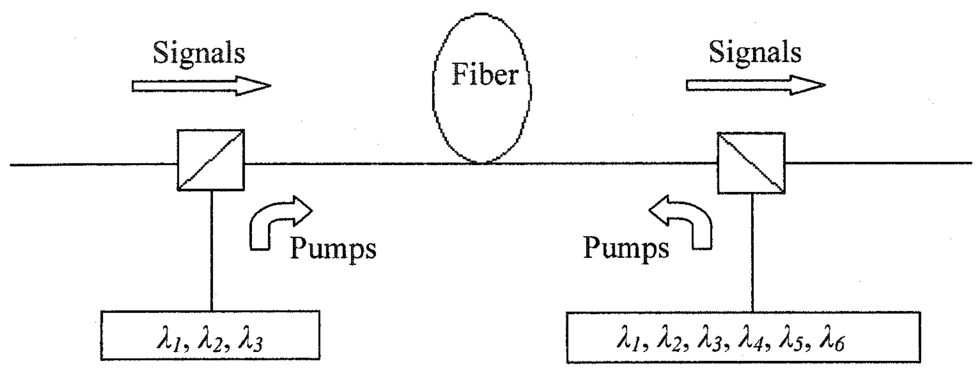

Fig. 2-3 Noise-flattening pump configuration. $\lambda_2 > \lambda_1, \lambda_3 > \lambda_2,$ **etc…**

The third primary noise source is Double-Rayleigh Scattering (DRS). Forward Rayleigh scattering has no overall effect on the amplifier since the photon is scattered in the same direction as it was originally propagating in, and with negligible (femtosecond) delay. On the other hand, Rayleigh backscattering gives rise to a coherent signal propagating in the reverse direction of the original signal but with the same frequency. DRS arises when photons from this counter-propagating signal Rayleigh backscatter and once again propagate in the original signal direction. Depending on when the two scattering events occur, a certain delay will be introduced in these DRS photons and therefore they will appear as noise at the receiver. In [5], DRS is said to limit the gain obtainable by any single-stage FRA to 15 dB. Using multiple gain stages optically isolated from one another is a well-known means of reducing the DRS noise, as the counter-propagating wave is eliminated at mid-stage. This is shown in [16], where a method of measuring the DRS is examined and applied to both a single-stage and dual-stage design. In [13], a gain of 30 dB with acceptable bit-error rate (BER) was obtained using a dual-stage FRA design. In [14], where a filter was used to flatten the gain spectrum (the gain spectrum was not initially flat since only two pumps were employed), it was shown that an amplifier with such a loss element placed in the gain fiber may also exhibit lower Rayleigh noise than an amplifier with the same net gain but with no loss element.

Finally, there is a noise source that arises from the short upper-state lifetime of Raman amplification. The nearly instantaneous gain may lead to a coupling of pump fluctuations to the signal. Launching the pump counter-propagating to the signal has the effect of introducing an effective upper-state lifetime equal to the transit time through the fiber [5], which mitigates this noise. If the pumps co-propagate with the signals, extreme pump power stability is required.

2.3 Polarization Dependence of Raman Gain

The Raman gain coefficient is strongly polarization dependent; it can be up to ten times higher when the signal and pump are co-polarized than when they are orthogonally-polarized [20]. However, the polarization-dependent gain (PDG) in actual systems strongly depends on the Polarization Mode Dispersion (PMD) of the fiber. The PMD usually scrambles the states of polarization (SOP) of the pumps and signals in different ways over the interaction length, and therefore in fibers with higher PMD, the gain's dependence on polarization is lower [20]-[21]. Using a counter-propagating scheme also has the effect of minimizing the correlation between the SOP of the pumps and signals. In [21], counter-propagation of the pump reduced the PDG to nearly zero, see Fig. 2-4.

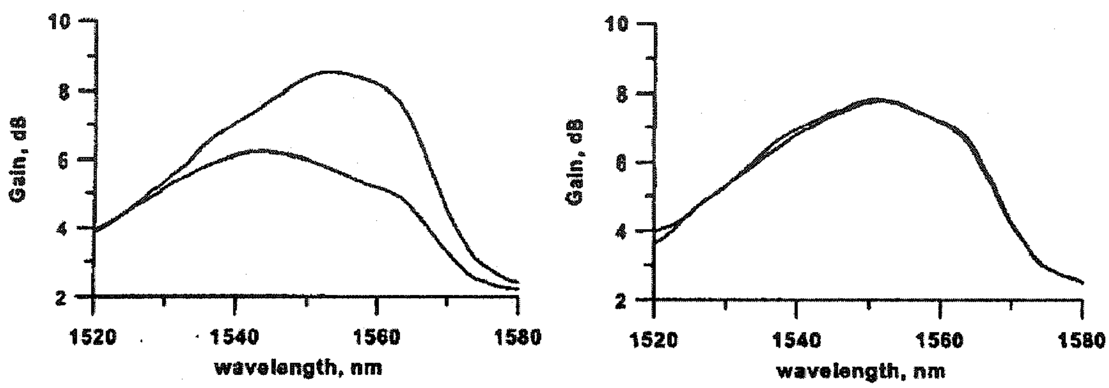

Fig. 2-4 Raman gain provided to signal at 1552 nm over 15 km of DCF fiber, pumped at 1452 nm co-propagatevely (left) and counter-propagatevely (right). In each case, the curves represent the gain for orthagonal pump polarizations. [21]

2.4 Enabling Technologies for FRAs

Raman amplification in optical fibers was first observed in the 1970's by Stolen and Ippen [31] though the phenomenon remained mostly a laboratory curiosity until 1985 when successful experiments were carried out by Aoki et al. [33]. It was applied by Mollenauer et al. in optical soliton transmission. At this time, however, obtaining sufficient gain required several hundred milliwatts of pumping power, and there was no alternative to solid-state lasers [35]. Research on Raman amplifiers was overshadowed by the advent of the EDFA, which provided the required functionality (gain) for single-channel optical systems using only a few milliwatts of pump power. But by the early

2000s, practically every ultralong-haul (over 800 km) and long-haul (300 to 800 km) transmission system employed Raman amplification [5]. This emergence of the FRA was motivated by the need to improve spectral efficiency, but was enabled by technological advances in three main areas [5]: high-powered pump laser diodes, fiber optic components and optical fibers for efficient Raman gain.

Perhaps the most significant development that led to the commercialization of FRAs was in the area of high-powered 14xx pump laser diodes, currently available in excess of 500 mW [4]. These lasers have sufficient compactness, power, wavelength stability and reliability to be incorporated into commercial systems. There are three main sources of noise that are associated with the pumps, which must be dealt with: stimulated-Brillouin scattering (SBS), relative-intensity noise (RIN) and mode-partition noise (MPN). FBG-stabilized laser diodes (FBG-LDs) have a broad linewidth, which results in very low SBS and MPN but in high RIN. Distributed feedback laser diodes (DFB-LDs), which have narrow linewidth, have high SBS but low RIN and MPN. Finally, Fabry-Perot (FP) lasers, which have many narrow linewidth modes have high RIN and MPN but maintain low SBS. Inner-grating multi-mode lasers (IGMs), are specifically tailored for Raman applications, and achieve an optimum tradeoff between the above mentioned noise sources [4].

Second, fiber-optic components that replace bulk-optics, such as wavelength division multiplexers (WDM) are now readily available for splicing into all-fiber systems. This enables a practical system to be built which is cost-effective and much less sensitive to environmental conditions.

Finally, fibers which have a higher effective Raman gain coefficient but that maintain relatively low loss are now available. The effective Raman gain coefficient is defined in Equation 2-3. The Raman gain coefficient g_R is related to the fiber's intrinsic characteristics (material composition) while A_{eff} refers to the confinement of the mode-field. For higher g_R there is greater Raman interaction over a given area, and by reducing the mode size, the interaction is more confined and therefore more efficient.

$$g_{R(eff)} = \frac{g_R}{A_{eff}} \qquad \textbf{(Equation 2-3)}$$

Dispersion Compensating Fiber (DCF) offers a 10-fold increase in the effective Raman gain coefficient compared to standard Single-Mode Fiber (SMF). Part of this increase is attributed to the effective area (approximately 23 μm^2 for DCF versus 85 μm^2 for SMF), while the rest of the increase is due to the intrinsic properties of the fiber. HNLF is designed specifically to achieve high Raman gain. Table 2-1 compares the parameters of SMF, dispersion shifted fiber (DSF), and four types of HNLF [4]. This is especially significant for the development of DFRAs: if high-gain fiber with low loss is available, shorter fiber lengths may be used to achieve higher gains and lower NF. Fig. 2-5 plots the effective Raman gain parameter versus pump-to-signal frequency separation for typical SMF, DSF, DCF and commercially available HNLF. Research in this area is ongoing: new potential technologies that could lead to an increase in g_R and a decrease in A_{eff} include holey fibers and bi-doped HNLFs [4].

	SMF	DSF	HNLF-A	HNLF-B	HNLF-C	HNLF-D
Attenuation coefficient (dB/km)	0.20	0.21	0.83	0.37	0.41	1.16
A_{eff} (μm^2)	80	50	12.0	14.2	14.6	9.7
Nonlinearity ($W^{-1}km^{-1}$)	1.3	2.7	17.5	12.9	12.6	25.1

Table 2-1 Attenuation, effective area and nonlinearity parameters for six different fiber types.

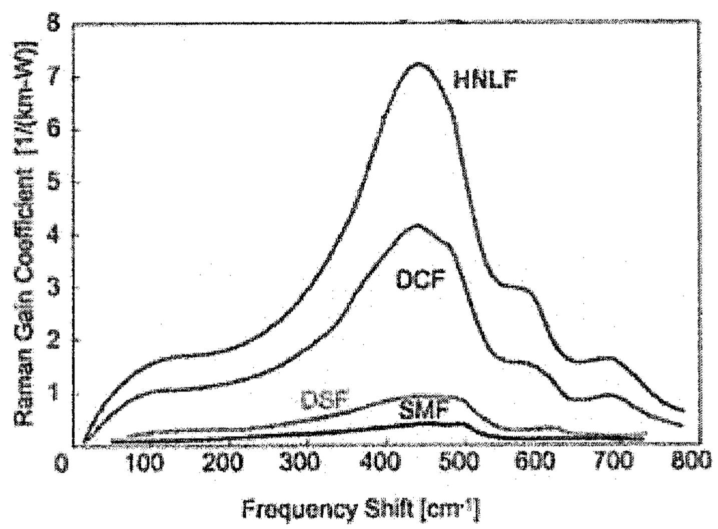

Fig. 2-5 Effective Raman Gain Coefficients for different fiber types. [36]

3.0 The Steady-State Raman Model

3.1 The Small-Signal Model

In the small-signal regime where pump depletion due to signal gain is neglected, the evolution of the signal and pump power levels may be described as in Equation 3-1 below, where P_p represents the pump power, P_s is the signal power, z is the distance, g_R / A_{eff} is the effective Raman gain coefficient, λ is the pump wavelength, and α_s and α_p are the attenuation coefficients at the signal and pump wavelengths, respectively [1].

$$\frac{dP_s}{dz} = \frac{g_R}{\lambda \cdot A_{eff}} P_p P_s - \alpha_s P_s \qquad \textbf{(Equation 3-1)}$$

$$\frac{dP_p}{dz} = -\alpha_p P_p$$

The signal is assumed to receive gain from the pump and loss from fiber attenuation, while the pump is assumed to experience loss only due to fiber attenuation. This simplified model may be used to extract an estimate of the effective Raman gain coefficient of a particular fiber, given the gain, the propagation distance, the attenuation coefficients, the wavelengths and the powers of the pump and signal.

3.2 The Full Model

In order to accurately analyze the steady-state behavior of an FRA, including gain-clamping behavior, a model that can accommodate multiple pumps, DWDM signals, ASE noise, and lasing signals is needed. This model assumes that the pumps, the DWDM signals and the lasing signals have an infinitesimally narrow bandwidth, while the ASE noise signals have a defined bandwidth or resolution 'Δv', as shown in Fig. 3-1. Accuracy is improved with smaller noise resolution. The frequency of each ASE signal is taken to be the center of each rectangle in Fig. 3-1.

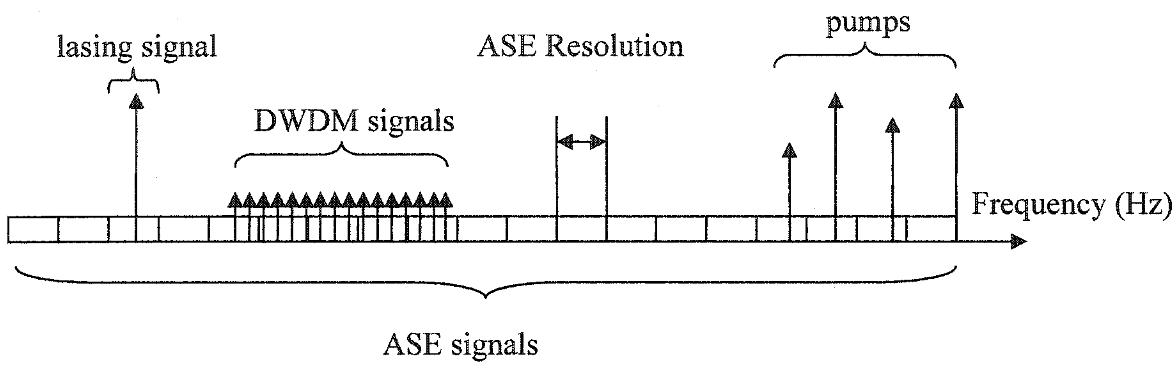

Fig. 3-1 The four different signal types in the full model.

The power evolution of each signal follows Equation 3-2, except that the fifth term of this equation applies **only to ASE signals**:

$$\frac{dP_v^{\pm}}{dz} = -\alpha_v P_v^{\pm} + \varepsilon_v P_v^{\mp} + P_v^{\pm}\sum_{\mu>v}\frac{g_{\mu v}}{A_\mu}(P_\mu^+ + P_\mu^-) - P_v^{\pm}\sum_{\mu<v}\frac{v}{\mu}\frac{g_{v\mu}}{A_v}(P_\mu^+ + P_\mu^-)$$

$$+2hv\sum_{\mu>v}\frac{g_{\mu v}}{A_\mu}\cdot(P_\mu^+ + P_\mu^-)\cdot\left[1+\frac{1}{\exp\left[\frac{h(\mu-v)}{kT}\right]-1}\right]\cdot\Delta v$$

$$-4hvP_v^{\pm}\sum_{\mu<v}\frac{g_{v\mu}}{A_v}\cdot\left[1+\frac{1}{\exp\left[\frac{h(v-\mu)}{kT}\right]-1}\right]\cdot\Delta v \qquad \text{(Equation 3-2)}$$

Subscripts μ and v denote optical frequencies, α_v is the attenuation coefficient at frequency v, ε_v is the Rayleigh-backscattering coefficient, A_v and A_μ are the effective areas at frequency v and μ respectively, k is the Boltzmann constant, T is temperature and $g_{\mu v}$ is the Raman gain parameter at frequency v due to a pump at frequency μ. The physical significance of each term in Equation 3-2 is described in Table 3-1.

Term	**Physical Significance**	**Impact on P_v**
1	Fiber attenuation	Loss
2	Double-Rayleigh backscattering	Gain
3	Raman interaction with higher frequency signals	Gain
4	Raman interaction with lower frequency signals	Loss
5	ASE generated at this signal frequency, by higher frequency signals (applies to ASE signals only)	Gain
6	ASE generated by this signal, at lower frequencies	Loss

Table 3-1 Physical significance of terms in Equation 3-2.

Each signal has a forward and backward propagating wave, denoted in Equation 3-2 by superscripts + and – respectively. The forward and backward propagating waves interact with each other via Rayleigh backscattering. The overall number of coupled equations is equal to twice the number of signals being modeled, e.g. for a system with 5 pumps, 50 DWDM signals, ASE signals spaced from 1500 to 1600 nm with a resolution of 100 GHz, and 1 lasing signal, there are a total of 362 coupled equations to be solved.

In order to completely specify the system, boundary conditions also need to be defined. Table 3-2 summarizes the boundary conditions used for the different signal types. It is important to note that the pumps and DWDM signals may be arbitrarily and independently chosen to enter the amplifier from either end, e.g. assuming the fiber extends horizontally, the pump and the signal may be chosen to enter either from the left (at $z = 0$) or from the right (at $z = L$).

Signal Type	**Direction**	**Boundary Value**	**Boundary Location**
Pump	Forward (+)	Input to system	$Z = 0$ or L
Pump	Backward (-)	0	$Z = 0$ or L (opposite of above)
DWDM Signal	Forward (+)	Input to system	$Z = 0$ or L
DWDM Signal	Backward (-)	0	$z = 0$ or L (opposite of above)
ASE Noise	Forward (+)	0	$z = 0$
ASE Noise	Backward (-)	0	$z = L$
Lasing Signal	Forward (+)	[Lasing Signal (-) at $z = 0$] * R_1	$z = 0$
Lasing Signal	Backward (-)	[Lasing Signal (+) at $z = L$] * R_2	$z = L$

Table 3-2 Boundary condition definitions. R_1 and R_2 are the reflectivities of FBG_1 (located at $z = 0$) and FBG_2 (located at $z = L$) respectively, see Fig. 1-5 (b).

The NF is defined below in Equation 3-3 [12]. The first term is a result of the **shot-noise** while the second term accounts for the ASE generated in the FRA.

$$NF = \frac{1}{G} + \frac{P_{ASE}}{G \cdot h \cdot \nu \cdot \Delta\nu} \qquad \textbf{(Equation 3-3)}$$

3.3 The Simulation Program

3.3.1 Selecting the Appropriate Solver

A computer program was created to implement the full steady-state FRA model described in the previous section. At the heart of this program is the Matlab© library function bvp4c™, which is a boundary-value problem solver for ordinary differential equations (ODEs) based on the **relaxation method**. In this method, the ODEs are replaced by approximate finite-difference equations on a mesh of points that span the amplifier length [3]. These mesh points are optimally selected by the solver for the quickest convergence time, and they are not necessarily uniformly spaced. The relaxation method converges much more slowly than another type of boundary-value problem ODE solver known as the **shooting method**, but it is preferred since it converges for a wider range of input conditions. More specifically, when the solution is as shown in Fig. 3-2, the shooting method cannot converge. In this figure, the pumps are counter-propagating (right to left), and so the left boundary is unknown. The 1450 nm and 1480 nm pumps are completely depleted (i.e. have no power remaining) at the point $z = 1500$ m, and therefore the correct value at the left boundary should be close to zero. The shooting method works by making a guess at the unknown boundary, solving the signals in the forward direction (left-to-right), verifying the solution at the known boundary and then refining the guess. This is repeated until the solution agrees with the known boundary condition. The shooting method does not work in this case since the initial guess needs to be very close to zero; when making even a very small refinement to a near-zero guess, the obtained solution at the known boundary changes drastically. On the other hand, the relaxation method, which works by making guesses over all of the mesh points and not just at the unknown boundary, can easily handle this case. The result is said to relax to the true solution [3].

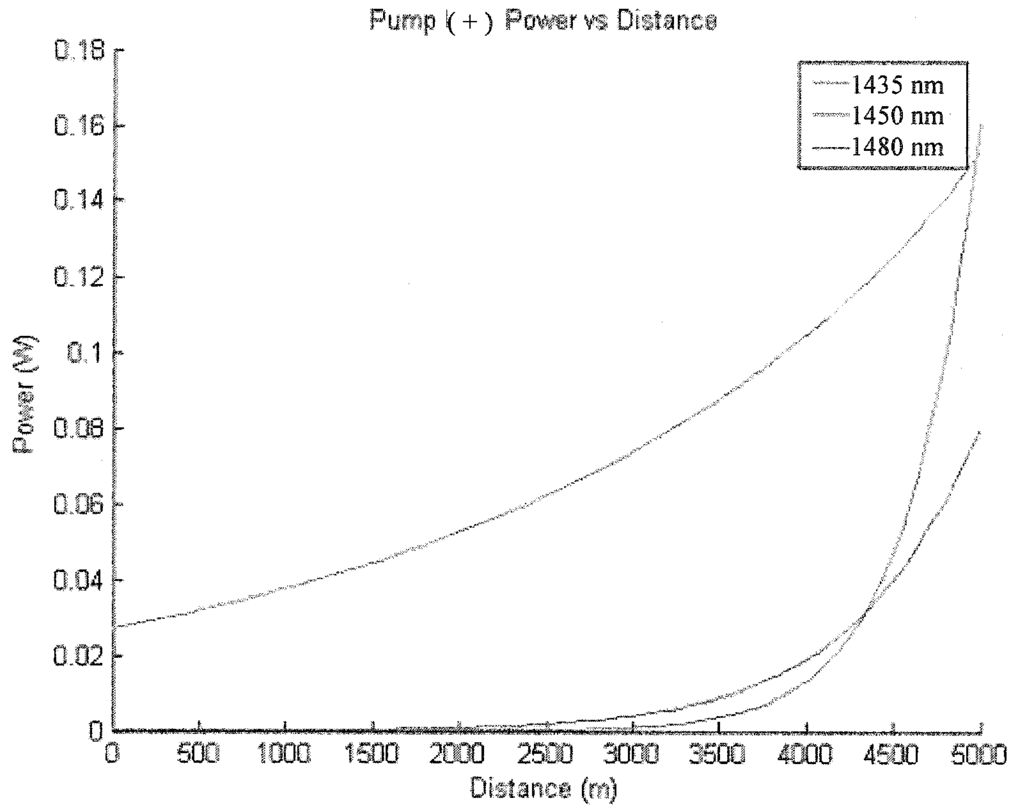

Fig. 3-2 Solution for which relaxation method converges, but shooting method does not.

3.3.2 Amplifier Parameters

In this section, the fixed amplifier parameters which are used to obtain the simulated results in this thesis are defined. This includes the temperature T, the noise resolution Δv and the fiber parameters (attenuation coefficient α, Rayleigh-backscattering coefficient ε and effective Raman gain parameter g_R / A_{eff}).

Effective Raman gain parameter g_R / A_{eff}:

The effective Raman gain spectrum that was used in the simulations is shown in Fig. 3-3 and has a peak value of approximately $6 \cdot 10^{-3}$ [$m^{-1} \cdot W^{-1}$] at a frequency shift of 14.5 THz, which is typical of commercially available HNLF (see Fig. 2-5).

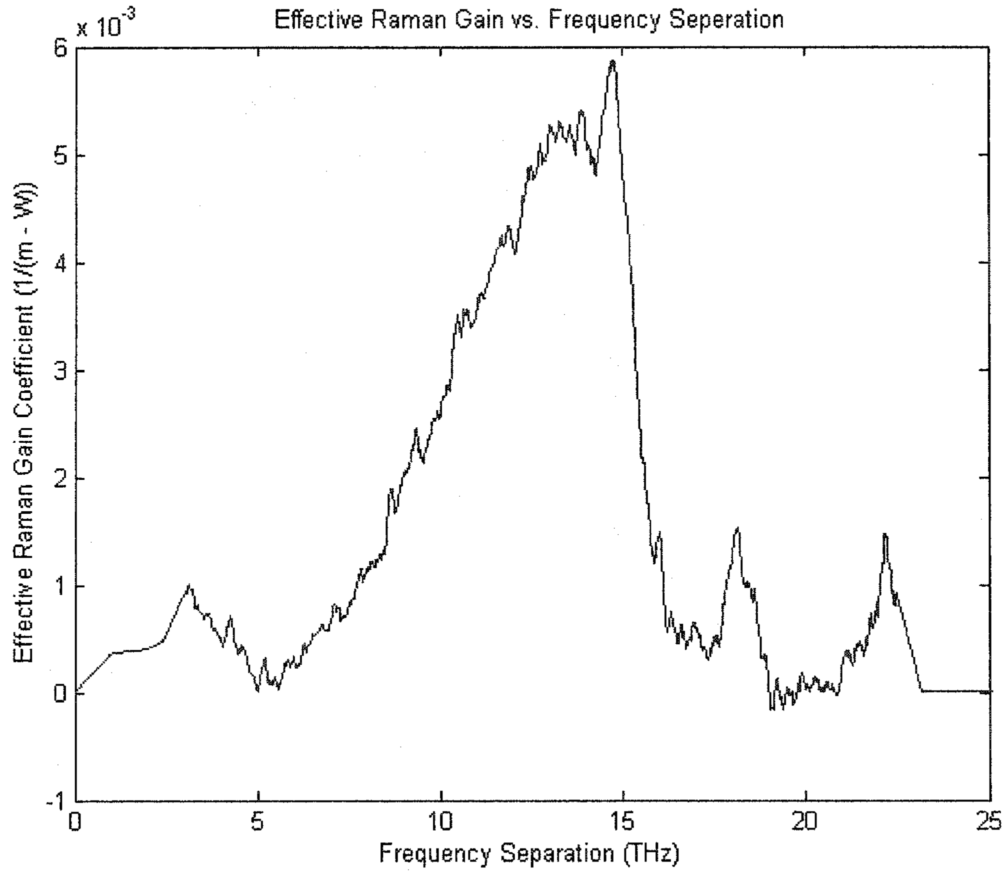

Fig. 3-3 Effective Raman gain parameter used in simulation program. Typical of commercially available HNLF.

Attenuation Coefficient α:

The attenuation coefficient shown in Fig. 3-4 was used, which roughly corresponds to the loss in certain HNLF.

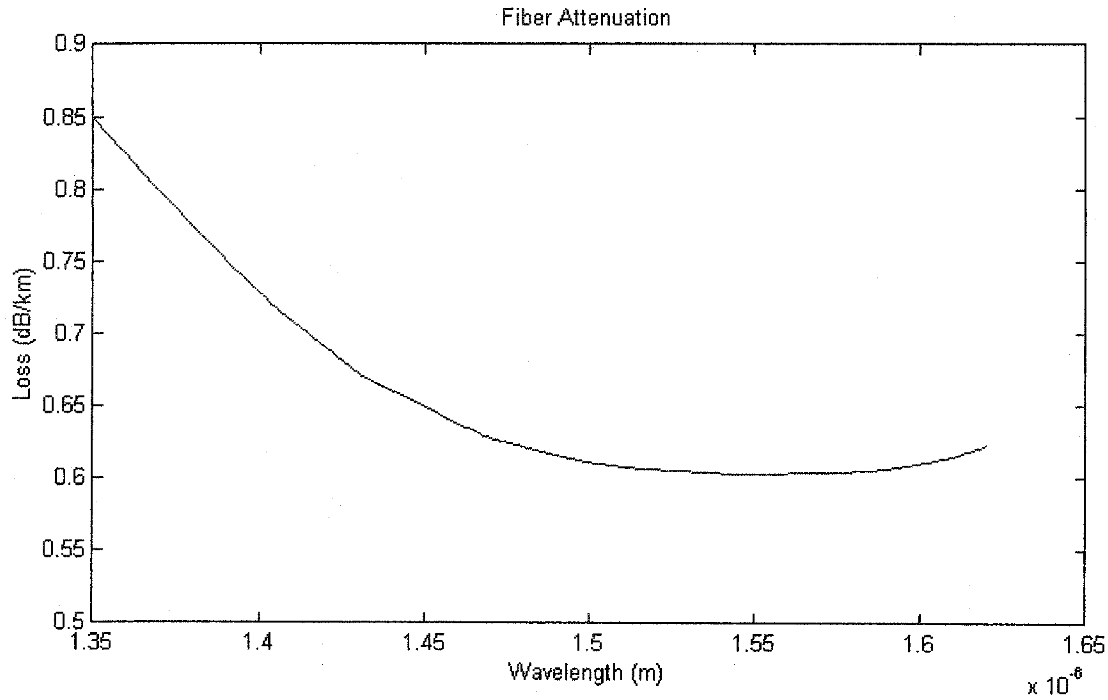

Fig. 3-4 Attenuation spectrum, typical of certain types of HNLF

Rayleigh backscattering coefficient ε:

The Rayleigh backscattering coefficient was assumed constant for all wavelengths:

$\varepsilon = 1\times10^{-7}m^{-1}$.

Temperature *T*:

The temperature was set to 300 Kelvin for all simulations, approximately room temperature. The physical effect most sensitive to temperature is the thermal noise, which is evident from Equation 3-2.

Noise Resolution Δv:

There is a tradeoff between the accuracy of the noise power calculation and the convergence time. It was shown that the results obtained using Δv = 200 GHz were approximately equivalent to the results obtained using Δv = 100 GHz, and the convergence time was much shorter (using the same computer, the convergence time was under an hour per full simulation with $\Delta\nu = 200$ GHz, while it is over four hours for $\Delta\nu = 100$ GHz). Therefore all of the simulations were performed using a noise resolution of 200 GHz. In order to obtain the noise power for a specific DWDM signal (required to calculate NF), a data extrapolation was used.

3.3.3 Amplifier Input Conditions

The amplifier input conditions are given in this section. The only unknown inputs (which are to be optimized) are the wavelength and reflectivities of the FBGs.

Fiber Length

A 5000 meter fiber length was used.

Pump Wavelengths and Powers

The pumps were located at 1435 nm, 1450 nm and 1480 nm, with input powers of 200 mW, 200 mW and 300 mW respectively. Although this does not result in a perfectly flat gain spectrum, the analysis presented in this chapter also applies to a gain-flattened system. In fact, it will be shown below that in an optimal GC-DFRA, the gain-flattening design may be performed prior to the gain-clamping design, since the addition of the feedback lasing signal should not affect the gain spectrum shape of the amplifier.

DWDM Signal Wavelengths and launch powers

The wavelength range for the DWDM input signals was chosen in accordance to the high-gain region (within 9 dB of the peak gain). As such, a total of 71 signals were spaced at 100 GHz from 1540 to 1598 nm. The total launch power was uniformly distributed amongst the signals, whereas in a practical system, this may generally not be the case. Although this could potentially have a small influence on the overall performance of the amplifier (even though pump-to-pump and pump-to-feedback signal interactions are strongest by far), we maintain this assumption for simplicity.

In certain simulations, the total input signal power was varied -15 dBm to + 15 dBm in increments of 3 dB. This translates into a range of individual signal launch powers of approximately -33 dBm to -3 dBm, which is typical of optical communications networks. Often mentioned in the analysis that follows is the **small-signal** behavior of the amplifier, or the unsaturated behavior; this refers to a total input signal power of -15 dBm (-33 dBm per signal).

Pump and signal directions:

The counter-propagating amplifier configuration was considered in this thesis. The DWDM signals propagated from left-to-right and the pumps from right-to-left. Using the notation for the forward (+) and reverse (-) waves described in Section 3.2, DWDM signals (+) travel from left-to-right, DWDM signals (-) from right-to-left, pumps (+) from right-to-left, and pumps (-) from left-to-right.

ASE noise band:

Also chosen in accordance with the high-gain band of the amplifier, the ASE noise band is taken to be from 1520 nm to 1620 nm. The noise is assumed to be zero outside this band. The simulation program also allows the noise calculation to be disabled, which reduced the convergence time of each simulation to less than ten minutes. It was found that the ASE has a small (but not negligible) effect on the gain results so that if only an estimate of the gain was required, then the simulation was performed without ASE.

4 Simulation Analysis of the GC-DFRA

4.1 Overview

Using the computer simulation program, the behavior of the GC-DFRA shown in Fig. 4-1 was analyzed. The main design objective was to obtain uniform gain-clamping behavior over the entire wavelength band being amplified, i.e. each DWDM signal should experience the same amount of clamping. For a given set of inputs (pump wavelengths and powers, fiber parameters, etc…), the design parameters are the reflectivity values for the two gratings, FBG_1 and FBG_2, denoted (R_1%, R_2%), and more importantly, the feedback signal wavelength λ_f. The ensuing analysis will demonstrate that the choice of λ_f determines the uniformity of the gain-clamping while the main role of the (R_1, R_2) parameters is only to control the gain-versus-critical power tradeoff. To this effect, once a feedback wavelength has been selected for analysis, the reflectivity parameters are varied in order to obtain the desired gain levels.

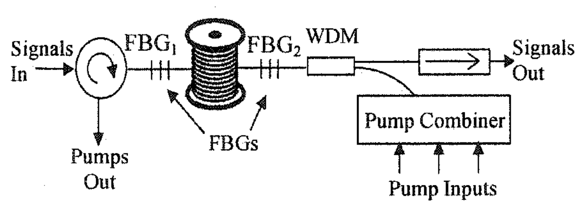

Fig. 4-1 Schematic of GC-DFRA.

The analysis is presented as follows. First, the performance of an unclamped system is demonstrated in Section 4.2 and the shortcomings of this system are discussed. In Section 4.3, the role that each pump has in providing gain is examined; this is of central importance for identifying appropriate wavelengths for λ_f. Section 4.4 analyzes a GC-

DFRA with λ_f set at 1595 nm, which gives insight as to where λ_f should be located to achieve uniform gain-clamping. This led to a set of criteria, given in Section 4.5, for systematically locating feedback wavelengths that meet the desired objectives. In Section 4.6, possible values for λ_f that could satisfy these criteria are examined, and two values are kept for a detailed analysis and are presented in Section 4.7. Since most of the analysis in this section is based on the gain characteristics, ASE is only included for the simulation of the unclamped amplifier in Section 4.2 and for the detailed analysis in Section 4.7.

4.2 The Unclamped Raman Amplifier

The gain and NF spectra of the unclamped DFRA are shown in Fig. 4-2 for a total input signal power ranging from –15 dBm to +15 dBm (in 3 dB increments).

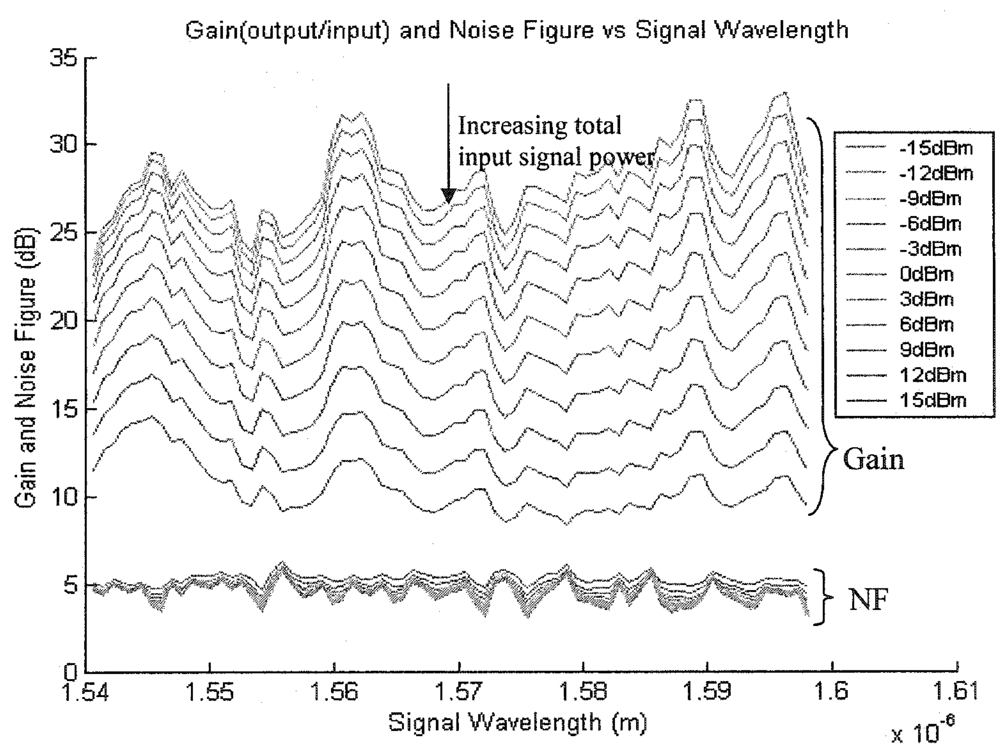

Fig. 4-2 Gain and noise figure spectra of the unclamped DFRA, with input signal powers varied.

It is evident that the gain is a strong function of the total input signal power. This is further highlighted in Fig. 4-3, where the gain and NF for a single DWDM signal at 1575.3 nm are shown as a function of total input signal power. Clearly, gain control is required to maintain the gain constant as the input signal power varies.

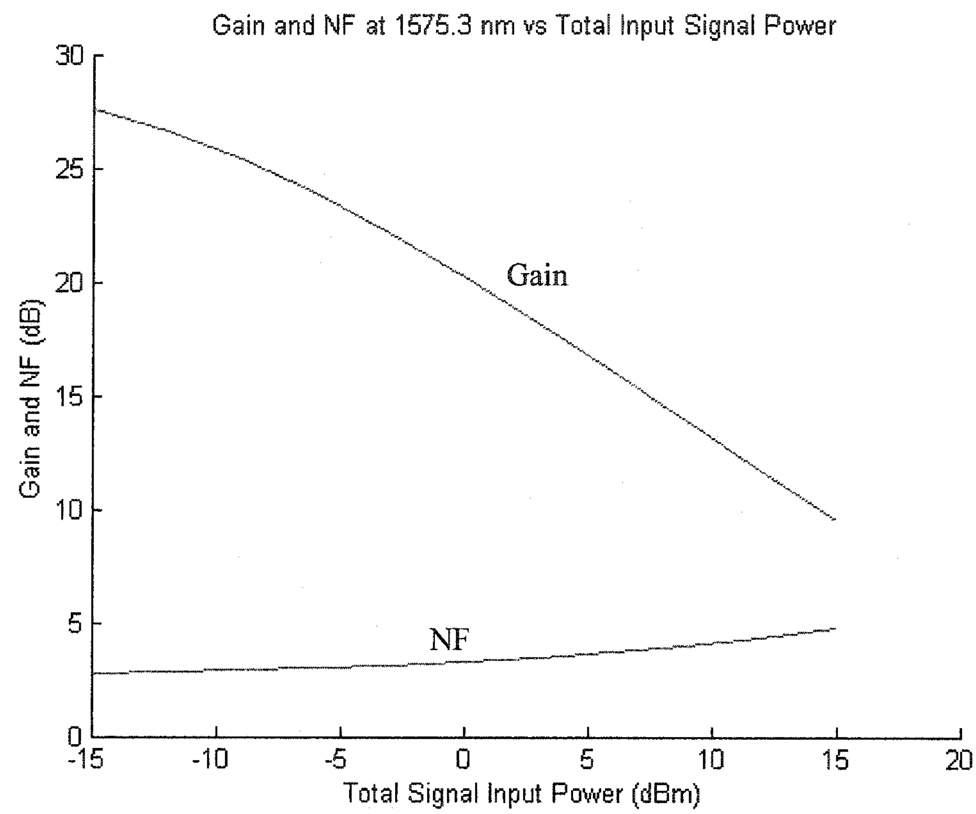

Fig. 4-3 The gain and the NF are strongly dependent on the total input signal power.

4.3 Role of the Pumps in the Unclamped Amplifier

A pump not only provides gain to the DWDM signals, but it also provides gain to other pumps at longer wavelengths (except for the longest wavelength pump, in this case the 1480 nm). Table 4-1 shows the role that each pump has in terms of its peak gain band (which begins at a 10 THz separation and ends at a 15 THz separation from the pump) and of the gain it provides to the other pumps.

Pump wavelength	Peak Gain Band	g_R / A_{eff} at 1450nm	g_R / A_{eff} at 1480nm
1435 nm	1510 to 1550 nm	$4.36 \cdot 10^{-4}$ [$W^{-1}m^{-1}$]	$4.20 \cdot 10^{-4}$ [$W^{-1}m^{-1}$]
1450 nm	1525 to 1565 nm	N/A	$6.15 \cdot 10^{-4}$ [$W^{-1}m^{-1}$]
1480 nm	1560 to 1600 nm	N/A	N/A

Table 4-1 Role of each pump in the amplification process.

As an example, we consider the 1435 nm pump. Fig. 4-4 demonstrates its effect on the gain spectrum. It has a direct effect on the signals from 1520 nm to 1555 nm, while from 1555 nm to 1600 nm, it provides gain mostly indirectly by pumping the 1450 nm and 1480 nm pumps. In fact, it does so evenly in this case (note in Table 4-1 that the gain coefficient from 1435 nm to 1450 nm and from 1435 nm to 1480 nm is almost the same), and so the gain spectrum in the wavelength range of 1555 nm to 1598 nm shifts up / down without changing in shape.

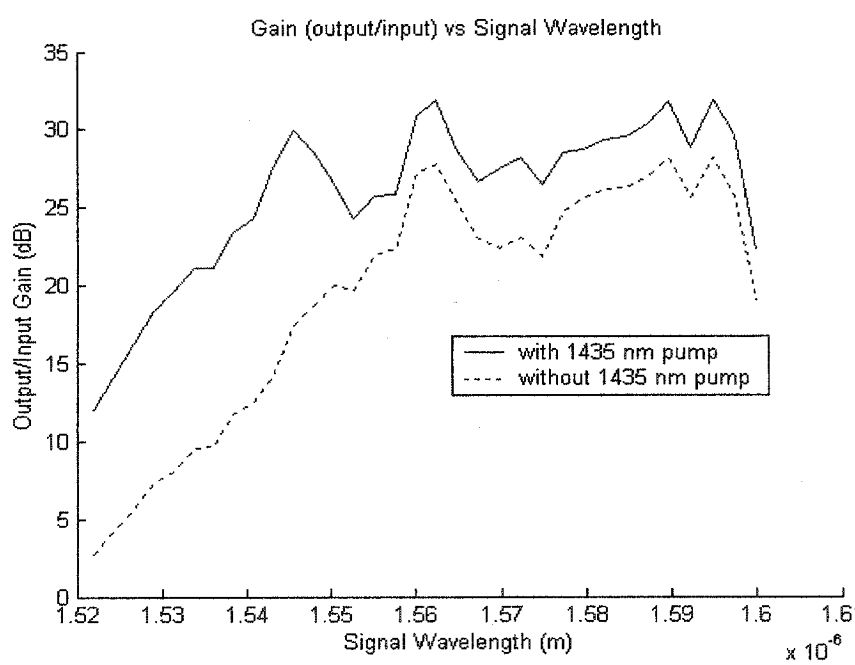

Fig. 4-4 Small-signal gain spectrum with and without the 1435 nm pump.

4.4 Performance of a GC-DFRA with Feedback at 1595 nm

In this section, a GC-DFRA with λ_f set at 1595 nm is studied. It will be shown that this choice of λ_f does not give the desired amplifier behavior, namely the gain-clamping performance is not uniform. Also note that the feedback signal is located directly in the DWDM signal band; in a practical system the cross-talk between the lasing signal and the DWDM signals would be a problem, but we ignore this effect for the purpose of our analysis. Fig. 4-5 contrasts the small-signal gain spectrum of the amplifier without and with the feedback signal at 1595 nm for *(R_1, R_2)* = (20%, 20%). For the GC-DFRA, the gain spectrum shape has been altered considerably compared to the unclamped DFRA, especially for signals at longer wavelengths.

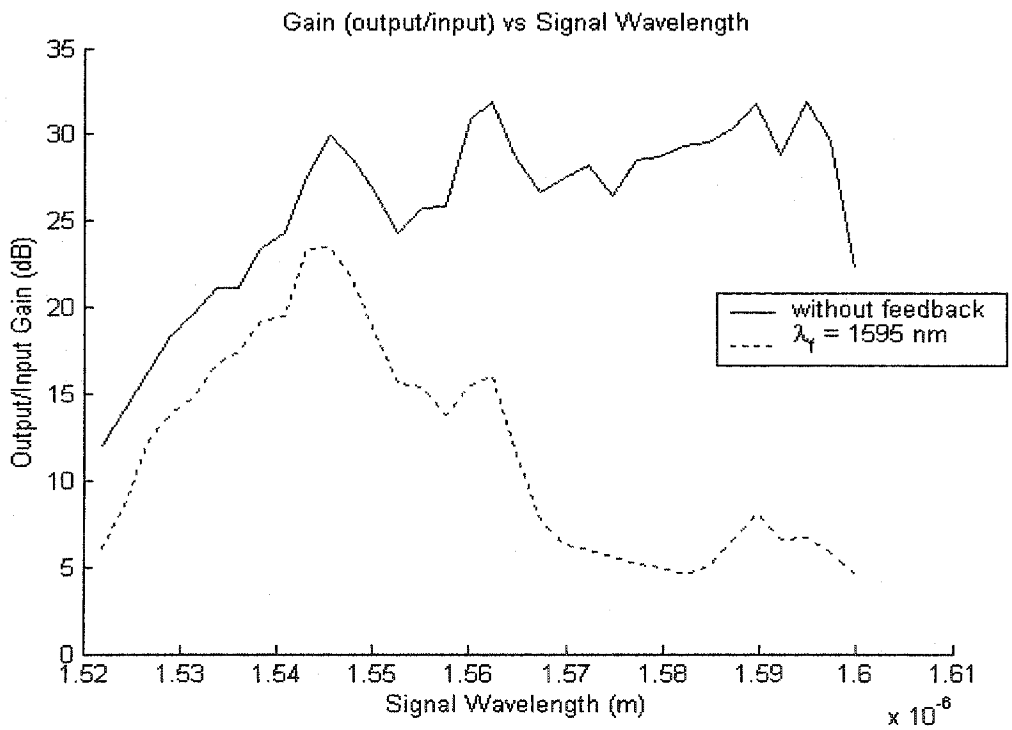

Fig. 4-5 Gain spectrum for no feedback and with a feedback signal at 1595 nm.

In order to understand why the gain spectrum is altered in this manner, it is intuitive to examine how the lasing signal affects the power of each pump. Fig. 4-6 shows the g_R / A_{eff} value that each pump has at the feedback wavelength. The 1480 nm pump is directly on the gain coefficient's peak ($g_R / A_{eff} = 5.67 \cdot 10^{-3}$ [$m^{-1} \cdot W^{-1}$]), while the other two pumps have near-zero coefficients ($g_R / A_{eff} = 0.33 \cdot 10^{-3}$ [$m^{-1} \cdot W^{-1}$] for the 1450 nm pump and $g_R / A_{eff} = 0.16 \cdot 10^{-3}$ [$m^{-1} \cdot W^{-1}$] for the 1435 nm pump). In the pump power evolution plots in Fig. 4-7, the 1480 nm pump is shown to be depleted very strongly in the presence of the feedback signal, while the other two pumps actually increase in power (this is because they now provide less power to the 1480 nm pump via pump-to-pump gain, since the 1480 nm pump is weaker). The drop in power in the 1480 nm pump explains the lower gain in the longer DWDM signal band.

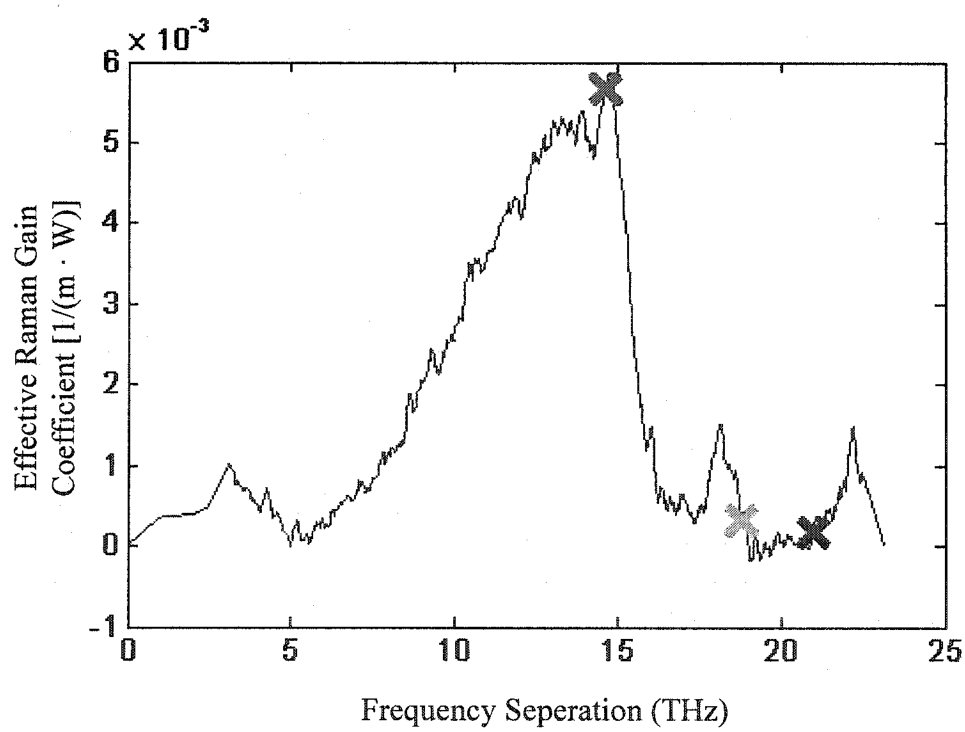

Fig. 4-6 Effective Raman gain coefficient values for pumps to feedback signal at λ_f = 1595 nm. 1435 nm pump (blue), 1450 nm pump (green), 1480 nm pump (red).

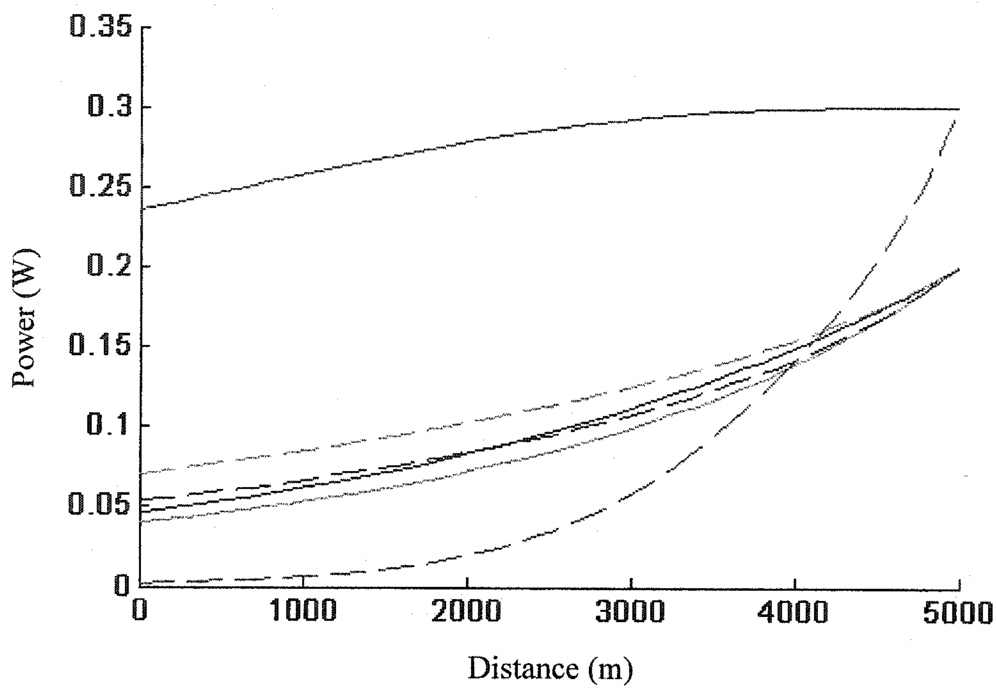

Fig. 4-7 Pump power evolution without (solid lines) and with feedback signal at λ_f = 1595 nm. 1435 nm pump (blue), 1450 nm pump (green), 1480 nm pump (red).

The gain spectra for different input signal powers are shown in Fig. 4-8. Gain-clamping is very strong for the longer DWDM band (the gain remains approximately constant even up to 15 dBm of total input power); however, it is less noticeable in the shorter DWDM band, and so the objective of uniform clamping is not met. This is further shown in the gain vs. input signal power plots in Fig. 4-9: the gain-clamping effect is much stronger for a signal at 1589.5 nm than for a signal at 1550.1 nm (but the gain is also lower).

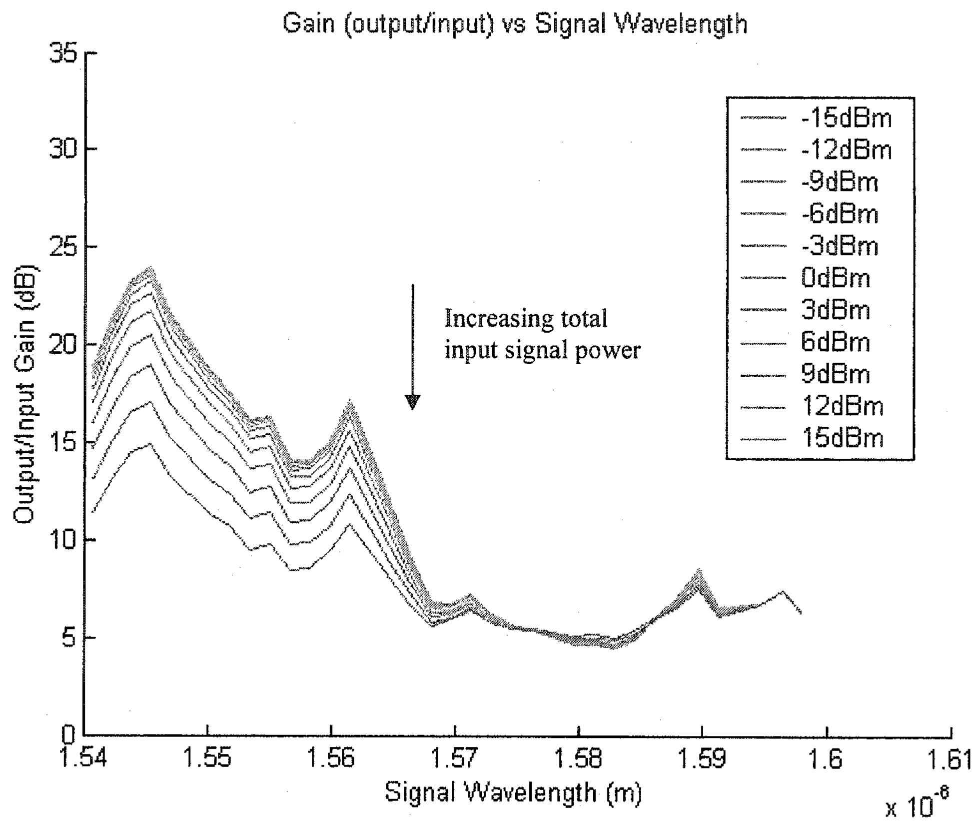

Fig. 4-8 Gain spectrum for feedback signal at 1595 nm with (R_1, R_2) = (20%, 20%). The total input signal power is varied from -15 to + 15 dBm.

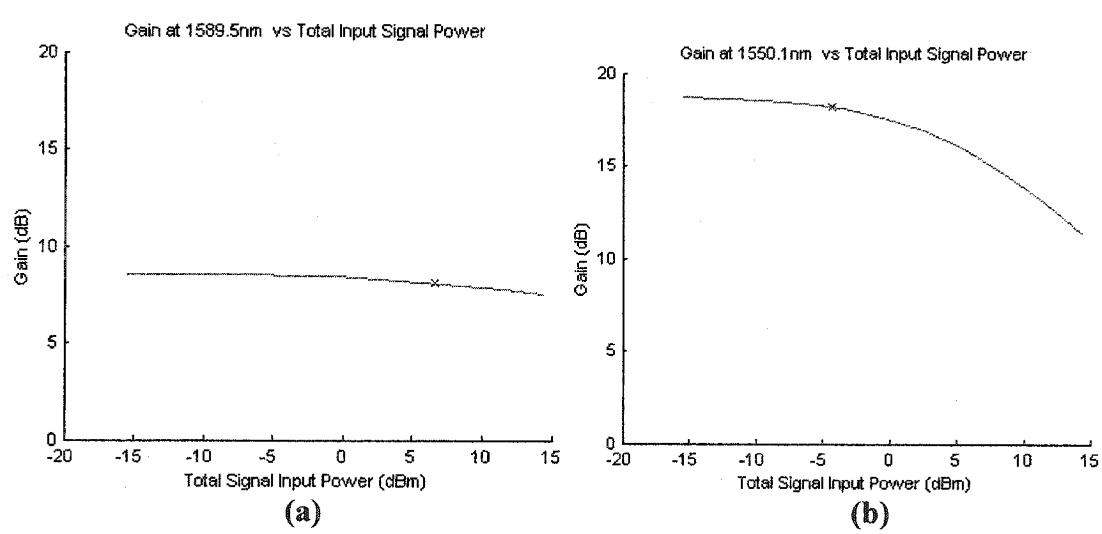

Fig. 4-9 Gain clamping is stronger in the long wavelength band (a) than in the shorter wavelength band (b). In each plot the 'x' indicates the critical power, defined in this thesis as a 0.5 dB decrease from the small-signal gain.

In summary, locating the feedback signal at 1595 nm is not ideal. First, the 1480 nm pump is depleted too strongly, resulting in low gain in the longer wavelength band. Also, the gain-clamping is very pronounced in this band (6.5 dBm critical power) while it is much more moderate for the lower wavelength signals (-5 dBm critical power). The analysis of this system gives us insight in establishing criteria for identifying locations for λ_f that could achieve uniform gain-clamping.

4.5 Criteria for Designing a Uniformly Gain-Clamped DFRA

Based on the results from the previous section, we can infer the following. For gain-clamping to be uniform, the feedback signal must be chosen so that the pumps are depleted in such a way that the gain spectrum shape is not altered from the unclamped case; instead, there is a uniform shift in the gain over the amplifier bandwidth. This is based on the observation that clamping is strongest for wavelengths corresponding to pumps which are depleted more strongly; thus for uniform clamping, there should be a uniform depletion of all pumps. Two important conclusions can now be drawn. First, to deplete the pumps more uniformly, the feedback wavelength should be located either above or below the high gain region. More importantly, by suitably locating the feedback wavelength, we have the desirable feature that the gain-flattening design process may be accomplished **separately** from the gain-clamping design process.

Direct or indirect depletion of the pumps by the feedback signal accounts for most of the change in the gain spectrum of a GC-DFRA (compared to the unclamped case). Direct depletion occurs when there is Raman gain directly between a pump and the feedback signal. Indirect depletion occurs when a pump provides gain to a second pump that is depleted directly by the feedback signal (via pump-to-pump interaction). Note that in the system being considered, the 1480 nm pump is at the longest wavelength and therefore it can only be depleted directly as it does not provide gain to any other pump.

4.6 Identification of Potential Feedback Signal Wavelengths

In Section 4.4, a feedback signal wavelength was arbitrarily chosen at 1595 nm and the performance of the amplifier was evaluated. In this section, the criteria established in Section 4.5 are used to arrive at first-pass designs of a uniform GC-DFRA.

The following three scenarios are considered: (1) the 1480 nm and 1450 nm pumps are depleted directly, (2) only the 1480 nm pump is depleted directly, and (3) the 1480 nm and 1435 nm pumps are depleted directly. The feedback wavelengths 1624.8 nm, 1662 nm and 1607 nm correspond respectively to these three scenarios, and also satisfy the criteria established in Section 4.5 (specifically, they result in a relatively uniform shift in the gain spectrum compared to the unclamped case). The analysis for each of these feedback wavelengths is presented in Sections 4.6.1, 4.6.2 and 4.6.3, respectively. A summary of their performance is given in Section 4.6.4.

4.6.1 $\lambda_f = 1624.8$ nm

As seen in the gain coefficient plot for a feedback wavelength of 1624.8 nm in Fig. 4-10, the effective Raman gain coefficients for the 1450 nm and 1480 nm pumps are almost equal and much lower than the peak ($g_R / A_{eff} = 1.32 \cdot 10^{-3}$ [$m^{-1} \cdot W^{-1}$] and $g_R / A_{eff} = 1.42 \cdot 10^{-3}$ [$m^{-1} \cdot W^{-1}$], respectively). For the 1435 nm pump, there is no direct power transfer to the lasing signal since g_R / A_{eff} is zero; however there is indirect transfer of photons to the feedback signal via the other two pumps (through pump-to-pump interaction), and therefore the 1435 nm pump is indirectly depleted by the feedback signal.

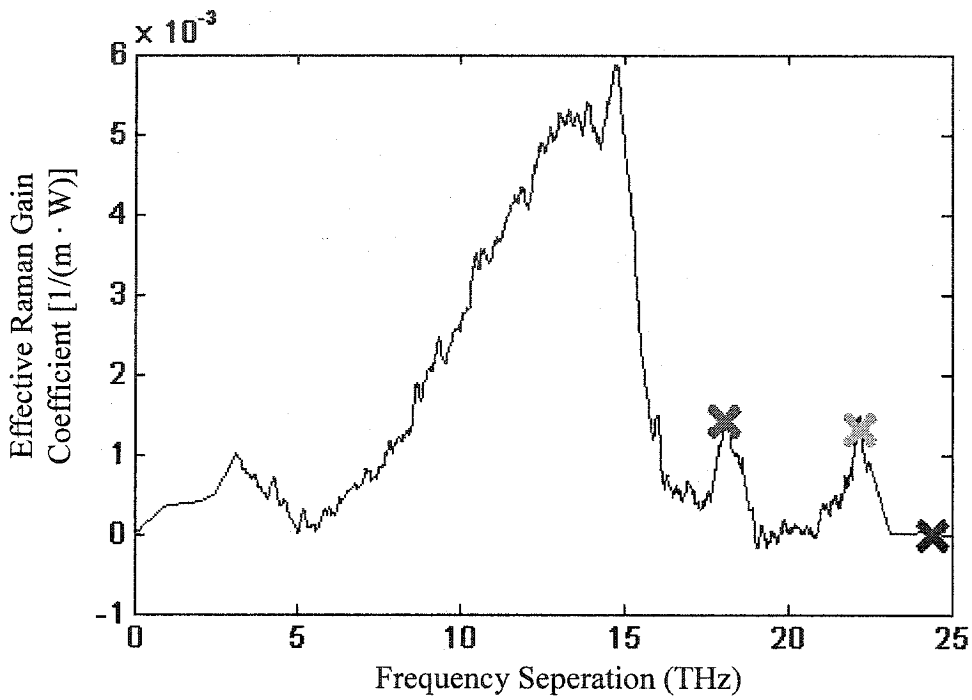

Fig. 4-10 Effective Raman gain coefficient values for pumps to feedback signal at λ_f = 1624.8 nm. 1435 nm pump (blue), 1450 nm pump (green), 1480 nm pump (red).

As shown in Fig. 4-11, the gain spectrum shape of the unclamped and clamped DFRAs [using λ_f = 1624.8 nm and (R_1, R_2) = (25%, 25%) and small-signal input power] are quite similar, with a maximum peak-to-peak variation in the gain, i.e. difference in amplifier gain with and without gain-clamping, of 3.3 dB (ideally this value should approach 0 dB difference). Since the pumps are uniformly depleted by the feedback signal, there is little change in the gain spectrum shape. Note that there is slightly stronger depletion in the lower and higher bands (gain difference is higher) and less depletion in the center band.

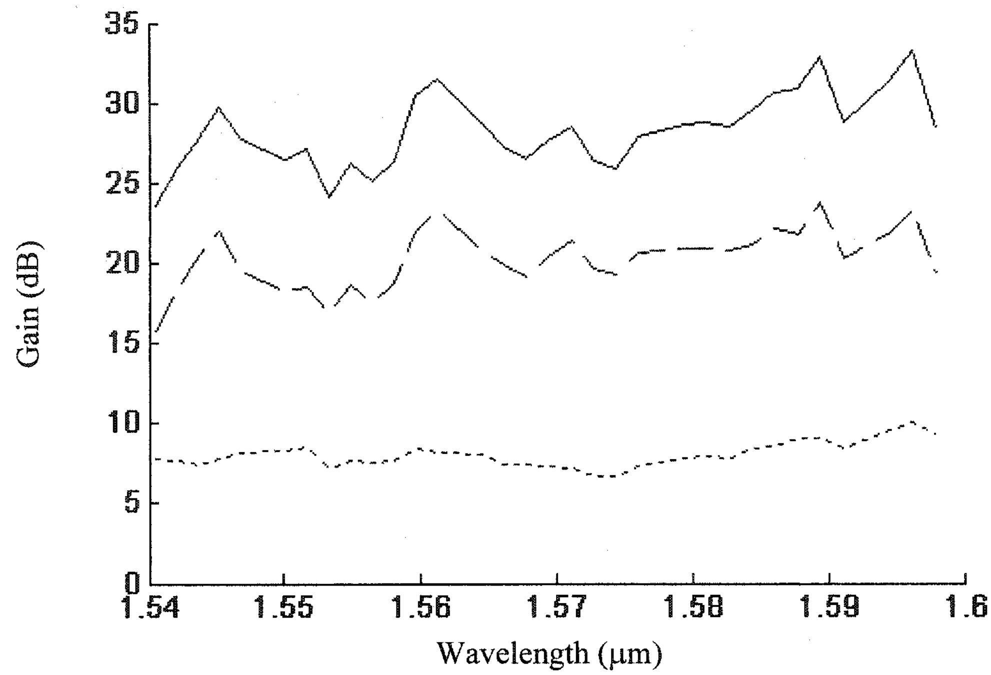

Fig. 4-11 Gain spectrum of DFRA without (solid line) and with (dashed line) feedback signal at λ_f = 1624.8 nm [(R_1, R_2) = (25%,25%)]. In both cases, the total input signal power is -15 dBm. The dotted line represents the gain difference.

The pump power evolution for this case is shown in Fig. 4-12. Comparing this with the pump power evolution for the case where λ_f = 1595 nm (see Fig. 4-7), we note that the amount of depletion of the 1450 and 1480 nm pumps is more even (there is now less depletion of the 1480 nm pump, and more of the 1450 nm pump). The 1435 nm pump has more power when the feedback signal is present than when it is not, which is again attributable to less pump-to-pump interaction due to the lower powers of the 1450 nm and 1480 nm pumps, which are depleted by the feedback signal.

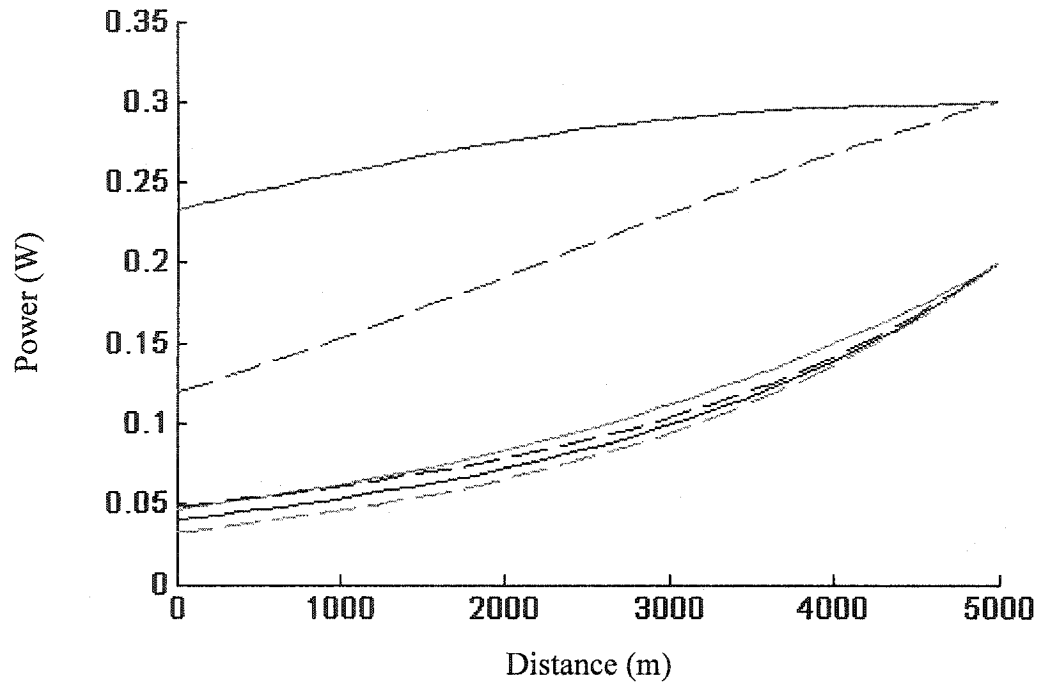

Fig. 4-12 Pump power evolution without (solid lines) and with (dashed lines) feedback signal at λ_f = 1624.8 nm. 1435 nm pump (blue), 1450 nm pump (green), 1480 nm pump (red).

4.6.2 λ_f = 1662 nm

When the feedback wavelength is set at λ_f = 1662 nm, only the 1480 nm pump interacts directly with the feedback signal with $g_R / A_{eff} = 1.47 \cdot 10^{-3}$ [$m^{-1} \cdot W^{-1}$], while both the 1435 nm and 1450 nm pumps interact only indirectly, as shown in Fig. 4-13. Again, as can be seen in Fig. 4-14, the gain spectrum shape of the unclamped and clamped DFRAs [using λ_f = 1662 nm and (R_1, R_2) = (35%, 35%)] are quite similar, with a gain difference variation of under 2.2 dB, owing to the uniform depletion of the pumps. Depletion is strongest in the center DWDM wavelengths.

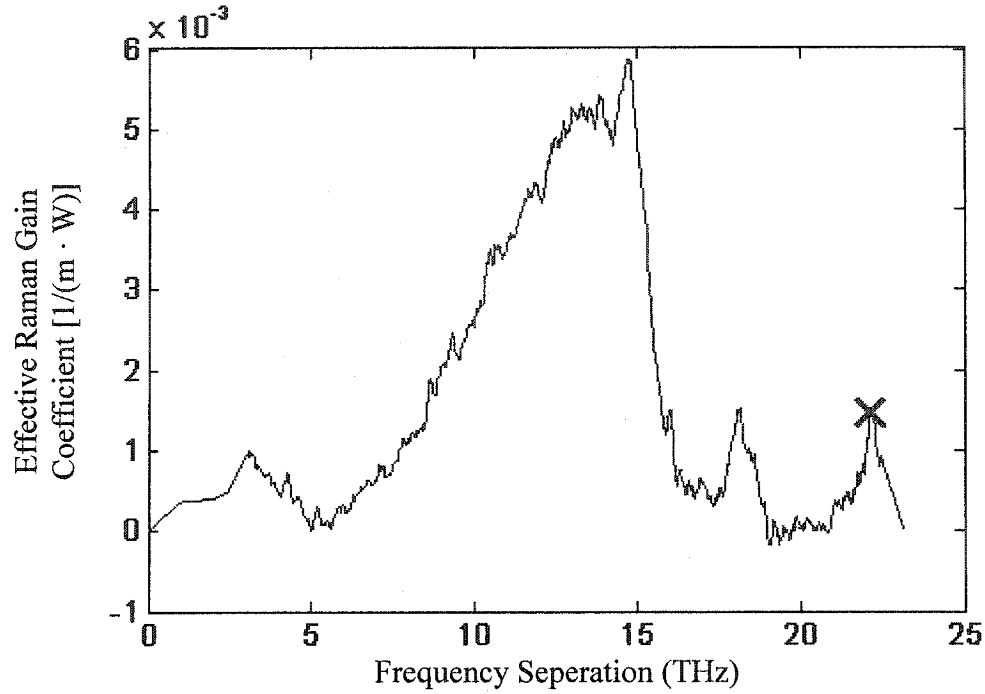

Fig. 4-13 Effective Raman gain coefficient values for pumps to feedback signal at λ_f = 1662 nm. Only the 1480 nm pump interacts directly with the feedback signal.

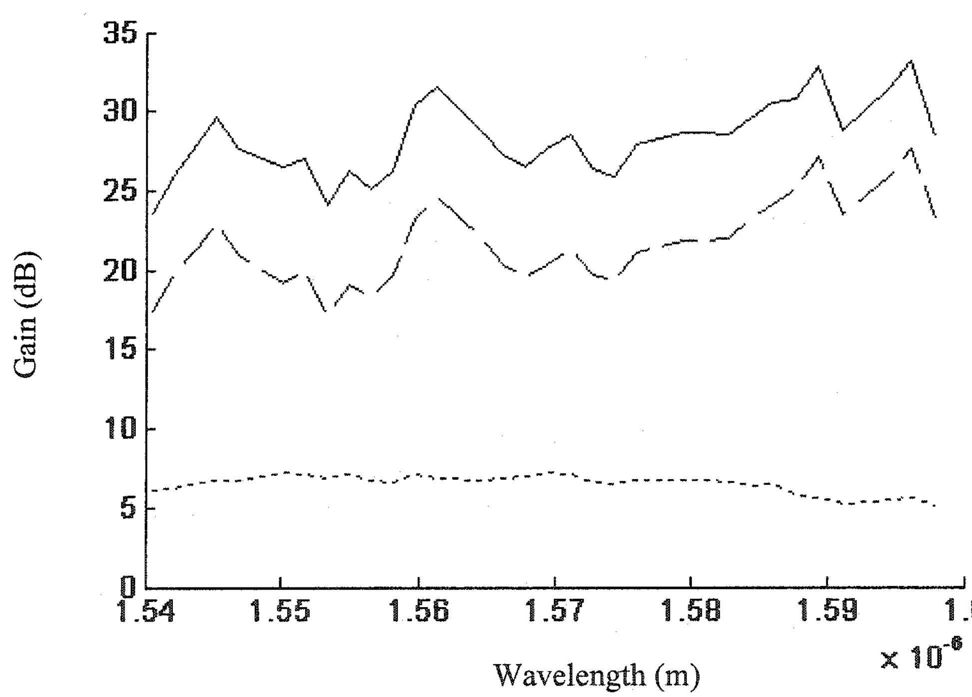

Fig. 4-14 Gain spectrum of DFRA without (solid line) and with (dashed line) feedback signal at λ_f = 1662 nm [(R_1, R_2) = (35%,35%)]. In both cases, the total input signal power is -15 dBm. The dotted line represents the gain difference.

4.6.3 $\lambda_f = 1607$ nm

When the feedback wavelength is set to $\lambda_f = 1607$ nm, the interaction with the feedback signal is direct for the 1480 nm pump ($g_R / A_{eff} = 1.45 \cdot 10^{-3}$ [$m^{-1} \cdot W^{-1}$]), mostly indirect for the 1450 nm pump ($g_R / A_{eff} = 0.11 \cdot 10^{-3}$ [$m^{-1} \cdot W^{-1}$]), and both direct and indirect for the 1435 nm pump ($g_R / A_{eff} = 0.94 \cdot 10^{-3}$ [$m^{-1} \cdot W^{-1}$]), as can be seen in Fig. 4-15.

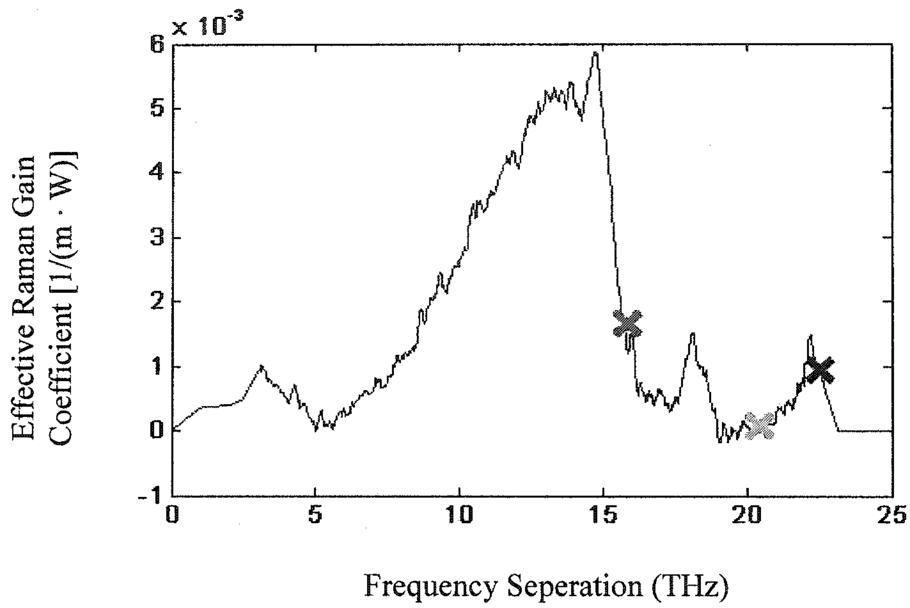

Fig. 4-15 Effective Raman gain coefficient values for pumps to feedback signal at $\lambda_f = 1607$ nm. 1435 nm pump (blue), 1450 nm pump (green), 1480 nm pump (red).

As shown in Fig. 4-16, there is a gain-tilt towards the longer band for a clamped amplifier with $\lambda_f = 1607$ nm and $(R_1, R_2) = (25\%, 25\%)$. The maximum variation in the gain difference between the unclamped and clamped amplifiers is 4.8 dB. In Fig. 4-17, the evolution of pump powers for $\lambda_f = 1607$ nm is contrasted with $\lambda_f = 1662$ nm (which was shown to result in more uniform depletion). As expected, the 1480 nm pump is weaker for $\lambda_f = 1607$ nm since it is depleted directly by the feedback signal and also receives less pump-to-pump gain from the 1435 nm pump.

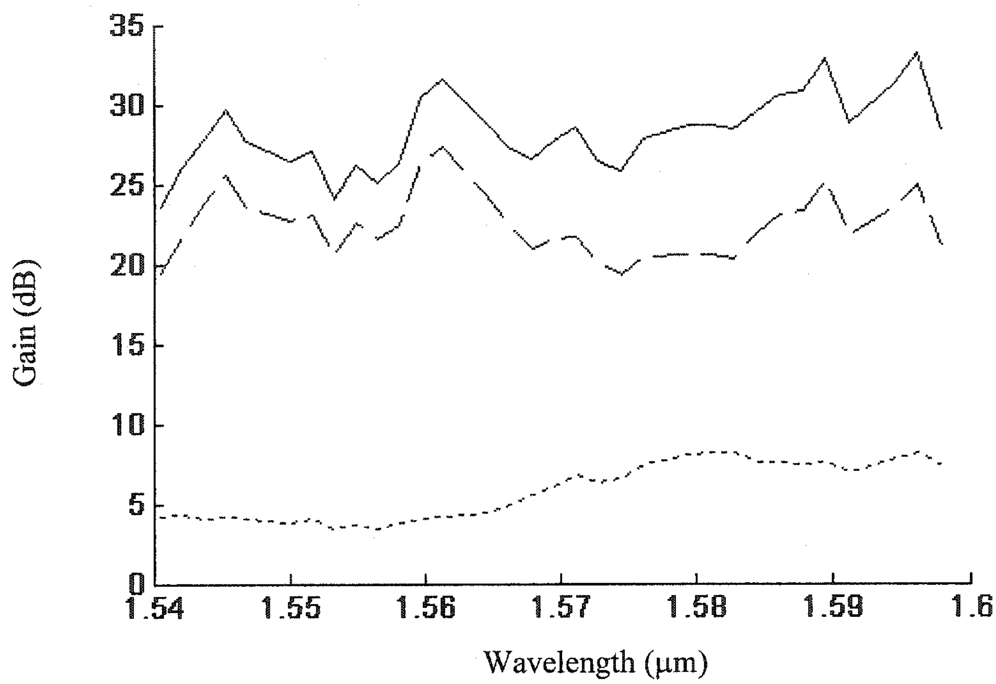

Fig. 4-16 Gain spectrum of DFRA without (solid line) and with (dashed line) feedback signal at λ_f = 1607 nm [(R_1, R_2) = (25%,25%)]. In both cases, the total input signal power is -15 dBm. The dotted line represents the gain difference.

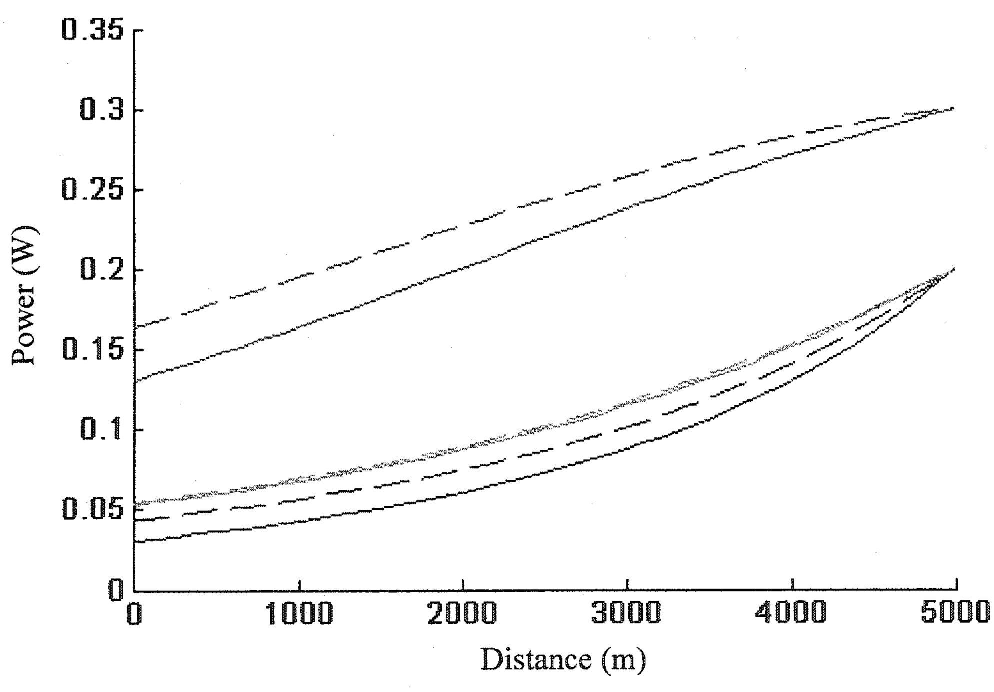

Fig. 4-17 Pump power evolution when λ_f = 1607 nm (solid lines) and 1662 nm (dashed lines). 1435 nm pump (blue), 1450 nm pump (green), 1480 nm pump (red).

4.6.4 Summary of potential feedback wavelength identification process

Based on the gain spectra plots presented in the previous subsections for clamped amplifiers having feedback wavelengths at 1624.8 nm, 1662 nm and 1607 nm, certain inferences can be made as to their respective clamping uniformity performance. In particular, the gain-clamping is expected to be stronger in signal bands where the gain depletion due to the introduction of the feedback signal was also stronger. For λ_f = 1624.8 nm, the gain-clamping should be slightly weaker in the middle of the DWDM band (see Fig. 4-11), for λ_f = 1662 nm gain-clamping should be weakest for longer wavelength signals (see Fig. 4-14), while for λ_f=1607 nm gain-clamping should be weakest for shorter wavelength signals (see Fig. 4-16). In each case however, since the unclamped amplifier gain-spectrum shape is relatively well maintained, the gain-clamping uniformity should be much better than for an amplifier with λ_f = 1595 nm (which was shown to be very non-uniform in Section 4.4).

The above inferences are all verified in Fig. 4-18, which shows the gain spectra with total input signal powers of -15 dBm, -9 dBm and -3 dBm for the three feedback wavelengths discussed above. Clearly, the gain-clamping is much more uniform when λ_f = 1624.8 nm, 1662 or 1607 nm rather than when λ_f = 1595 nm. Furthermore, in each case, gain-clamping is strongest where gain depletion was strongest.

Also note that the feedback signal causes a small gain-tilt for increasing signal power, noticeable especially in the shorter wavelength signals in Fig. 4-18 (a) and (b).

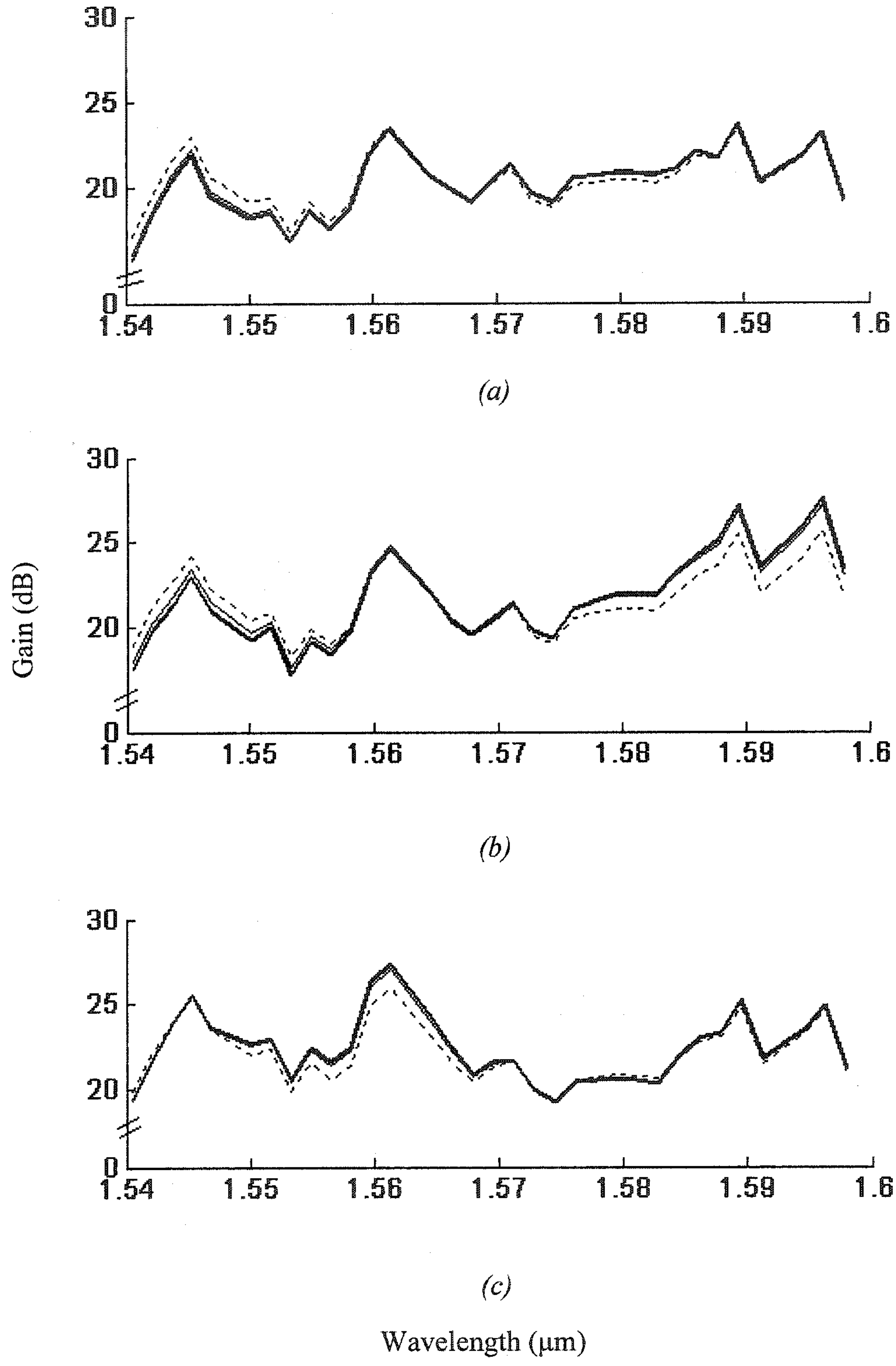

Fig. 4-18 Gain-spectra for three input power levels (-15 dBm, thick solid line; -9 dBm, solid line; -3 dBm, dotted line) for DFRAs clamped at (a) λ_f = 1624.8 nm with (R_1, R_2) = (25%, 25%), (b) λ_f = 1662 nm with (R_1, R_2) = (35%, 35%) and (c) λ_f = 1607 nm with (R_1, R_2) = (25%, 25%).

Normally, as the input signal power to an amplifier increases, the gain should decrease: in these cases, there is a small increase in the gain when the input signal power is increased from -15 dBm to -3 dBm. This effect is discussed further in the following section.

The full analysis for GC-DFRAs with λ_f = 1624.8 nm and λ_f = 1662 nm, including noise analysis, and a more quantitative comparison of gain-clamping uniformity, is presented in the following section.

4.7 Complete Analysis of Two GC-DFRA Designs

As shown in the previous section, locating the feedback signal at 1624.8 nm and 1662 nm gives (relatively) uniform pump depletion. In this section, we give an in-depth analysis of the gain, noise and gain-clamping performance for these two feedback wavelengths.

As will be shown below, for λ_f = 1624.8 nm, FBG reflectivities of (R_1, R_2) = (20%, 30%) will be used since this overall system maintains relatively high gain (on average, only 8 dB lower than the unclamped amplifier), while demonstrating strong gain-clamping performance. For λ_f = 1662 nm, FBG reflectivities of (R_1, R_2) = (30%, 50%) are used since this configuration exhibits similar gain. This enables a comparison of these two systems, which is presented in Section 4.7.3.

4.7.1 Full Analysis for Feedback Signal at 1624.8nm

We begin by varying the grating reflectivity and note its effect on the gain. While maintaining R_1 at 20%, R_2 is varied from 20% to 50% in increments of 10%. The small-signal gain and NF spectra for these cases are shown in Fig. 4-19. It is clear that as R_2 is increased, the gain decreases and the NF increases. For (R_1, R_2) = (20%, 30%), the decrease in gain from the unclamped DFRA is 7.2 dB, 6.3 dB and 8.7 dB at 1555.7 nm, 1575.3 nm and 1593.7 nm, respectively. Meanwhile, there is a corresponding increase in the NF at these wavelengths of 0.8 dB, 0.35 dB and 0.6 dB, which is explained as follows. When the degree of clamping is increased (i.e. the reflectivity is increased), both the gain G and the ASE power P_{ASE} decrease at the DWDM signal wavelengths since the pumps are depleted by feedback signal. From Equation 3-3, a decrease in the gain results in an increase in the NF while a decrease in the ASE power results in a decrease of the NF. Although these two factors oppose each other, it is evident from Fig. 4-19 that the overall change in the NF is an increase. It may therefore be concluded that the decrease in the gain is the dominant effect.

However, this increase in the NF is more pronounced for the shorter DWDM wavelengths for the following two reasons. First, thermal noise is present and so the ASE power is higher in the shorter band. Second, the feedback signal further reduces the gain of the shorter wavelength signals via direct Raman interaction (the signals directly amplify the feedback signal). This effect is even more significant for λ_f = 1662 nm, as will be explained in Section 4.7.2.

Changing the reflectivity also plays a role in the effectiveness of the gain-clamping. Shown in Fig. 4-20 (a) and (b) are the gain spectra for different total input signal powers for *(R_1, R_2)* = (20%, 20%) and *(R_1, R_2)* = (20%, 30%), respectively. As expected, there is stronger gain-clamping when *(R_1, R_2)* = (20%, 30%), although the gain is lower.

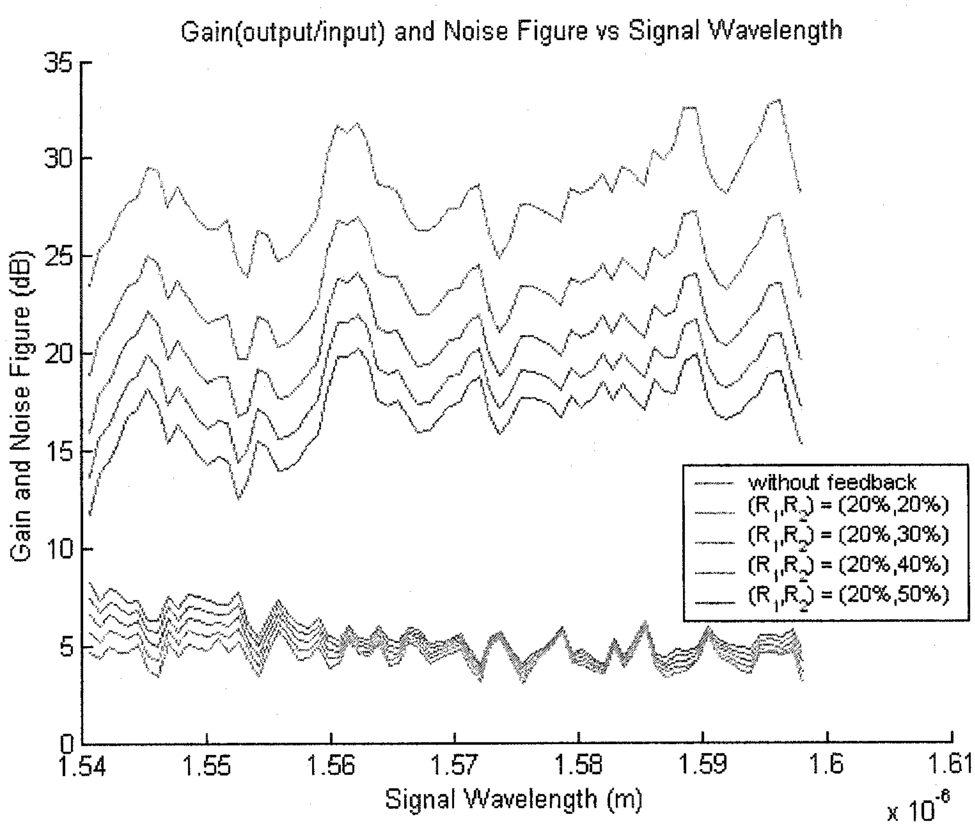

Fig. 4-19 Small-Signal Gain for feedback signal at 1624.8 nm and varying reflectivity.

Another effect we observe in Fig. 4-20 is the gain-tilt with increasing input signal power in the shorter DWDM signal band, i.e. as the input signal power increases, the gain also increases slightly (also observed in Section 4.6.4). This may be explained as follows: since the feedback signal power is much lower in the 0 dBm case, more of the 1435 nm pump's power goes to amplifying the signals rather than providing gain to the feedback signal indirectly via the other two pumps. The same applies to the 1450 nm pump, since it also interacts indirectly with the feedback signal.

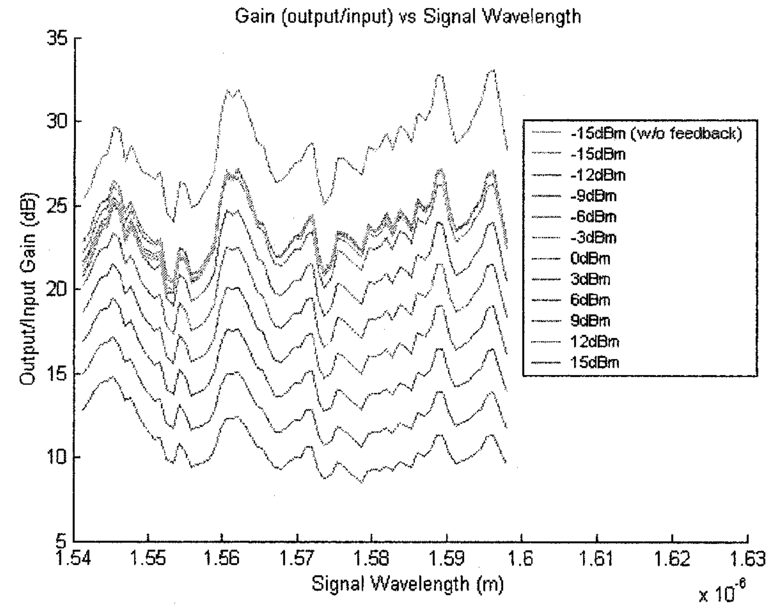

(a)

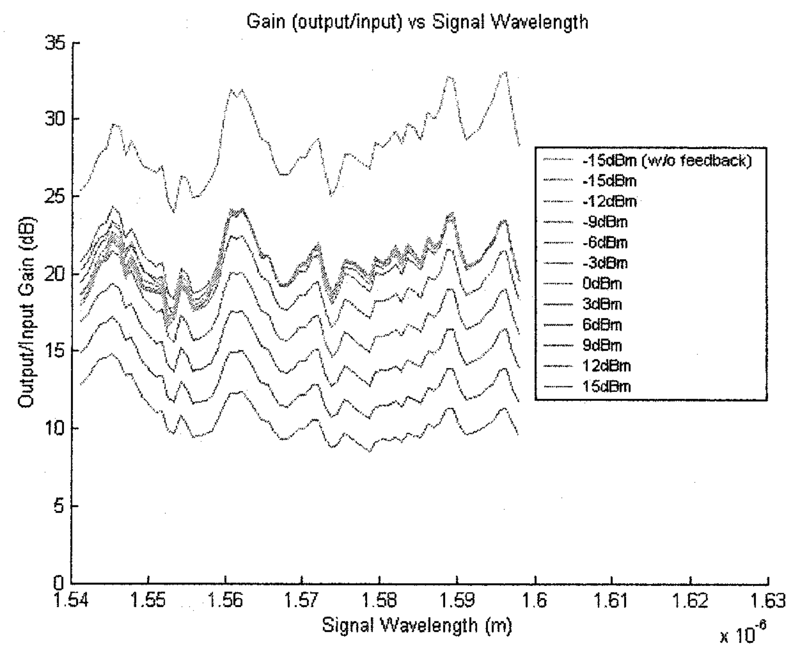

(b)

Fig. 4-20 Gain spectrum plots for varying total input signal power. In (a) *(R_1,R_2)* = (20%, 20%) and in (b) *(R_1,R_2)* = (20%, 30%). Also shown in each case is the small-signal gain for the unclamped amplifier.

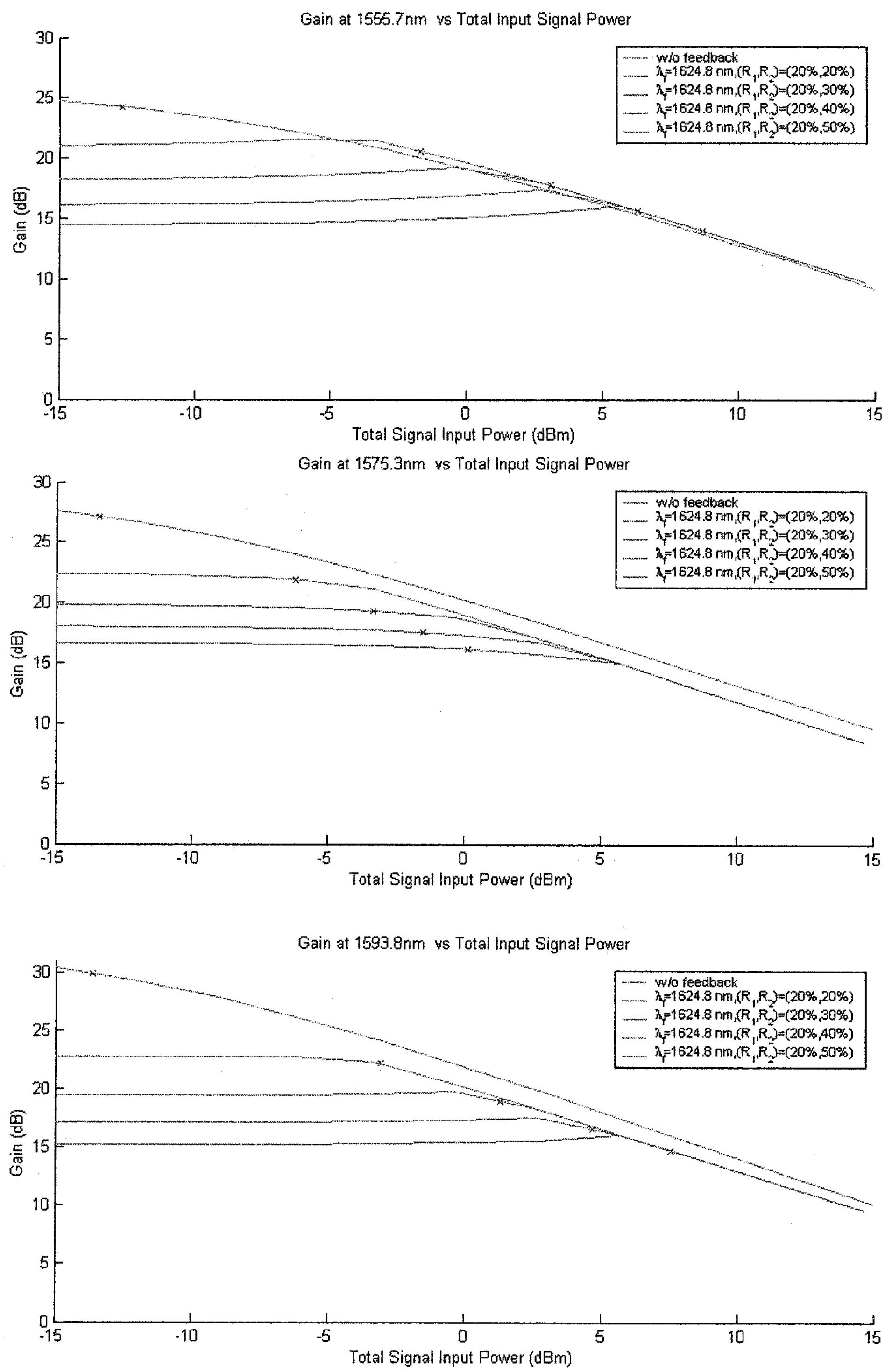

Fig. 4-21 Gain vs. total input signal power for signals at 1555.7, 1575.3 and 1593.8 nm. The critical power is indicated by an 'x'. Shown in each plot, for comparison purposes, is the result of the unclamped amplifier.

Fig. 4-21 shows gain at different signal wavelengths as a function of total input signal power for different feedback levels. The critical power, which we define as the input signal power at which the gain decreases by 0.5 dB from the small-signal gain value (i.e. for -15 dBm total input power), is also indicated. As the feedback level is increased, the critical power also increases. For (R_1, R_2) = (20%, 30%), the critical powers are 3.1, -3.3 and 1.3 dBm for signals at 1555.7 nm, 1575.3 nm and 1593.8 nm respectively, and therefore clamping is shown to be strongest at shorter and longer wavelengths and slightly weaker in the center band.

As a performance metric to assess the uniformity of gain-clamping, we determine the maximum input power before which the gain of **all** DWDM signals decreases by 0.5 dB of its corresponding small-signal gain value. This gives the worst-case critical power of a particular system, which we denote as $P_{crit,w\text{-}c}$, and it occurs at the DWDM signal wavelength where the gain-clamping is least effective. For λ_f = 1624.8 nm and (R_1, R_2) = (20%, 30%), $P_{crit,w\text{-}c} \approx$ -3.5 dBm, and it occurs at a signal wavelength of 1578.6 nm.

4.7.2 Full Analysis for Feedback Signal at 1662 nm

Due to the weaker depletion of the pumps when λ_f = 1662 nm, higher FBG reflectivities are required in order to achieve gain-clamping. In Fig. 4-22, the small-signal gain spectrum is shown with R_1 set at 30% and R_2 varied from 30% to 60% in increments of 10%. The decrease in the gain from the unclamped amplifier for signals at 1555.7 nm, 1575.3 nm and 1593.7 nm is of 6.7 dB, 6.2 dB and 6.0 dB, respectively, and the corresponding increase in the NF is of 1.7 dB, 1.1 dB and 0.4 dB, when (R_1, R_2) = (30%, 50%).

Since the feedback signal at 1662 nm is at the Raman gain peak with respect to the shorter wavelength DWDM signals, there is considerable power transfer from these DWDM signals to the feedback signal, which deteriorates the NF, as explained above. This effect is even more noticeable when the reflectivity of FBG_2 is increased, since the power of the feedback signal also increases and therefore it depletes the power of the lower DWDM signals to a greater extent, as is evident from Fig. 4-22.

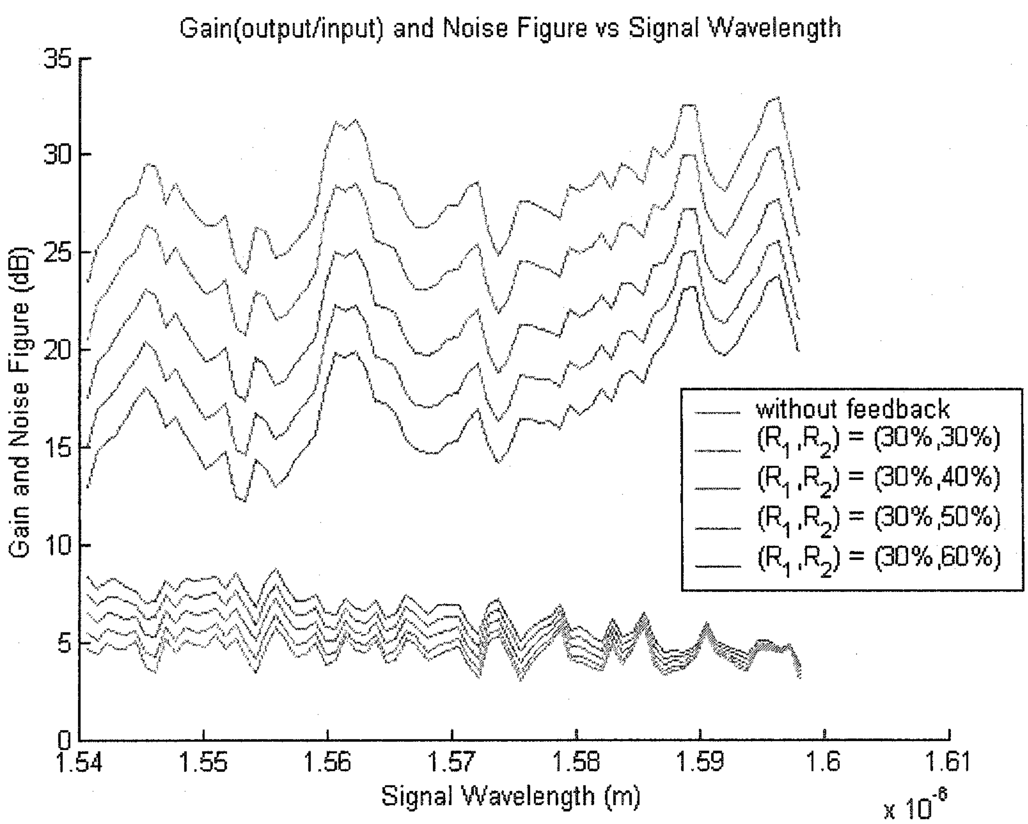

Fig. 4-22 Small-signal gain for feedback signal at 1662 nm and varying reflectivity. Also shown is the small-signal gain of the unclamped DFRA.

This is further supported by the plots in Fig. 4-23, which show the feedback signal power evolution for input powers at 0 dBm and 9 dBm, for λ_f = 1624.8 nm and 1662 nm. For λ_f = 1624.8 nm, as the input signal power is increased to 9 dBm, the DWDM signals draw most of the pump power, leaving insufficient gain for lasing at the feedback wavelength. For λ_f = 1662 nm, the feedback signal power persists for an input signal power of 9 dBm since there is power transfer from the DWDM signals to the feedback signal.

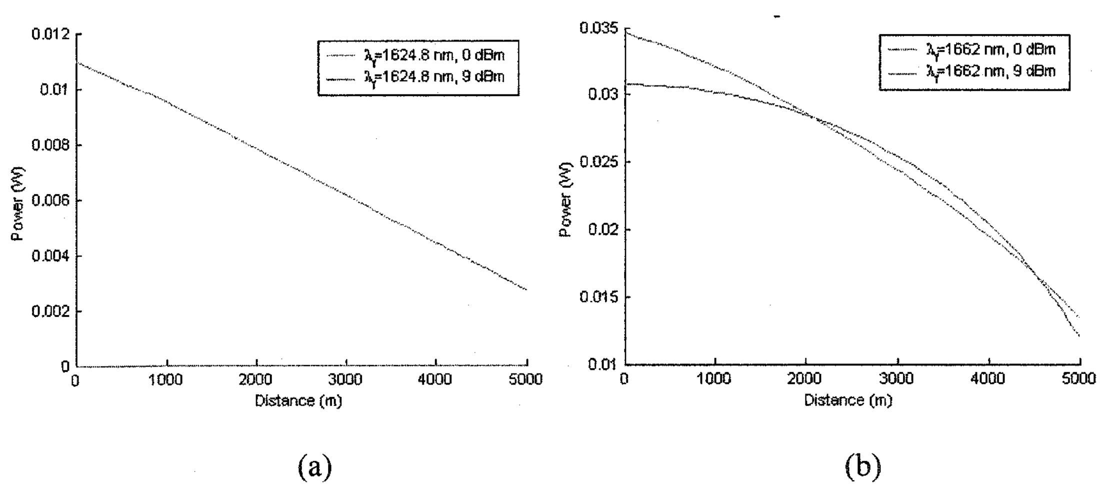

Fig. 4-23 Feedback signal power evolution for input signal powers of 0 and 9 dBm for (a) λ_f = 1624.8 nm and (b) λ_f = 1662 nm. In both cases, the backward propagating (from $z = L$ to $z = 0$) component of the feedback signal is shown.

Shown in Fig. 4-24 are the gain spectra for different total input signal powers, when λ_f = 1662 nm and (R_1, R_2) = (30%, 50%). $P_{crit,w\text{-}c}$ for this system is ≈ -6.1 dBm, and it occurs at a signal wavelength of 1596.3 nm, at which point the gain-clamping is weakest.

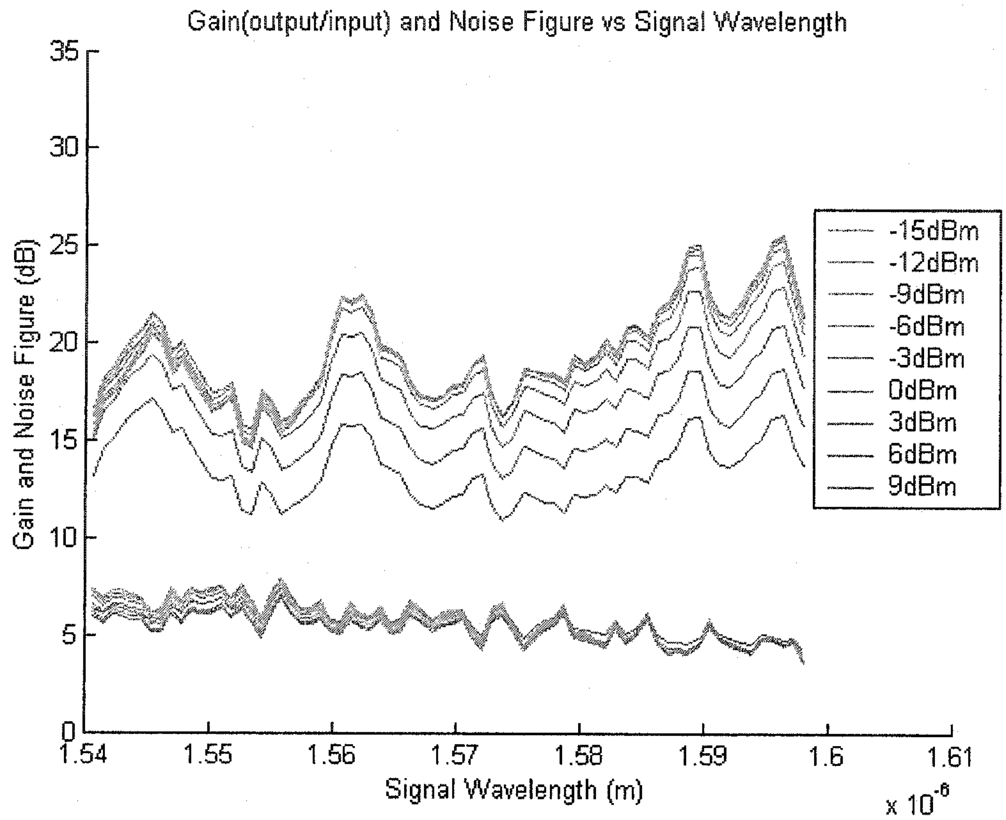

Fig. 4-24 Gain spectrum plots for λ_f = 1662 nm, (R_1, R_2) = (30%, 50%), with the total input signal power varied.

Fig. 4-25 shows the plots of gain vs. input signal power at different signal wavelengths for different feedback levels. As the feedback level is increased, the critical power also increases. For (R_1, R_2) = (30%, 50%), the critical powers are 2.19 dBm, -3.04 dBm and -6.03 dBm (total input power) for signals at 1555.7 nm, 1575.3 nm and 1593.7 nm, respectively. The clamping is therefore much stronger in the shorter wavelength band, and weaker in the longer wavelength band.

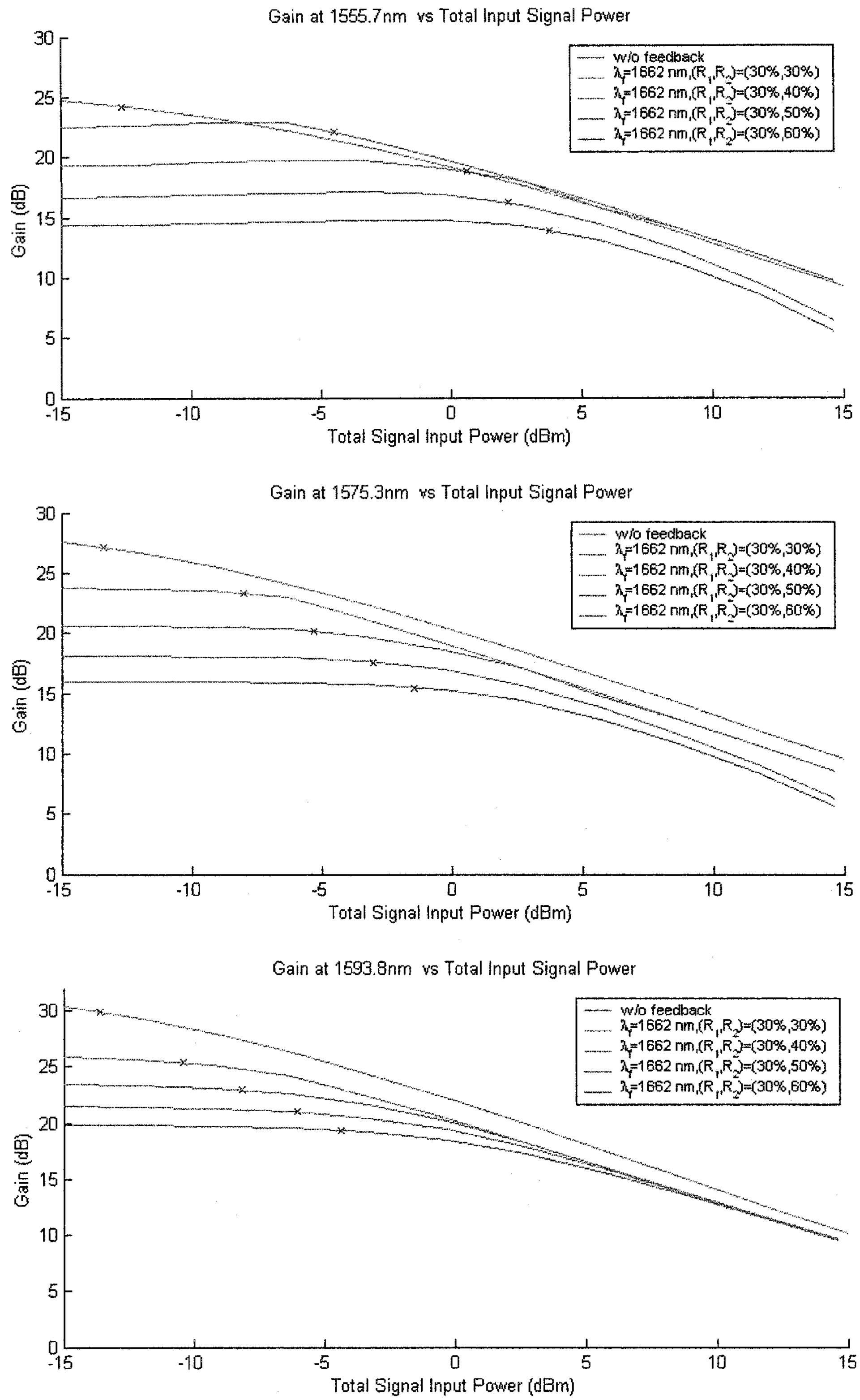

Fig. 4-25 Gain vs. total input signal power for signals at 1555.7 nm, 1575.3 nm and 1593.8 nm. The critical power is indicated by an 'x'. Shown in each plot, for comparison purposes, is the unclamped result.

4.7.3 Comparison of GC-DFRAs with λ_f = 1624.8 nm and 1662 nm

Due to the complex interactions between the feedback signal, DWDM signals, and pumps, a strict comparison between the performance of the GC-DFRAs with feedback signals located at 1624.8 nm and 1662 nm is not possible, since the gain spectra cannot be precisely overlapped. However, for purposes of illustration, the small-signal gain and NF for these two cases are shown in Fig. 4-26. For λ_f = 1624.8 nm, there is higher gain at the shorter wavelengths, while for λ_f = 1662 nm, there is higher gain at the longer wavelengths. This is due to the depletion of the lower wavelength signals by the feedback signal for λ_f = 1662 nm, as was explained above. This effect also leads to a deterioration of the NF: it is considerably greater for the shorter wavelengths for λ_f = 1662 nm than for λ_f = 1624.8 nm (even where the gain is almost equal in both cases), while in the longer band the NFs are almost equal, even though the gain is greater for λ_f = 1662 nm. These results suggest that λ_f = 1624.8 nm has better NF performance.

Fig. 4-27 compares the critical powers of the two systems for signals at 1555.7 nm, 1575.3 nm and 1593.8 nm. In the first and last case, λ_f = 1624.8 nm gives a higher critical power, while for the second case, λ_f = 1662 nm gives a slightly higher critical power (but lower gain). Meanwhile, the NF is higher for λ_f = 1662 nm in all three cases.

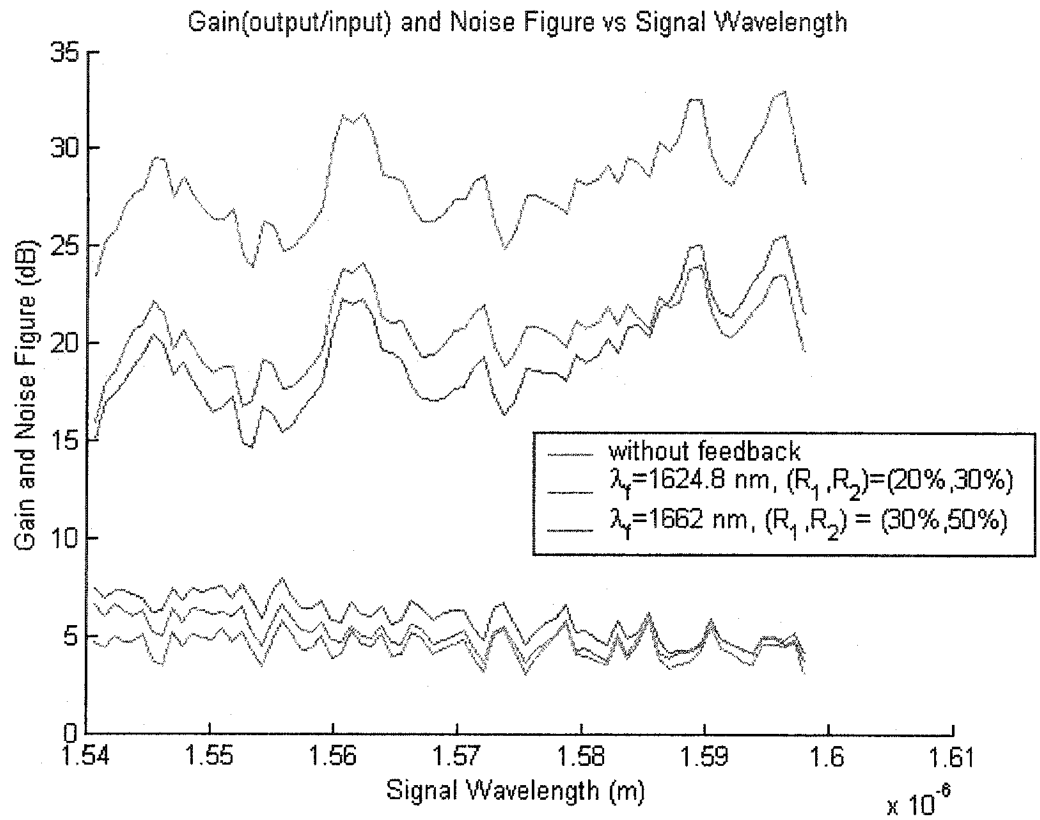

Fig. 4-26 Small-signal gain and noise figure for the different feedback configurations and for the unclamped amplifier.

In summary, in terms of NF and critical power (taken for signals at 1555.7 nm, 1575.3 nm and 1593.8 nm) for systems with similar gain with λ_f = 1624.8 nm and λ_f = 1662 nm, the former seems to outperform the latter. Also, as was seen in Sections 4.7.1 and 4.7.2, the λ_f = 1624.8 nm system has a higher $P_{crit,w\text{-}c}$ of -3.5 dBm, compared to -6.1 dBm for the λ_f = 1662 nm system, and therefore λ_f = 1624.8 nm gives better gain-clamping uniformity.

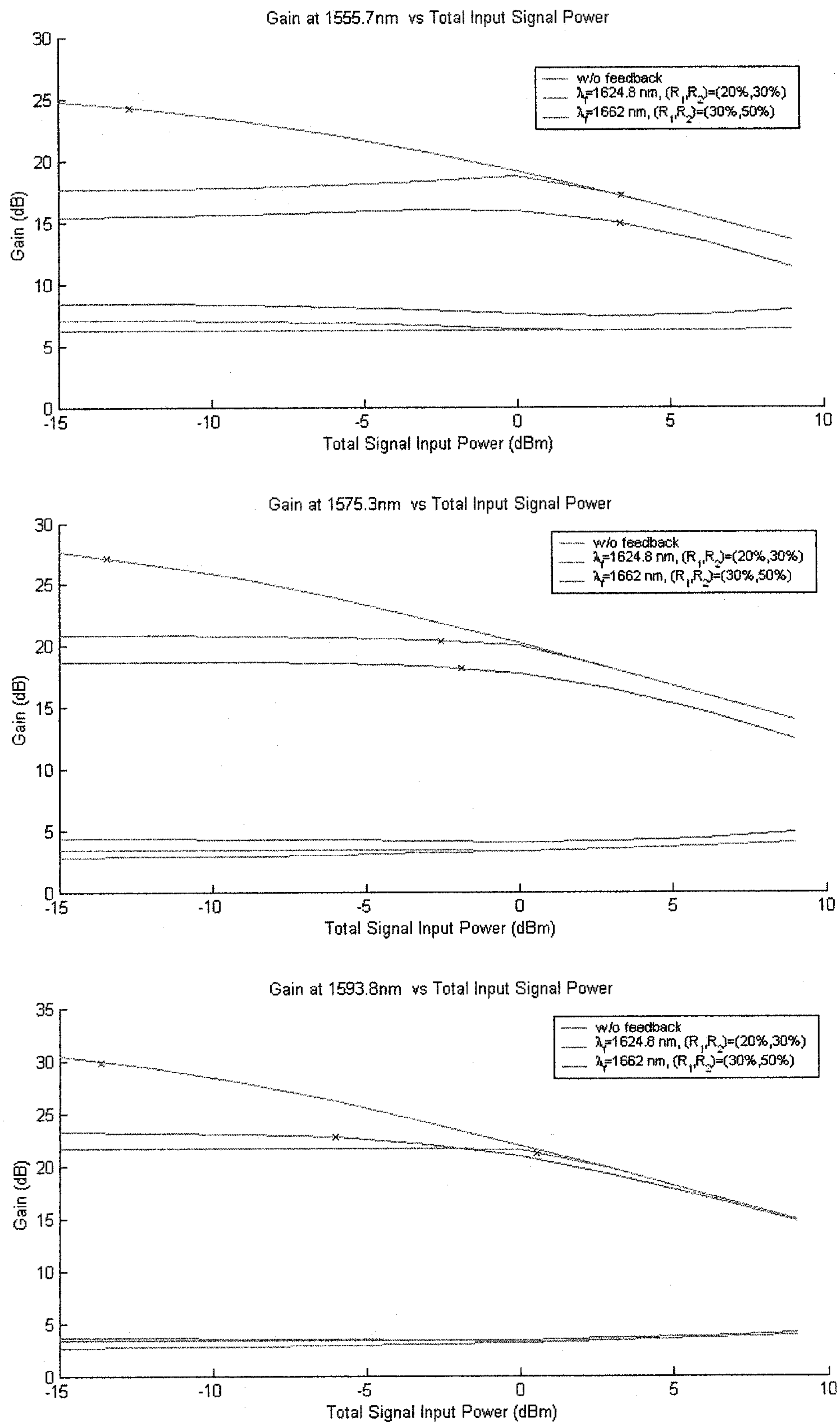

Fig. 4-27 Gain and noise figure vs. input signal power at 1555.7 nm, 1575.3 nm and 1593.8 nm for the two different feedback configurations and for the unclamped amplifier.

5 Experiments

The purpose of the experimental analysis was to replicate the gain-clamping effect that was demonstrated in the simulations. The components used in the simulations did not exactly match the simulated components (due to availability), and therefore an exact match of results was not expected. Most notably, DCF was used in the experiment while data for HNLF was used in the simulations. Nevertheless, basic amplifier features were verified.

The remainder of this chapter is organized as follows. In Section 5.1, the setup of the experiment is given. In Section 5.2, the amplifier's parameters are discussed and in Section 5.3, the measured small-signal gain and NF of the unclamped amplifier are given and compared to values obtained using the simulation program (with input parameters matching the experimental setup). In Section 5.4, the unclamped gain and NF are shown for multiple DWDM inputs; as expected, increasing the power results in a decrease in gain. In Section 5.5, all-optical gain-clamping is demonstrated experimentally in the DFRA, using the FBG configuration.

5.1 Experimental Setup

The experimental setup, which uses two optical switches, is shown in Fig. 5-1. By setting both switches to the bottom path, a measurement of the input signals was obtained. By setting the switches to the upper path, the input signals traveled through the DFRA and the amplified signals could be measured. Measurement error was greatly reduced by using optical switches since they eliminated the need to manually change the system configuration, i.e. mounting and dismounting fiber connections, for measuring the input and amplified signals.

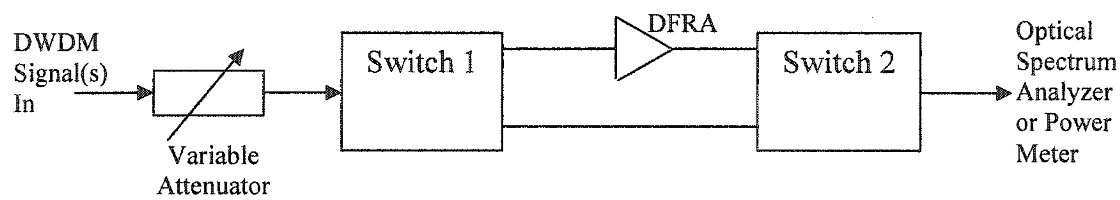

Fig. 5-1 Experimental setup for measuring amplifier gain and noise figure.

The gain is obtained by taking the difference in power between the amplified and the input signals. Note that the difference in insertion losses of the two paths must be taken into account. In order to calculate the NF, the amplifier measure feature on the Agilent 86142 optical spectrum amplifier was used. The ASE power is required to calculate the NF (as in Equation 3.3), and it is obtained as follows. First, the noise power of the signal source, P_{source}, is measured and stored. Next, the total noise power output by the amplifier, P_{tot}, is measured which contains both the ASE noise generated by the amplifier and the source noise which has now been amplified by gain G. As shown in Equation 5-1, the ASE power is simply the difference between the total noise power and the amplified source noise power. Note that the measured noise powers are dependent on the resolution bandwidth setting on the optical spectrum analyzer (OSA), which is analogous to the $\Delta\nu$ value used in the simulations.

$$P_{ASE} = P_{tot} - G \cdot P_{in} \qquad \textbf{(Equation 5-1)}$$

The *amplifier measure* function uses an interpolated value for the ASE power at the signal wavelength, i.e. the ASE power is measured on either side of the signal wavelength and the average is taken.

5.2 Amplifier Parameters

This section describes the parameters of the amplifier components for the GC-DFRA shown again in Fig. 5-2 for convenience. Note that for the unclamped amplifier, the FBGs are not included in the configuration.

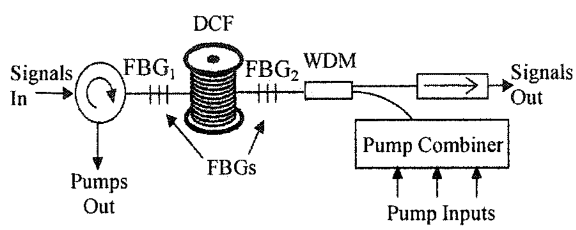

Fig. 5-2 Schematic of GC-DFRA.

5.2.1 The Pumps

Based on availability, pumps at 1435 nm, 1454 nm and 1480 nm were used. The 1435 nm and 1480 nm pumps were FBG stabilized laser diodes made by Fitel while the 1454 nm pump was a Raman fiber laser produced by MPB Communications. The launch powers (entering the DCF) of the pumps were 153 mW, 500 mW and 80 mW, respectively. Prior to entering the DCF fiber, the pump signals experience insertion losses due to the pump combiner and to the WDM coupler. Minimizing the losses of these components at the pump wavelengths plays a very important role in maximizing the efficiency of the amplifier. The WDM coupler used in our configuration had a loss of around 0.4 dB at the pump wavelengths, while the pump combiner, had a transmission spectrum as shown in Fig. 5-3; since the combiner is optimized for pumps at 1435 nm, 1450 nm, 1465 nm and 1480 nm, there was a loss of over 2 dB for the 1454 nm pump.

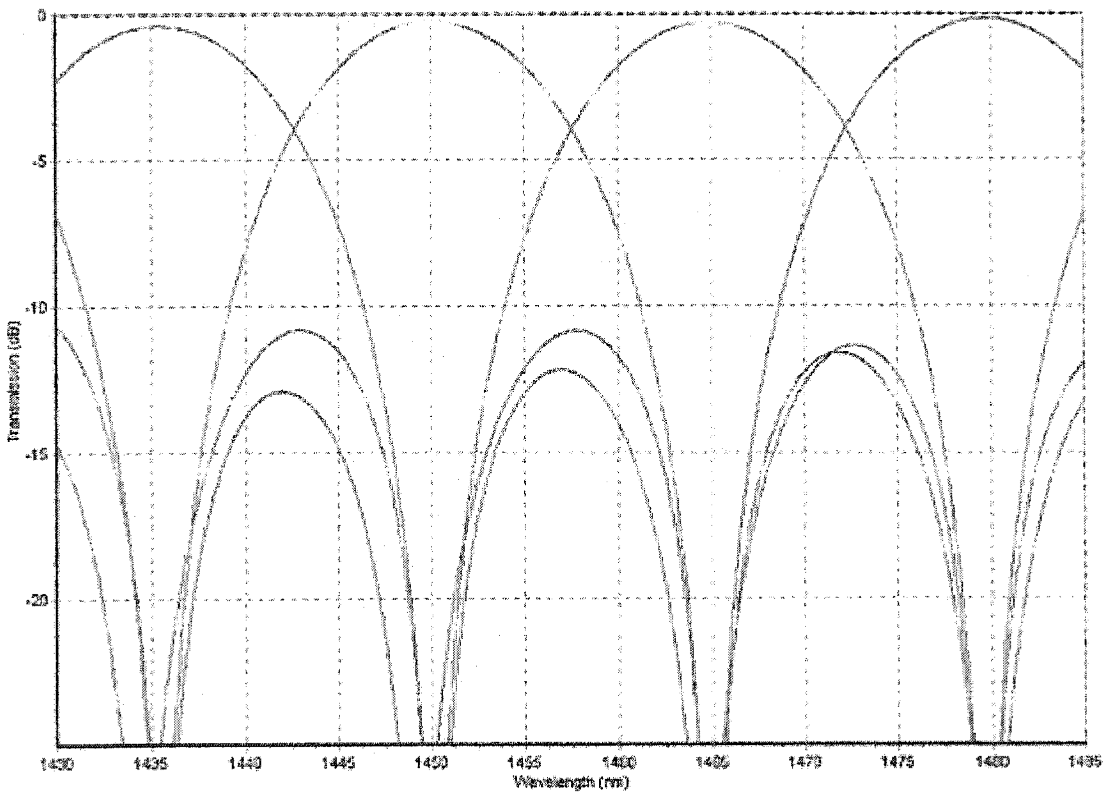

Fig. 5-3 Transmission Spectrum of pump combiner. There is a 2 dB loss at 1454 nm and less than 0.5 dB loss for 1435 and 1480 nm.

5.2.2 The DCF Fiber

A DCF module made by Corning Inc. was used as the Raman gain medium in the experimental configuration. Its specifications are given below.

Fiber Length:

6.9 km of DCF was enclosed in the fiber module.

Attenuation:

The measured attenuation spectrum of the fiber module is shown in Fig. 5-4. There is approximately 0.57 dB/km of attenuation at 1550 nm.

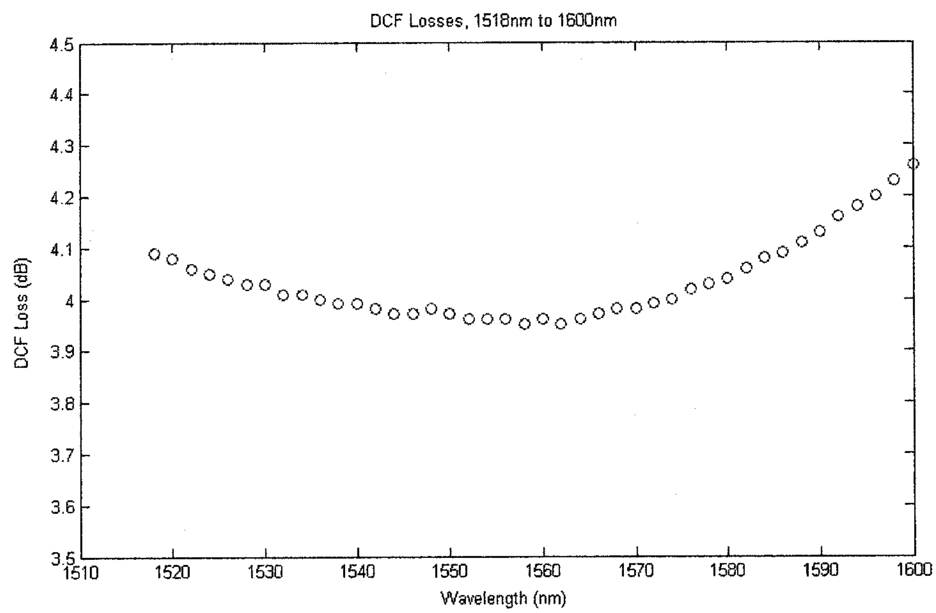

Fig. 5-4 Attenuation spectrum of DCF fiber module.

At the pump wavelengths of 1435 nm, 1454 nm and 1480 nm, the fiber attenuation was measured to be 6.95 dB, 5.66 dB and 4.96 dB, respectively.

Effective Raman Gain Coefficient:

The effective Raman gain coefficient of the DCF used in this experiment was not known precisely, however an approximation technique was used to obtain an estimate of this coefficient [37]. The approximation technique used is based on the small-signal gain model which was discussed in Section 3.1. A single FBG stabilized laser diode at 1450 nm was launched into the fiber with 161 mW of power, along with a low power probe signal (-30 dBm), which was swept from 1518 nm to 1600 nm in increments of 2 nm. In each case, the gain was noted. Using Equation 5-2, which is the approximate solution of the power evolution equation of the small-signal model, g_R / A_{eff} was deduced [37].

$$G \approx \exp\left(\frac{g_R}{A_{eff}} P_o L_{eff} - \alpha_s L\right)$$ **(Equation 5-2)**

$$L_{eff} = \frac{1}{\alpha_p}[1 - e^{-\alpha_p L}]$$ **(Equation 5-3)**

P_o is the input pump power (161 mW), α_s and α_p are the attenuation constants at the signal and pump wavelengths, respectively, and L is the fiber length. L_{eff} is the effective amplifier length, and is defined in Equation 5-3. All of these values were specified above. Fig. 5-5 shows the approximate effective Raman gain spectrum of the DCF as a function of frequency separation. Each measured point is marked with an 'x'. The remaining data points are obtained by approximation.

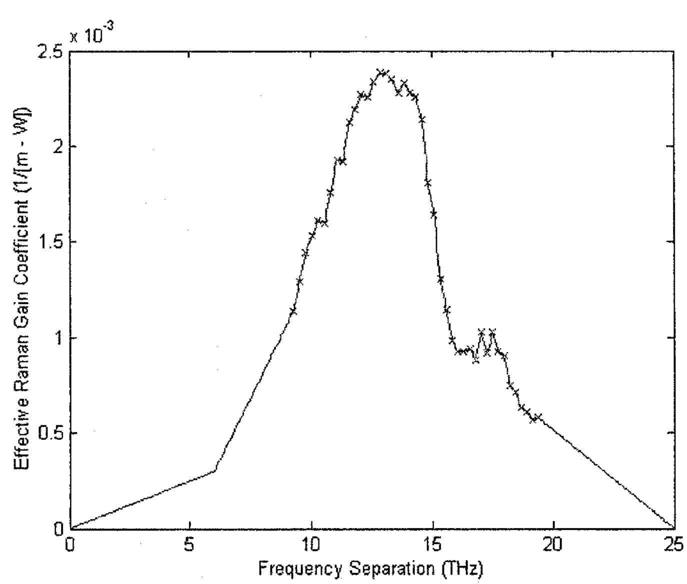

Fig. 5-5 Approximation of effective Raman gain coefficient of the DCF.

5.2.3 The Fiber Bragg Gratings

As was discussed in chapter 4, it is preferable to locate the feedback signal outside the high-gain region in order to maintain relatively high gain while still achieving gain-clamping. For this reason, and based on equipment availability, a feedback wavelength of λ_f = 1585 nm was selected. The normalized reflection spectra of the FBGs are shown in Fig. 5-6. FBG_1 was centered at λ_1 = 1585.1 nm and FBG_2 was centered at λ_2 = 1584.8 nm. Both gratings were over 90% reflective (93.2% and 94.5% for R_1 and R_2, respectively).

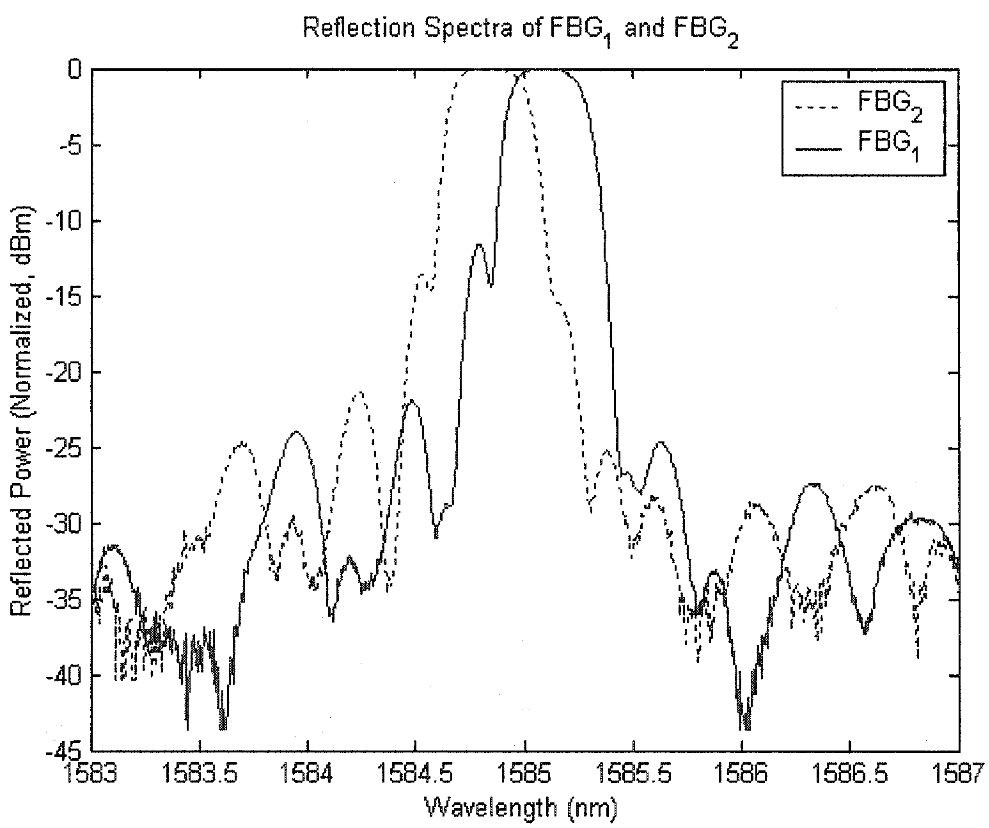

Fig. 5-6 Normalized reflection spectra of gratings (without tension). The center wavelengths are slightly offset.

FBG_1 was put on a stretch mount which allowed for strain-tuning; by stretching the grating, its center wavelength was varied from 1585.1 nm to 1585.4 nm, see Fig. 5-7. This gave a certain degree of freedom in tuning the feedback level in the cavity, as was done in [38] for a gain-clamped EDFA.

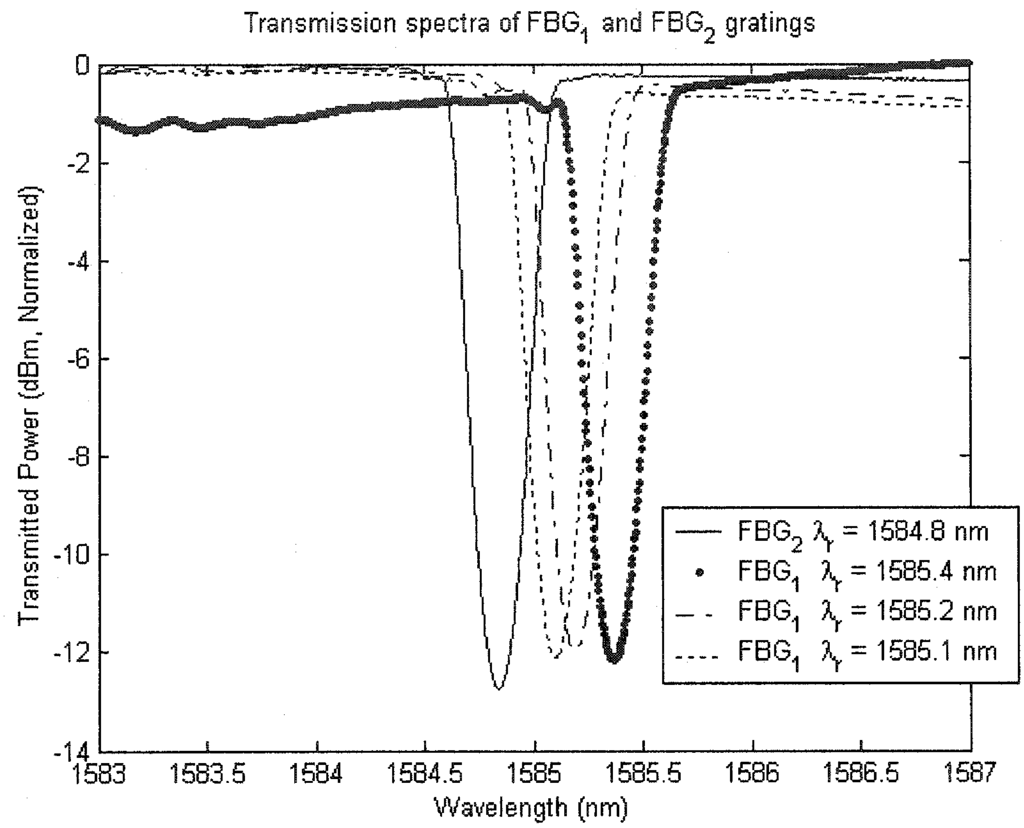

Fig. 5-7 FBG_1 and FBG_2 gratings have less overlap as tension in FBG_1 is increased.

5.2.4 Other components in the FRA

Besides the DCF, a circulator, a WDM coupler and an isolator also form part of the path which the DWDM signals traverse in the DFRA setup; these components introduce an additional loss of roughly 2 dB, which lowers the gain and increases the

NF (note that these additional losses are **not** accounted for in the simulations). This value may be improved through the use of components having lower loss.

5.3 Unsaturated Gain Spectrum Measurement

The small-signal gain and NF for the amplifier were measured by sweeping a single probe signal from 1518 nm to 1600 nm with an interval of 2 nm and an input power of -33 dBm. The result is shown in Fig. 5-8. The gain peak is at 1552 nm with a value of 21.8 dB and the corresponding NF is 6.6 dB. Note that the thermal noise contributes to a higher NF at the shorter wavelengths, as predicted by the full Raman model.

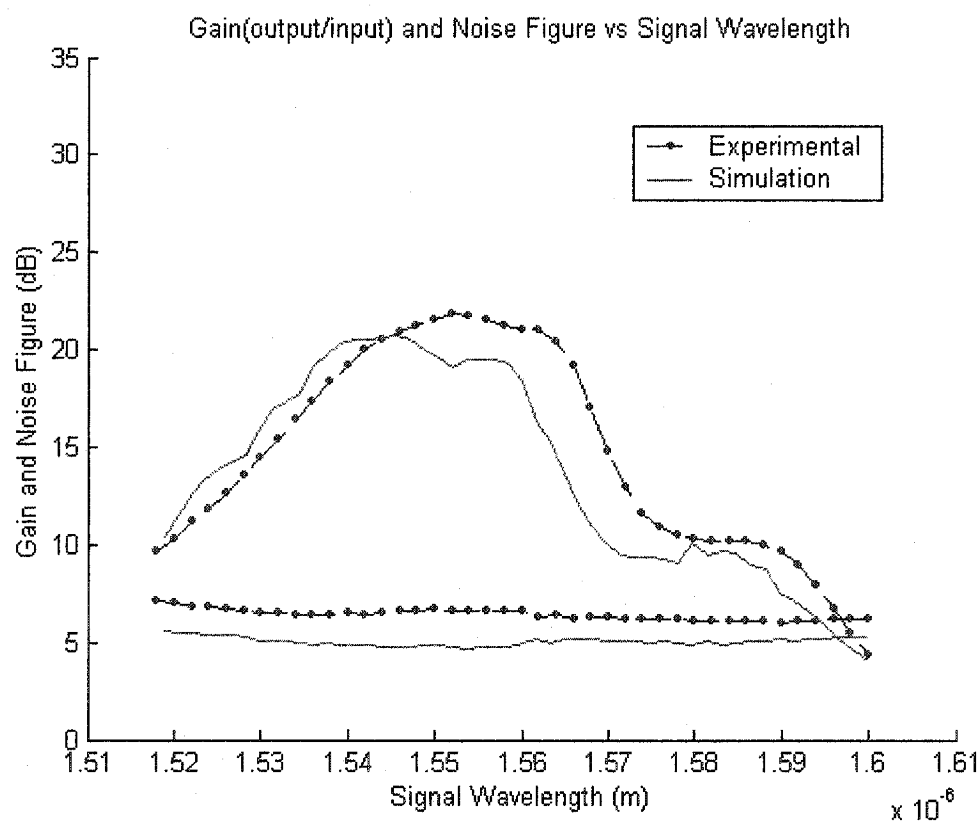

Fig. 5-8 Small-signal gain and noise figure, simulation and experiment.

Also shown in Fig. 5-8 are the simulated gain and NF, obtained using the amplifier parameters as described in Section 5.2. As can be seen, a very close agreement is obtained, the difference attributable in part to the fact that the gain parameter is approximate. The higher NF in the experimental result may be explained by the additional loss components in the DWDM signal's path (see Section 5.2.4), which are not accounted for in the simulations.

5.4 The Unclamped DFRA

Twelve DWDM signals at the ITU grid wavelengths 1527.99 nm, 1529.55 nm, 1531.12 nm, 1532.68 nm, 1534.25 nm, 1535.82 nm, 1537.40 nm, 1538.19 nm, 1538.98 nm, 1545.32 nm, 1550.12 nm and 1556.55 nm were multiplexed and launched into the amplifier (see Fig. 5-9).

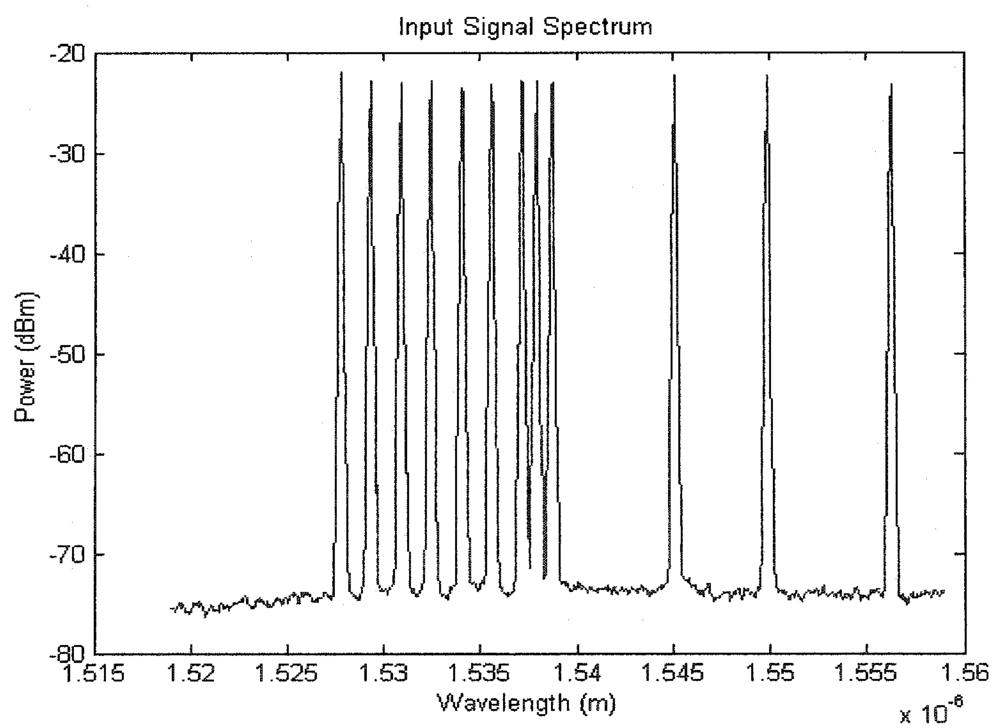

Fig. 5-9 Spectrum of multiple DWDM input signal to DFRA.

The launch power of these signals was maintained approximately equal (within 1 dB), and a broadband attenuator was used to collectively vary this total launch power from -20 dBm to +7 dBm total power, or -31 dBm to -4 dBm per signal. The gain and NF of the unclamped DFRA for different values of total input signal power are shown in Fig. 5-10.

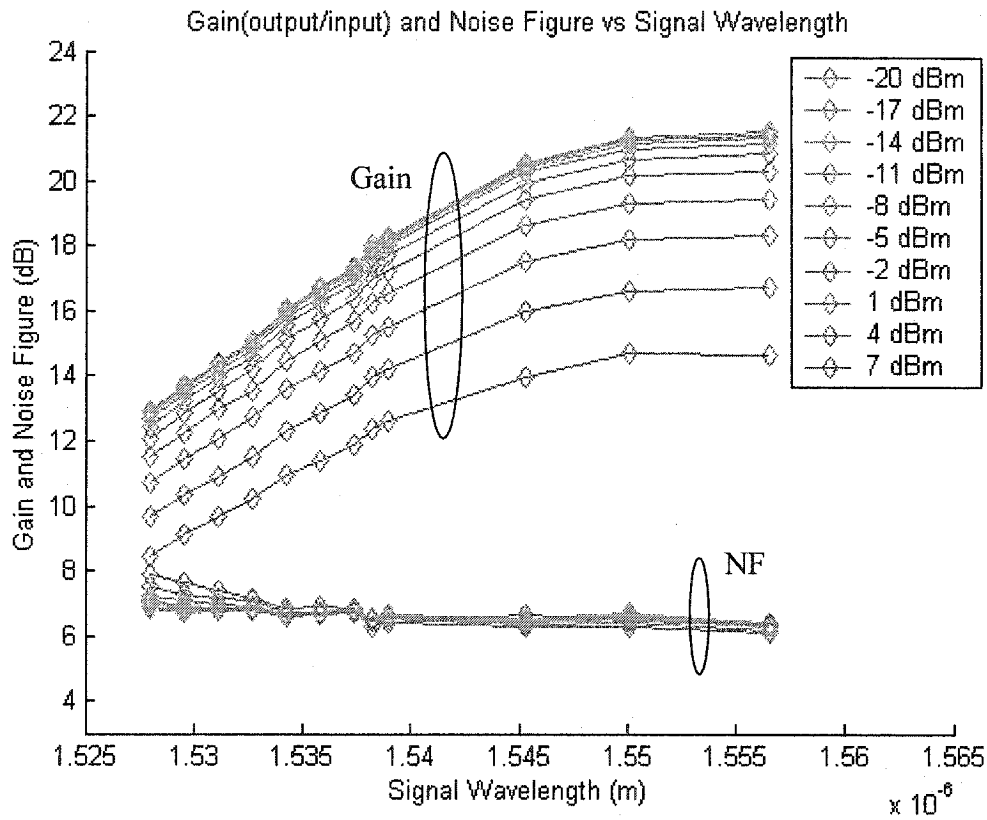

Fig. 5-10 Gain and noise figure of unclamped amplifier with total input power varied.

Fig. 5-11 plots the gain and noise figure for three different signals in the band. In each case, the amplifier reaches its saturation point for a total input signal power of -10 dBm (-21 dBm per channel), at which point the gain begins to decrease sharply, as was the case for the simulated unclamped DFRA presented in Section 4.2.

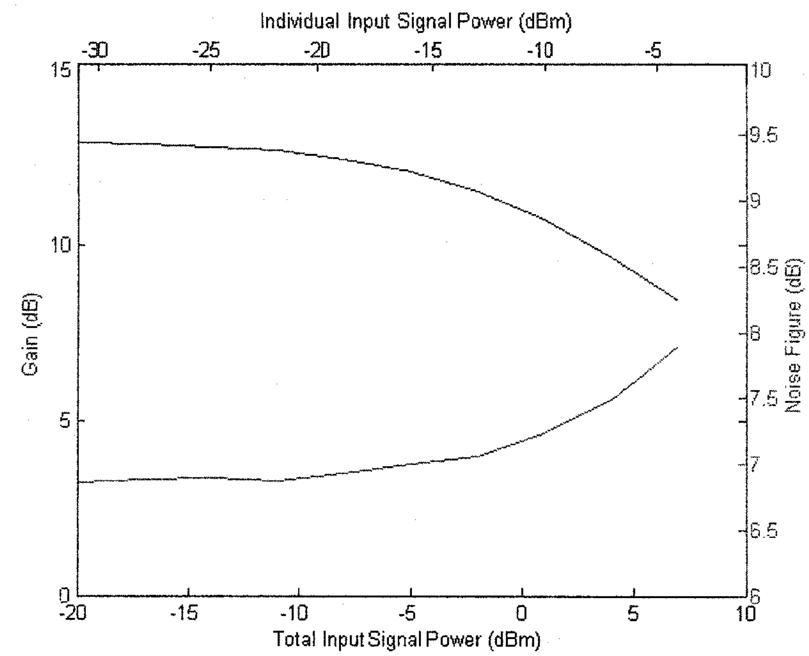

(a)

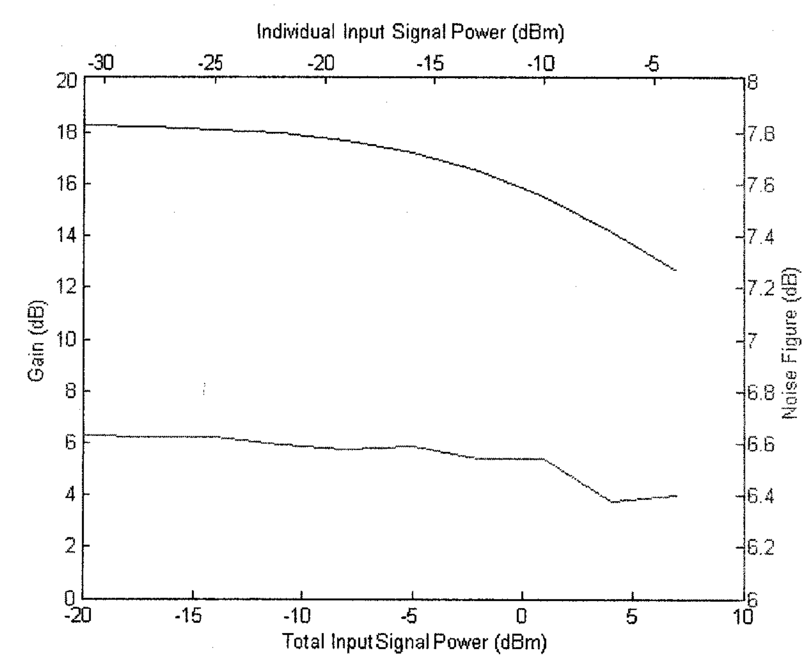

(b)

Fig. 5-11. Shows the saturation of the unclamped DFRA for signals at (a) 1527.99 nm, (b) 1538.98 nm and (c) 1550.12 nm. Note that the unexpected shape of the NF in (b) was probably due to a fluctuation during measurements.

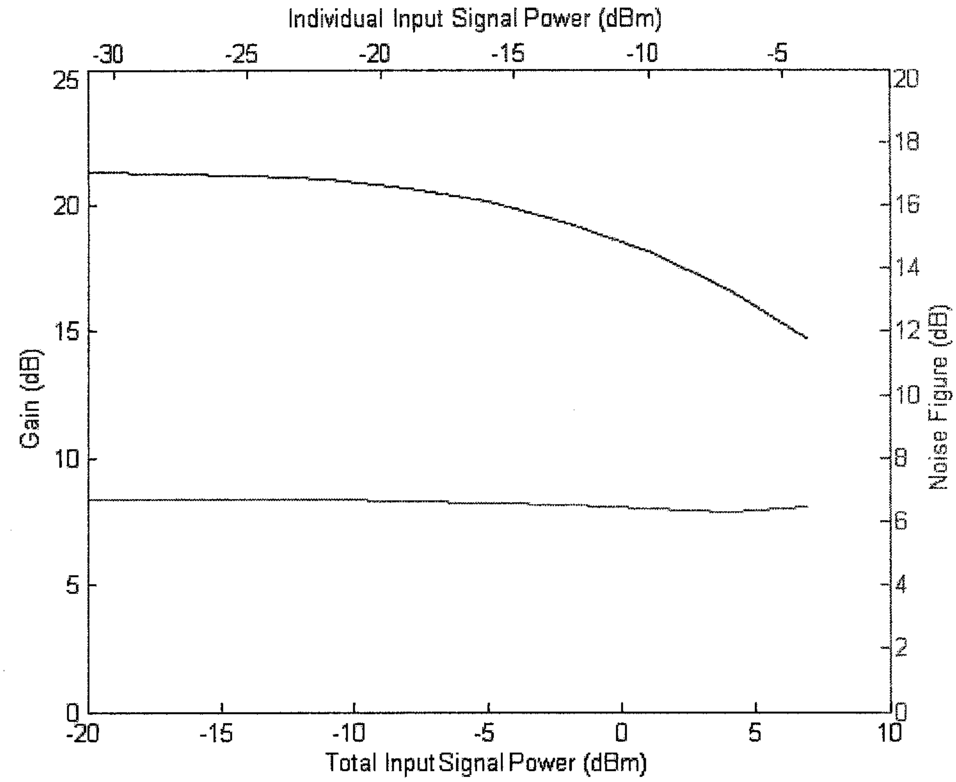

(c)

Fig 5-11 (con't). Shows the saturation of the unclamped DFRA for signals at (a) 1527.99 nm, (b) 1538.98 nm and (c) 1550.12 nm. Note that the unexpected shape of the NF in (b) was probably due to a fluctuation during measurements.

5.5 The GC-DFRA

Fig. 5-12 shows the twelve input DWDM signals from 1527.99 nm to 1556.55 nm along with the feedback signal at 1585.1 nm, at the output of the GC-DFRA. The signals were input with an approximate power of -30 dBm each (there were additional components, part of the experimental setup, located between the output of the amplifier and the OSA, and therefore power levels in Fig. 5-12 are lower than what is actually output by the amplifier).

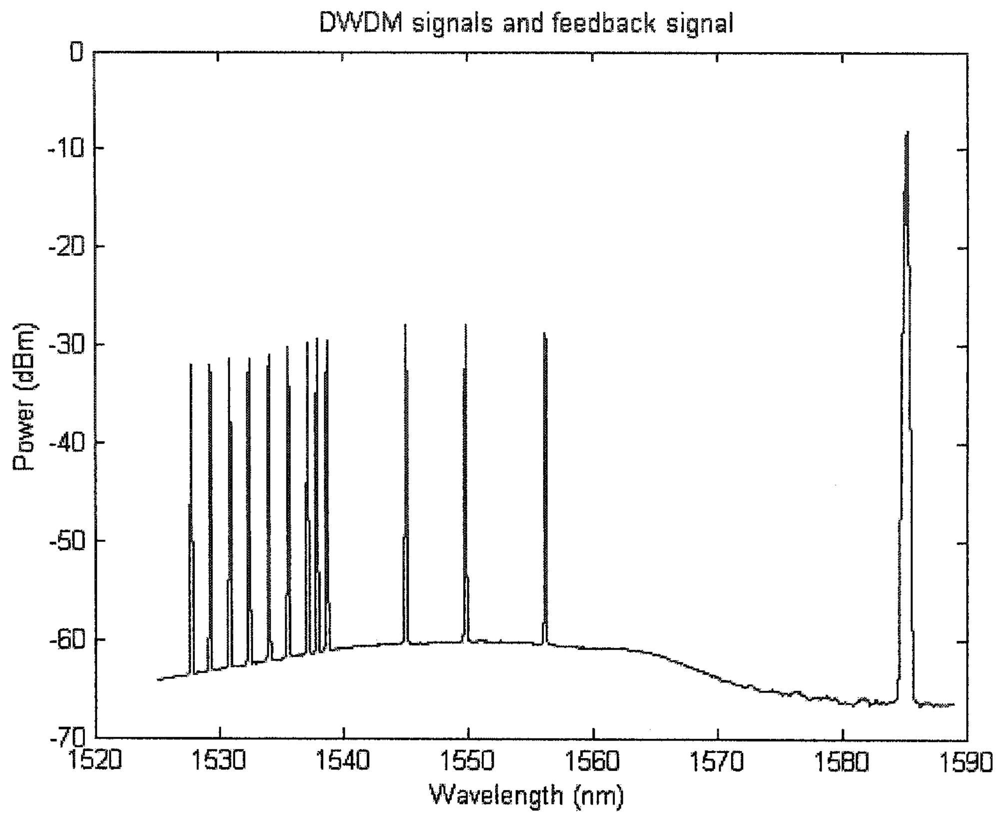

Fig. 5-12 DWDM signals and feedback signal.

As was mentioned above, the power and wavelength of the feedback signal may be varied by stretching one of the FBGs, in this case FBG_1. This tunes the wavelength response of the grating, which increases or diminishes the overlap of the reflection bands of the two gratings. As can be seen from Fig. 5-7, the highest degree of overlap between the reflection spectra of FBG_1 and FBG_2 occurs when FBG_1 is not stretched. As tension is applied, the overlap decreases. This gives a decrease in the feedback level in the cavity, which diminishes the depletion of the lasing signal on the pumps, which in turn results in higher gain but less efficient gain-clamping, i.e. lower critical power. The gain, NF and gain-clamping performance were analyzed for different values of applied strain on FBG_1, namely when its central reflective wavelength was tuned to $\lambda_r =$

1585.1 nm, 1585.2 nm and 1585.4 nm. The gain and NF for the three different feedback levels are illustrated in Fig. 5-13, Fig. 5-14 and Fig. 5-15, respectively. Gain-clamping behavior is indeed exhibited since the gain does not decrease as the input signal power is increased until a critical power of approximately + 5 dBm is reached (compared to -10 dBm for the unclamped amplifier).

For λ_r = 1585.1 nm, the gain is lowest with a peak value of 3.1 dB, since the feedback level is highest. For λ_r = 1585.2 nm, the peak gain is slightly higher, at 4.5 dB, while for λ_r = 1585.4 nm, the peak gain is highest at 7.9 dB. The corresponding NF values are 8.8 dB, 8.5 dB and 7.4 dB. Also, because the grating were not packaged during the measurements and therefore was exposed to vibration and/or air drafts, the results showed some variation with time (up to 1.5 dB difference in the gain measurement). This was especially noticeable for λ_r = 1585.4 nm (see Fig. 5-15) since the overlap was located on the slope portion of each of the gratings' reflection spectra, small disturbances in FBG_1's tension caused important fluctuations in the cavity's overall feedback level.

The gain and NF as a function of input signal power are shown for signals at 1527.99 nm, 1538.98 nm and 1550.12 nm in Fig. 5-16, Fig. 5-17 and Fig. 5-18, respectively. Results for the three feedback levels are provided. As expected, gain-clamping is strongest when the feedback level is highest; the tradeoff is that the gain is lower and the NF is higher.

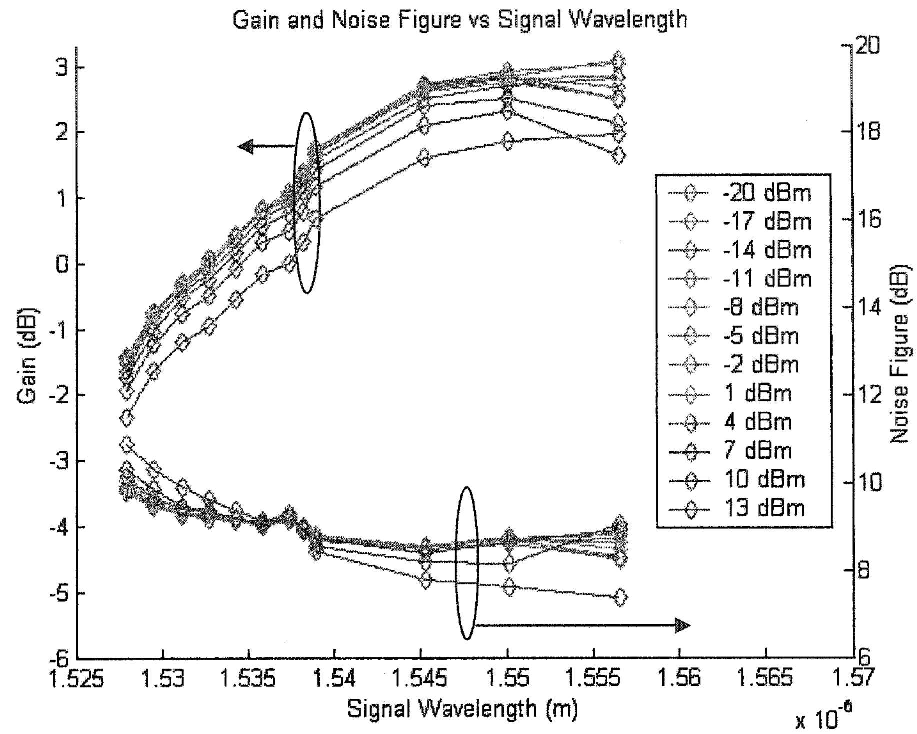

Fig. 5-13 λ_r = 1585.1 nm, feedback level is highest.

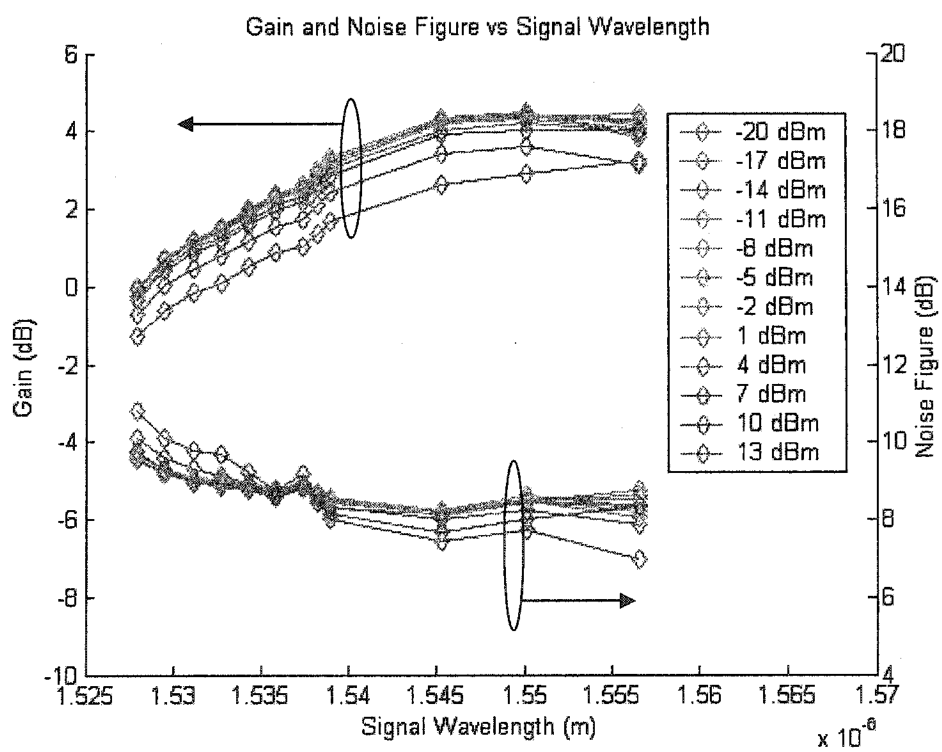

Fig. 5-14 λ_r = 1585.2 nm, middle feedback level in the cavity.

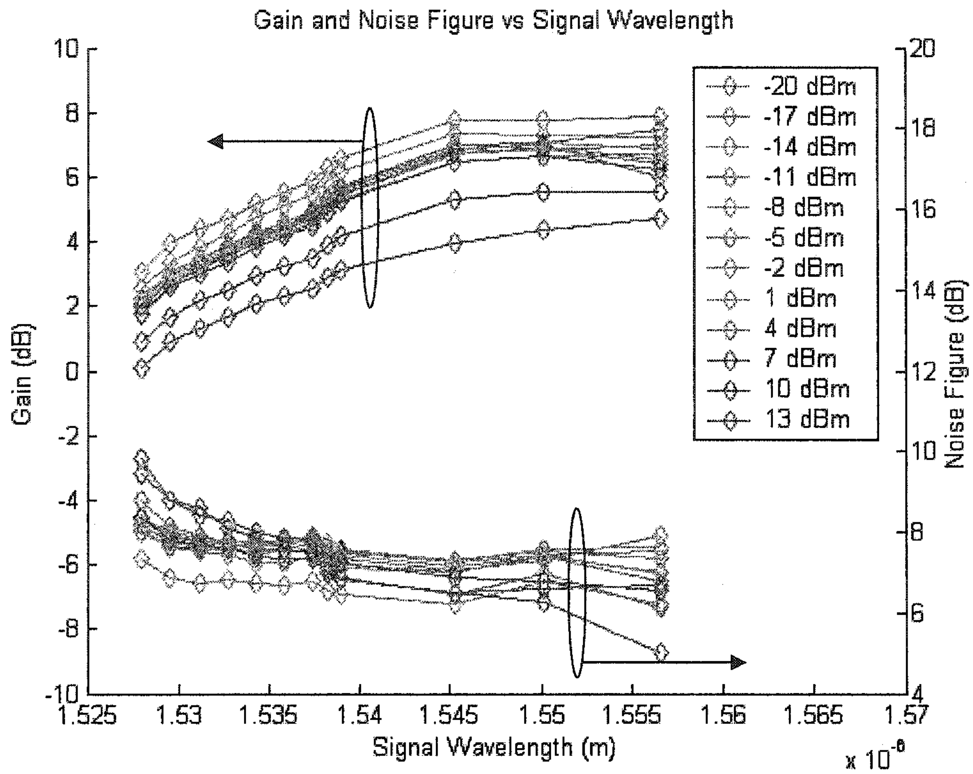

Fig. 5-15 λ_r = 1585.4 nm, lowest feedback level in the cavity.

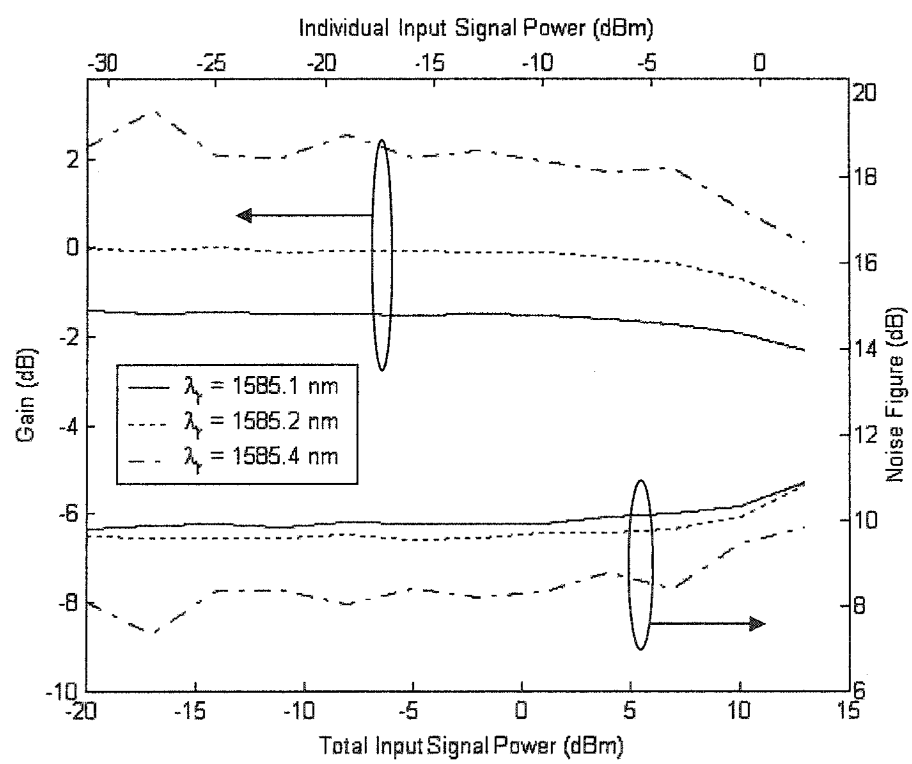

Fig. 5-16 Gain and NF vs. total input signal power for signal at 1527.99 nm.

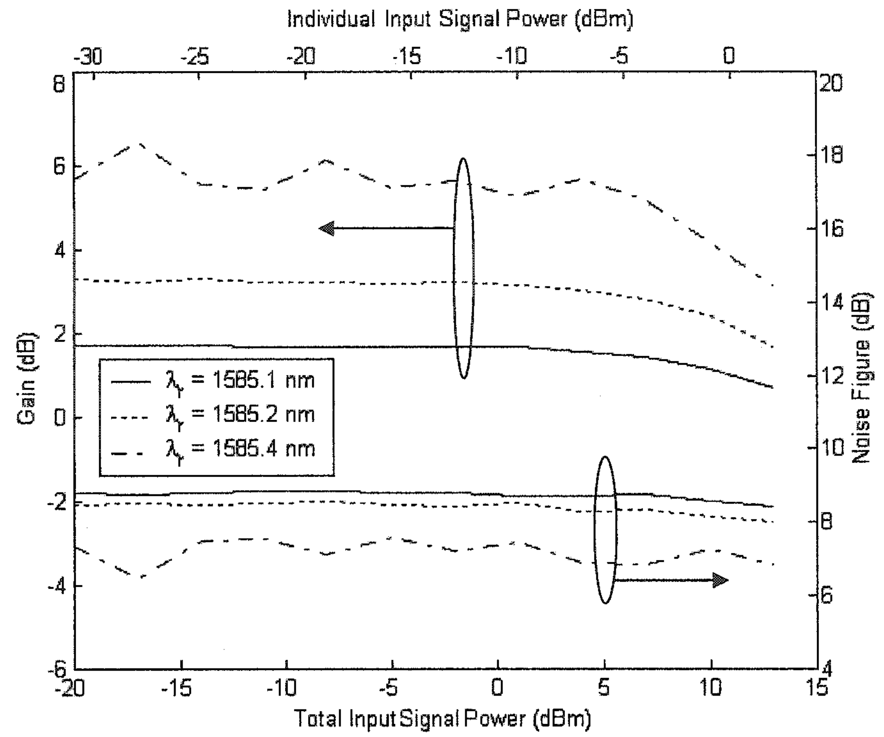

Fig. 5-17 Gain and NF vs. total input signal power for signal at 1538.98 nm.

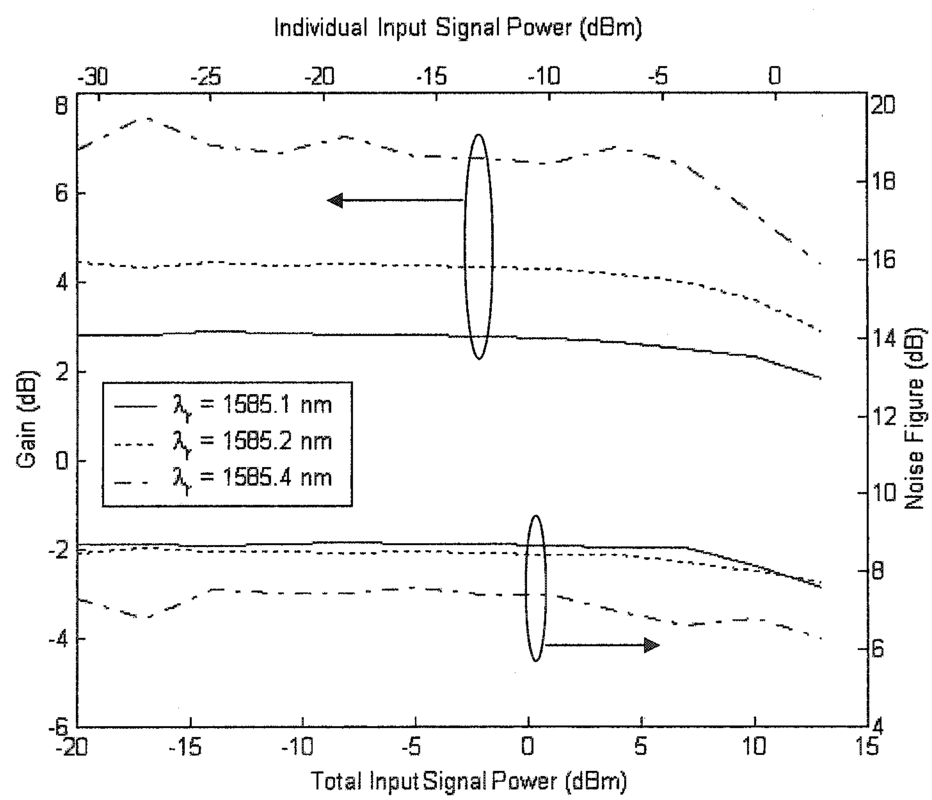

Fig. 5-18 Gain and NF vs. total input signal power for signal at 1550.12 nm.

5.6 *Summary of Experimental Analysis*

Gain-clamping using an FBG configuration was verified experimentally in this chapter. The feedback level in the cavity was varied by strain-tuning one of the gratings, which varied its central wavelength and consequently varied the degree of spectral overlap between the two gratings. The gratings that were used provided strong gain-clamping, in part due to their high reflectivity but also due to their wavelength location vis-à-vis the optical pumps. This resulted in a high critical power (over 5 dBm total input signal power) but also in a much lower gain (maximum of 7.9 dB) and high NF (7.4 dB, corresponding to maximum gain).

Also, the simulation program and the experiments were compared for the unclamped DFRA and they were shown to have similar gain and NF.

6 Conclusion

In this thesis, a systematic study of all-optical GC-DFRAs has been presented. In particular, a design achieving optical feedback through the use of FBGs has been explored, both through simulations and experiments.

The main challenge in designing a GC-DFRA is to locate an appropriate feedback wavelength which will achieve gain-clamping uniformly over the DWDM band being amplified. It was determined that by placing the feedback wavelength such that the pumps are evenly depleted allowed this objective to be met; more specifically, the introduction of the feedback signal should not affect the gain spectrum shape, i.e. the gain should only shift down uniformly. This has the added benefit that the gain-clamping design may be done separately from the gain-flattening design. How the feedback signal depletes the pumps is primarily dependent on the Raman gain coefficient corresponding to the frequency separation between the pumps and the feedback signal. Other factors, such as pump-to-pump interaction, DWDM signal interaction with the feedback signal also need to be considered when trying to locate a suitable feedback wavelength.

In the simulation portion of this thesis, a GC-DFRA spanning 58 nm which showed uniform gain-clamped performance and having a gain of over 20 dB was achieved for a set of given amplifier parameters (fiber length, effective Raman gain coefficient, fiber attenuation coefficient, pump locations and launch powers, etc…). The worst-case critical power of this amplifier was approximately -3 dBm. This same unclamped amplifier (i.e. without FBGs) was shown to saturate at a total input power of less than -15 dBm. The tradeoff in the gain (decrease) for the clamped amplifier was on the order of 7 dB, while the tradeoff in NF (increase) was of less than 1 dB, from the unclamped DFRA.

In the experimental portion of this thesis, gain-clamping for the FBG configuration was verified. Due to the availability of equipment, a feedback signal was located at 1585 nm, using gratings that were over 90 % reflective. The resulting feedback signal had too high a power which depleted the pumps too strongly, resulting in a system with low gain and high NF. Strain-tuning one of the FBGs allowed the feedback signal power to be lowered hence increasing the gain by 4.8 dB (from 3.1 to 7.9 dB) and lowering the noise figure by 1.6 dB (from 8.3 dB to 6.7 dB) for a signal at 1550.12 nm. Still, there is a very large gain and NF tradeoff from the unclamped amplifier, which had a gain of 21.8 dB and a NF of 6.6 dB near 1550 nm. As expected, gain-clamping was very strong in this case: the critical power was on the order of 7 dBm total input signal power. In order to properly design this amplifier to achieve uniform gain-clamping, high gain and low NF, the procedure developed in chapter 4 needs to be applied, which requires knowing the exact effective Raman gain coefficient. A feedback wavelength at a longer wavelength and FBGs with lower reflectivity would most certainly be needed for an optimum design.

In the future, a more thorough study of how the GC-DFRA would be affected by input signals being added and dropped non-uniformly across the wavelength band is needed.

Other issues that need to be explored include the maximum band that such a GC-DFRA configuration could support, the number of pumps that a single feedback signal could effectively deplete and whether multiple feedback signals could be used. Nevertheless, the results presented herein provide the basis for these deeper investigations.

References

[1] S. Namiki, Y. Emori, "Ultrabroad-band Raman amplifiers pumped and gain-equalized by wavelength-division-multiplexed high-power laser diodes", IEEE Journal on Selected Topics in Quantum Electronics, vol. 7, no. 1, pp. 3-16, Feb 2001.

[2] J. Kierzenka, L. F. Shampine, "A BVP Solver Based on Residual Control and the Matlab PSE", Mathworks Inc., Natick MA, USA.

[3] W. H. Press, B. P. Flannery, S. A. Teukolsky, W. T. Vetterling, Numerical Recipes in C: The Art of Scientific Computing, "Two Point Boundary Value Problems", Cambridge University Press, 2nd edition, January 1993.

[4] S. Namiki, "WDM Pumping and Highly Nonlinear Fibers for Raman Amplification", Raman '03, Center for Nonlinear Studies Workshop, 2003.

[5] M. N. Islam, "Raman Amplifiers for Telecommunications", IEEE Journal of Selected Topics in Quantum Electronics, vol. 8, no. 3, May/June 2002.

[6] P. Gavrilovic, "S-Band Discrete Raman Amplifiers: Technology and System Performance", LEOS 2001, vol. 2, pp. 471-472, Nov 2001.

[7] J. Auyeung, A. Yariv, "Spontaneous and Stimulated Raman Scattering in Long Low Loss Fibers", IEEE Journal of Quantum Electronics, vol. QE-14, no. 5, May 1978.

[8] H. Jiao, "Review: Raman Amplifier", Electrical and Computer Engineering Department, University of Maryland Baltimore County, website: research.umbc.edu/~ychen/ee635.

[9] B. D. Guenther, Modern Optics, J.W. Wiley, pp. 596-599, 1990.

[10] Y. Kang, “Calculations and Measurements of Raman Gain Coefficients of Different Fiber Types”, M. Sc. Thesis, Department of Electrical Engineering, Virginia State University, (2002).

[11] P. B. Hansen et al, “Capacity Upgrades of Transmission Systems by Raman Amplification”, IEEE Photonics Technology Letters, vol. 9, no. 2, February 1997.

[12] C.R.S. Fludger, V. Handerek, R.J. Mears, “Fundamental Noise Limits in Broadband Raman Amplifiers”, OFC 2001, vol.1, pp. MA5 1 – 3, March 2001.

[13] A.B. Puc, M.W. Chbat, J.D. Henrie, N.A. Weaver, H. Kim, A. Kaminski, A. Rahman, H. Fevrier, “Long-haul WDM NRZ Transmission at 10.7 Gb/s in S-band using cascade of lumped Raman amplifiers”, OFC 2001, vol. 4, pp. PD39-P1-3, March 2001.

[14] S.A.E. Lewis, S.V. Chernikov, J.R. Taylor, “Rayleigh noise suppression using a gain flattening filter in a broadband Raman amplifier”, OFC 2000, vol. 4, pp. 7-10, March 2000.

[15] N. Gryspolakis, “Theoretical Analysis of Two-Stage Discrete Fiber Raman Amplifiers”, M. Eng Thesis, Department of Computer and Electrical Engineering, McGill University (2003).

[16] S.A.E. Lewis, S.V. Chernikov, J.R. Taylor, “Characterization of double Rayleigh scatter noise in Raman amplifiers”, IEEE Photonics Technology Letters, vol. 12, no. 5, pp. 528-530, May 2000.

[17] S.S-H Yam, F-T. An, E.S-T. Hu, M.E. Marhic, T. Sakamoto, L.G. Kazovsky, "Gain-clamped S-band discrete Raman amplifier", OFC 2002, pp. 385-387, March 2002.

[18] Z. Xiang, L. Chao, S. Ping, H.H.M. Shalaby, C. Teehiang, "Dynamic gain control for discrete Raman fiber amplifier", CLEO 2001. pp. 144-145, May 2001.

[19] C.R.S. Fludger, V. Handerek, "Ultra-wide bandwidth Raman amplifiers", OFC 2002, pp. 60-62, March 2002.

[20] P. Ebrahimi, M.C. Hauer, Q. Yu, R. Khosravani, D. Gurkan, D.W. Kim, D.W. Lee, A.E. Willner, "Statistics of polarization dependant gain in Raman fiber amplifiers due to PMD", CLEO 2001, pp. 143-144, May 2001.

[21] S. Popov, E. Vanin, "Polarization dependence of Raman gain on propagation direction of pump and probe signal in optical fibers", CLEO 2001, pp. 146-147, May 2001.

[22] M.H. Eiselt, "Raman gain saturation and the need for dynamic gain control", IEEE / LEOS 2002 All-Optical Networking, Summer Topics, pp. WE1-43-44, July 2002.

[23] S. Kado, Y. Emori, S. Namiki, "Gain and noise tilt control in multi-wavelength bi-directionally pumped Raman amplifier", OFC 2002, pp. 62-63, March 2002.

[24] Y. Emori, S. Kado, S. Namiki, "Simple gain control method for broadband Raman amplifiers gain-flattened by multi-wavelength pumping", ECOC 2001, pp. 158-159, 2001.

[25] Bing Xia, "Theoretical and experimental analyses of all-optical gain-clamped L-band EDFAs", M.Eng. Thesis, Department of Electrical and Computer Engineering, McGill University, 2002.

[26] C.-J. Chen, J. Ye, W.S. Wong, Y.-W. Lu, M.-C. Ho, Y. Cao, M. J. Gassner, J. S. Pease, H.-S. Tsai, H.K. Lee, S. Cabot, Y. Sun, "Control of transient effects in distributed and lumped Raman amplifiers", Electronics Letters, vol. 37, pp. 1304-1305, October 2001.

[27] M. Karasek, M. Menif, "Protection of surviving channels in pump-controlled gain-locked Raman fiber amplifier", Optics Communications, vol. 210, pp. 57-65, September 2002.

[28] Y.D. Gong, P. Shum, C. Lu, T.X. Cheng, X. Zhou, Y.X. Wang, "Investigation of Raman fiber amplifier with all optical gain clamping ring", Proceedings of the SPIE, vol. 4906, pp. 43-46, 2002.

[29] J. Ning, X. Lu, Z. Chen, "Automatic gain control for Raman fiber amplifiers", Proceedings of the SPIE, vol. 4913, pp. 41-44, 2002.

[30] C.C. Wang, A. Srivastava, C.J. Chen, W. S. Wong, Y. Sun, "Recent advances in optical fiber amplifiers", Proceedings of SPIE, vol. 4581, pp. 149-157, 2001.

[31] R.H. Stolen, E. P. Ippen, "Raman gain in glass optical waveguides", Applied Physics Letters, vol. 22, no. 6, 1973.

[32] Y. Emori, S. Namiki, "Broadband Raman amplifier for WDM", IEICE Transactions on Communications, vol. E84-B, no. 5, pp. 1219-1223, May 2001.

[33] Y. Aoki, S. Kishida, K. Washio, K. Minemura, "Bit error rate evaluation of optical signals amplified via stimulated Raman process in an optical fiber", Electronic Letters, vol. 21, no. 5, pp. 191-193, 1985.

[34] L. F. Mollenauer, J. P. Gordon, M. N. Islam, "Soliton propagation in long fibers with periodically compensated loss," Journal of Quantum Electronics, vol. QE-22, no. 1, pp. 157-173, 1986.

[35] Y. Emori, S. Namiki, "Demonstration of broadband Raman amplifiers: a promising application of high-power pumping unit", Furukawa Review, No. 19, 2000.

[36] Sumitomo Electric, HNLF Datasheet, website: www.sumitomo.com.

[37] Dennis Derickson, <u>Fiber Optic Test and Measurement</u>, Prentice Hall PTR, 1998.

[38] S.Y. Ko, M.W. Kim, D. H. Kim, S. H. Kim, J. C. Jo, J. H. Park, "Gain control in erbium doped fiber amplifiers by tuning center wavelength of a fiber Bragg grating constituting resonant cavity", Electronic Letters, vol. 34, pp. 990-991, May 1998.

[39] P.C. Reeves-Hall, D.A. Chestnut, C.J.S. De Matos and J.R. Taylor, "Dual Wavelength pumped L- and U-band Raman amplifier", Electronics Letters, vol. 37, no. 14, pp. 883-884, July 2001.

Appendix 1

This paper was presented at the 2003 IEEE-Lasers and Electro-Optics Society (LEOS) Annual Meeting in Tucson, Arizona (Paper ThFF 1).

Design of All-Optical Gain-Clamped Discrete Fiber Raman Amplifiers

Theodore Zambelis, Nikolaos Gryspolakis, and L. R. Chen
Department of Electrical and Computer Engineering, McGill University, Montreal, PQ H3A 2A7 Canada

Abstract – Using numerical simulations, we design and analyze the performance of gain-clamped discrete fiber Raman amplifiers. In particular, we investigate the impact of the feedback wavelength on the gain-clamping properties.

Fiber Raman Amplifiers (FRAs) are of interest for DWDM applications, especially since the gain spectrum can be arbitrarily tailored through the selection of the pump wavelengths and powers. Ultra-broadband amplifiers (covering > 80 nm bandwidth) having a gain flatness of < 1 dB have been demonstrated [1-3]. With the introduction of high-powered 14xx pump laser diodes and the development of highly nonlinear fiber (HNLF) having a peak effective Raman gain coefficient roughly 10 times that of conventional silica fiber [3], discrete FRAs (DFRAs) are emerging as a viable optical amplifier technology.

As optical networks become increasingly "agile", optical amplifiers must be capable of operating in dynamic environments where the number and power of DWDM signals vary constantly with time. In particular, efficient gain control techniques are required to stabilize the amplifier gain profile and to minimize the impact of transient effects.

Gain-clamping in DFRAs using ring laser configurations [4] has been demonstrated as a means for providing gain control. However, in typical ring configurations, both feedback (lasing) and WDM signals are tapped so that we cannot control the level of feedback (i.e. the loss of the ring cavity which determines the amount of gain) without affecting the WDM signals. In this paper, we investigate the use of fiber Bragg gratings (FBGs) to create a standing wave cavity for gain-clamping, see Fig. 1. This configuration allows us to control the cavity loss for the feedback wavelength (by adjusting the FBG reflectivities) independently from the WDM signals. Furthermore, we optimize the design of gain-clamped (GC) DFRAs, especially in terms of the feedback wavelength for a given fiber Raman gain spectrum and pump wavelengths. So far, such studies have been lacking.

Our main design objective is to obtain uniform gain-clamping behaviour over the entire wavelength band being amplified, i.e. each wavelength should experience the same amount of clamping. For a given set of pump wavelengths and pump powers, the design parameters include the reflectivity of the two FBGs, denoted (R_1, R_2), and more importantly, the feedback (lasing) wavelength λ_f.

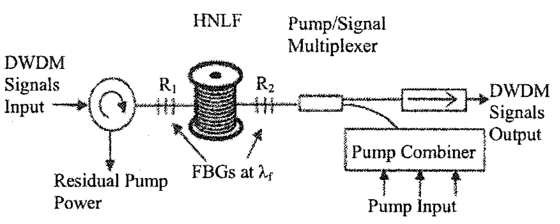

Fig.1. GC-DFRA configuration.

We use the full propagation equations in [2] to model the GC-DFRA and account for all interactions. We consider three pumps at 1435, 1450 and 1480 nm, each with a launch power of 200 mW (although this does not yield a perfectly flat gain spectrum, the analysis presented herein applies equally to a gain-flattened system). Sixty-seven DWDM signals were evenly spaced by 100 GHz in the range from 1545 nm to 1600 nm. Noise is calculated over an extended wavelength range with 200 GHz resolution [we use interpolation to extract the noise at specific signal wavelengths for determining the noise figure (NF)]. We use 5 km of fiber with a typical effective Raman gain spectrum shown in Fig. 2. The peak coefficient is 5.9 $(W\cdot km)^{-1}$, which is typical of currently available HNLF.

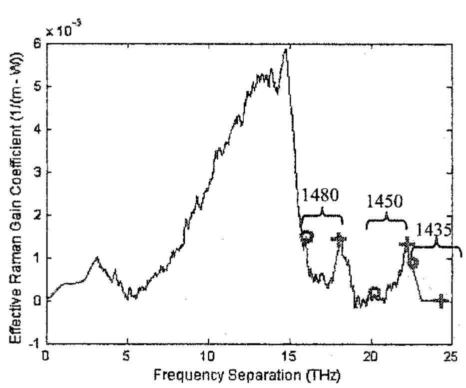

Fig.2. Raman gain coefficient with pump to lasing signal interaction indicated ('o' for λ_f = 1607 nm and '+' for λ_f = 1624.8 nm)

In order to satisfy our main objective, we found that the shape of the gain spectrum of the clamped amplifier had to be the same as that of the unclamped amplifier. In particular, the design with the best overall performance uses a feedback wavelength λ_f = 1624.8 nm. Fig. 2 illustrates the effective Raman gain coefficients for the feedback signal relative to the pump wavelengths. This is the optimum feedback wavelength since the 1450 nm and 1480 nm pumps are depleted by an equal amount (i.e. the pumps provide the same Raman gain for λ_f). The 1435 nm pump is not directly depleted by the feedback signal since the gain coefficient is zero; however, it is indirectly depleted since it provides gain to the other two pumps. Overall, the depletion of the 3 pumps is such that the introduction of the feedback signal does not alter the shape of the gain spectrum, see Fig. 3. On the other hand, if the feedback wavelength does not satisfy this constraint, e.g. for λ_f = 1607 nm, then the shape of the gain spectrum is not maintained.

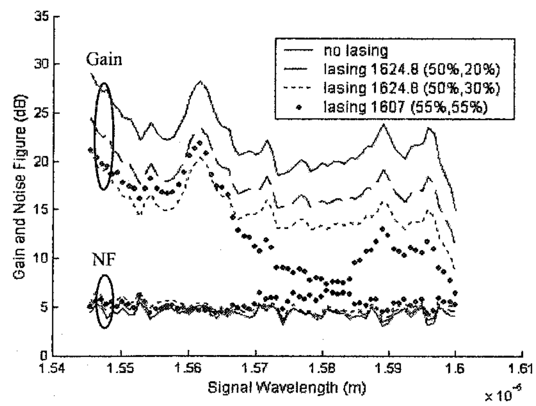

Fig.3. Small-signal gain (-15 dBm total input signal power) and NF for unclamped and clamped cases.

Fig. 4 shows the gain and NF as a function of the total input signal power for a signal wavelength of 1575 nm (with λ_f = 1624.8 nm). The amplifier clearly exhibits gain-clamped behavior. By varying (R_1, R_2), we can vary the amount of gain without changing the shape of the gain spectrum, see also Fig. 3.

Fig. 5 shows that the clamping behavior is more uniform over the amplifier bandwidth when λ_f = 1624.8 nm. In particular, when the total input signal power to the amplifier is increased from -15 dBm to 0 dBm, there is practically no change in gain for the signal wavelengths with λ_f = 1624.8 nm. However, with λ_f = 1607 nm, the gain varies by over 1 dB in the short wavelength region, i.e. the clamping is less effective from 1545 to 1570 nm compared to 1570 to 1600 nm.

In summary, we have investigated the performance of DFRAs clamped using FBGs. We find that in order to achieve uniform clamping performance for all wavelengths being amplified, the feedback wavelength must be chosen so that the depletion of the pumps is such that the introduction of the feedback signal does not alter the shape of the gain spectrum relative to the unclamped case.

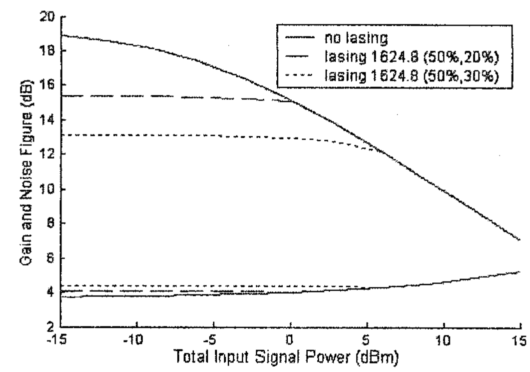

Fig.4. Gain and NF vs. total input signal power for unclamped and clamped cases for a signal at 1575 nm.

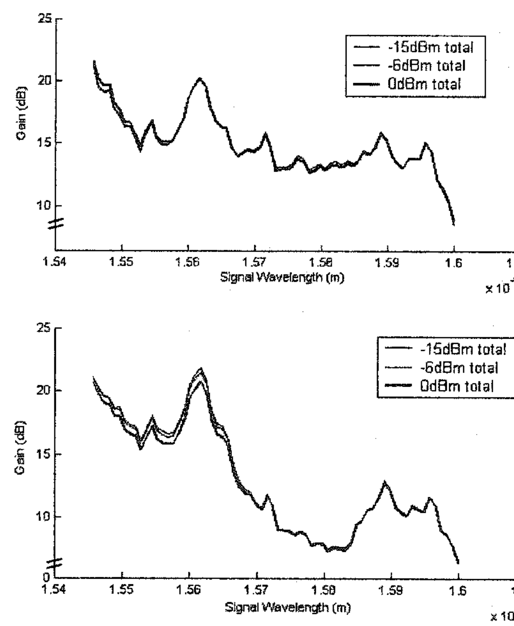

Fig.5. Gain spectra for different total input signal power for GC-DFRA with λ_f = 1624.8 nm (top) and 1607 nm (bottom).

References

[1] H. Kidorf, L. Rottwitt, M. Nissov, M. Ma, E. Rabarijaona, IEEE Photon. Technol. Lett., **11**, pp. 530 -532, 1999.

[2] S. Namiki and Y. Emori, IEEE J. Sel. Top. in Quantum Electron., **7**, pp. 3-16, 2001.

[3] S. Namiki, Raman'03, Center of Nonlinear Studies Workshop, 2003.

[4] X. Zhou, H. H. M. Shalaby, C. Lu, P. Shum, and T. Cheng, Proc. OFC'01, **3**, pp. 17-22, 2001.

Appendix 2

Photographs of the experimental setup.

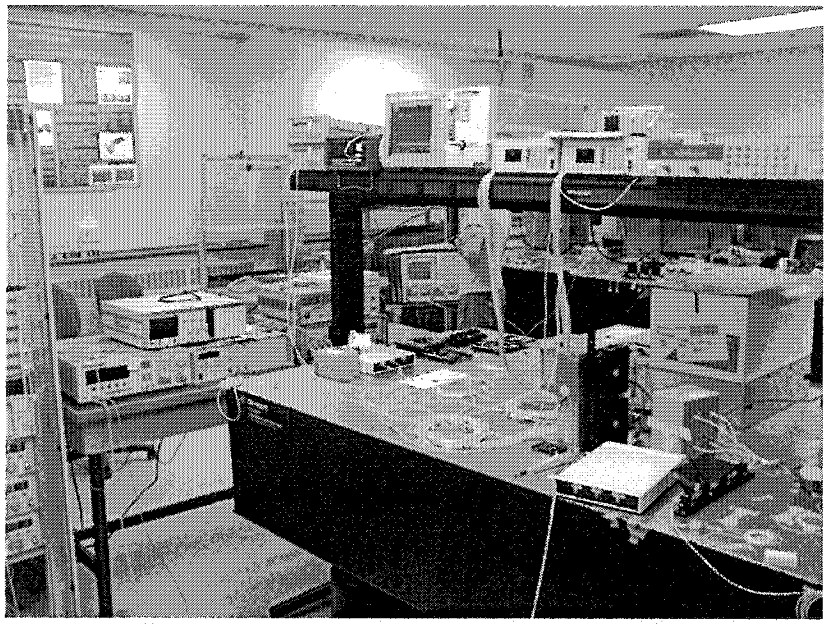

The GC-DFRA experimental setup.

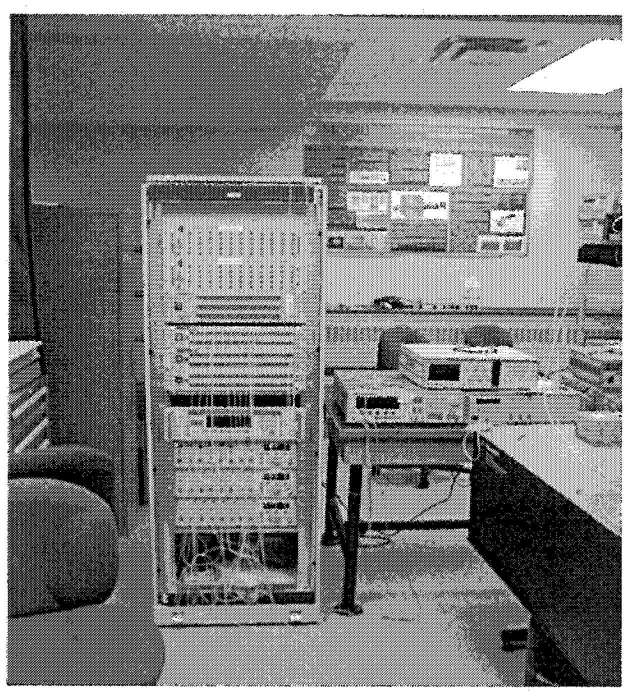

The DWDM signal sources and the multiplexer.

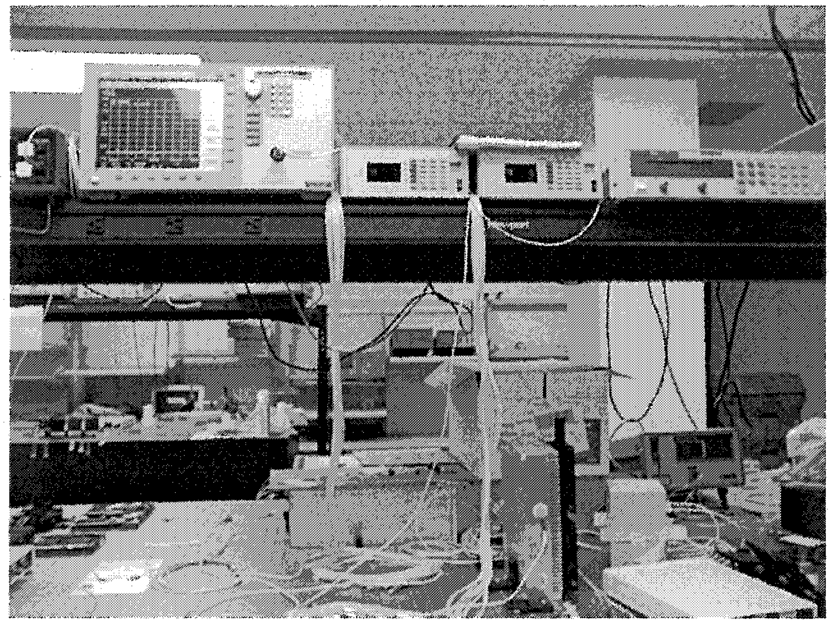

In the foreground are the two switches, the OSA (top) and the Raman fiber laser (below).

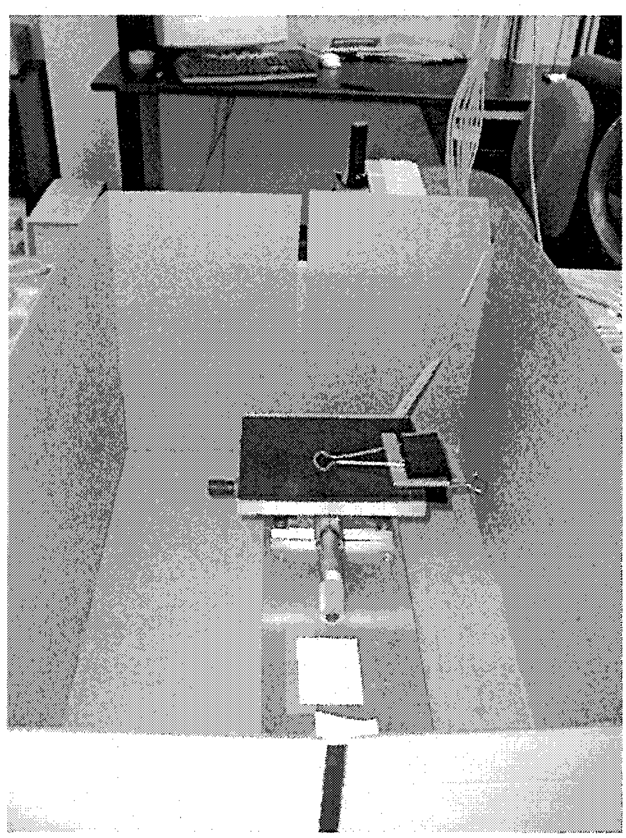

The FBG on a strain-mount. The box was used to reduce exposure to air-drafts.

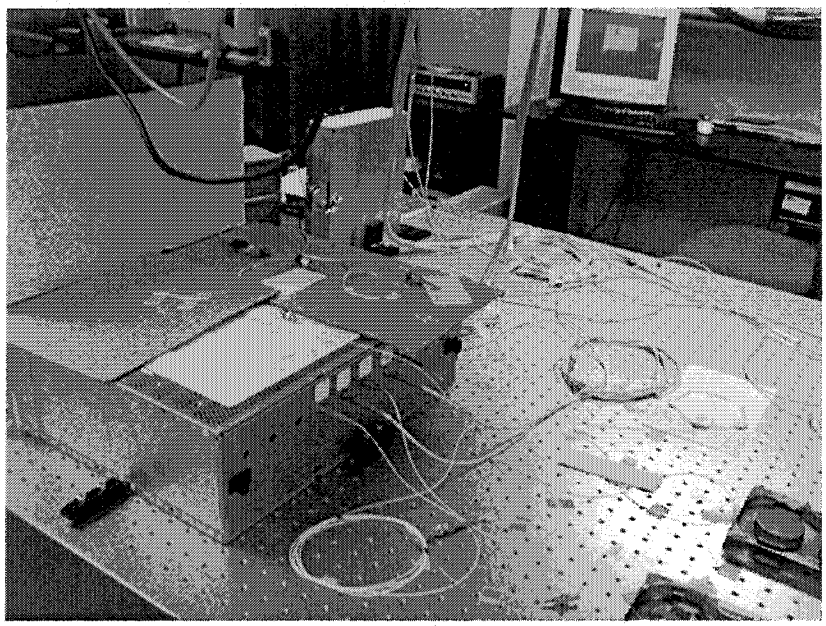

Most of the amplifier components were secured in this metal frame to avoid disturbance.

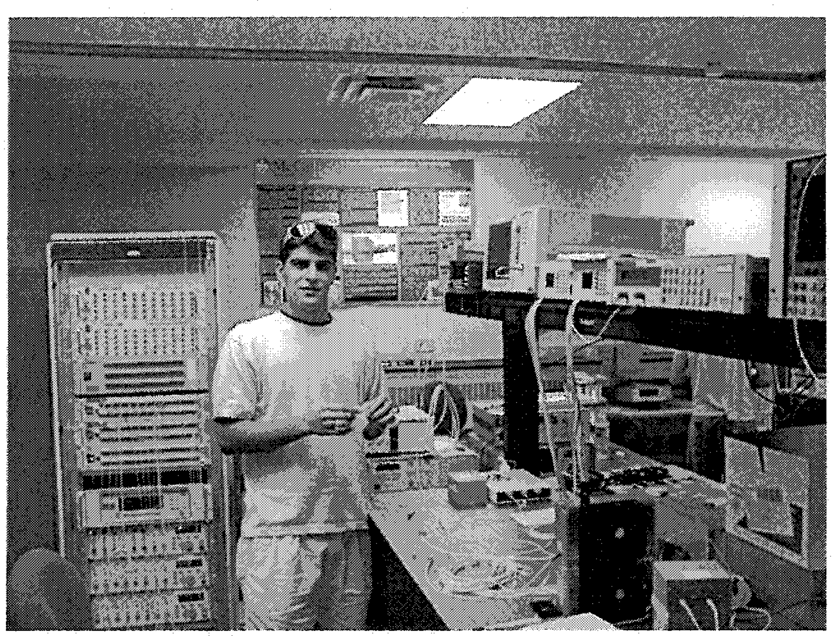

The author cleaning a fiber connector.